Progress Report 2024 — Laboratory for Waste Management

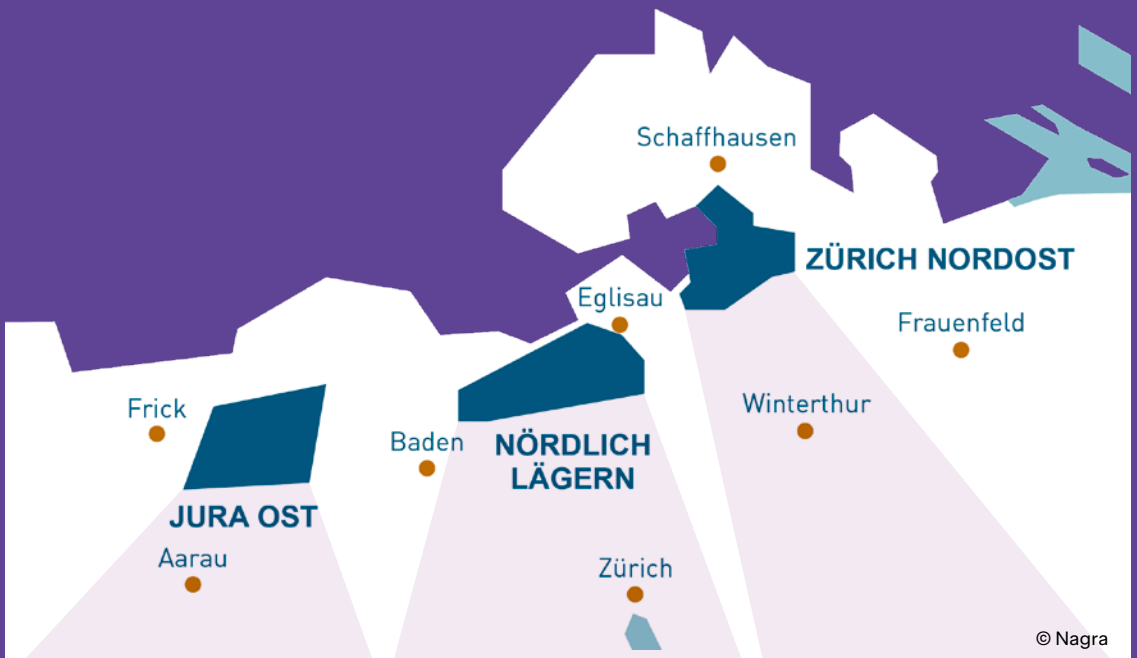

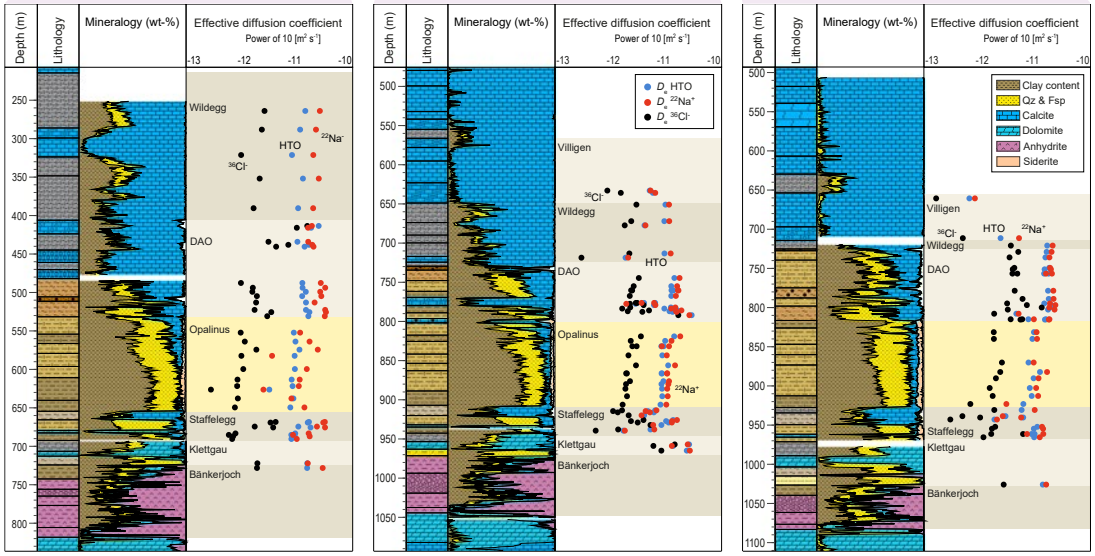

PSI Center for Nuclear Engineering and Sciences

PSI

Cover

Mineralogy and effective diffusion coefficients for HTO, Na^+ and Cl^- across stratigraphic sequences in potential siting regions for a deep geological repository in Northern Switzerland. The corresponding datasets were derived based on extensive field explorations, laboratory diffusion experiments on rock samples and thermodynamic modelling. Further details of the study are provided in Chapters 3 and 5. The schematic map showing siting showing the locations is reproduced with permission of Nagra.

Progress Report 2024
— Laboratory for Waste Management

PSI Center for Nuclear Engineering and Sciences

PSI

Preface

The mission of the Laboratory for Waste Management (LES) is to carry out a comprehensive research and development (R&D) programme in support of Swiss radioactive waste disposal options. In particular, LES maintains and further develops world-leading expertise in repository geochemistry, radionuclide migration, and design optimisation of engineered barrier systems and materials based on experimental studies and numerical simulations.

The Laboratory serves an important national duty by supporting the Swiss Federal Government and Nagra in their tasks to safely dispose of radioactive wastes from medical, industrial and research applications as well as from nuclear power plants. The research activities of LES cover fundamental aspects of repository geochemistry, radionuclide transport and retardation in geological and technical barriers. The project portfolio of LES is a balanced combination of experimental activities conducted in dedicated laboratories for handling radioactive isotopes, field experiments, and computer simulations. This work is directed towards repository implementation, and the results are used by Nagra in their comprehensive performance assessment studies. The finalisation of the documentation for Nagra's general licence application and the implementation of a repository in the next decades require expertise in model-based assessments of the *in situ* repository conditions for specific repository designs. The long-term strategy of LES is thus to develop the experimental and modelling expertise necessary for coupled description of relevant repository processes to assist safety- and economy-driven design optimisation of geological disposal of radioactive wastes in Switzerland.

Together with other laboratories in the PSI Center for Nuclear Engineering and Sciences, LES maintains best practices and standards in laboratory management and data processing according to the ISO 9001:2015 certified Integrated Quality Management System. This certification covers research and scientific services for agencies in the area of nuclear waste disposal and environmental sciences.

The present report summarises the research activities and results achieved in 2024. It gives a detailed overview of research projects, personnel management, national and international collaborations, and individual contributions achieved by scientists in the four research groups at PSI and the Mineralogy group at the University of Bern.

We gratefully acknowledge the support of our work by the PSI management, Nagra, and numerous research programmes within National and European funding agencies (e.g. SNSF, Swiss Nuclear, Eurad), as well as national and international industrial partners.

Table of Contents

1 OVERVIEW

Churakov S.V.

1.1 Introduction

This chapter provides an overall progress summary of activities in the Laboratory for Waste Management (LES) conducted from January 1st, 2024 to December 31st, 2024. The following chapters are organised thematically according to the six overarching research topics addressed by the LES team. These topics are multidisciplinary in nature and include contributions from different research groups at LES and the Mineralogy Group hosted by the Institute of Geological Sciences at the University of Bern.

1.2 General

The site selection process for geological disposal of radioactive waste in Switzerland has entered its licensing stage. In November 2024, Nagra has submitted the general licence application (Rahmenbewilligungsgesuch – RBG) for the geological disposal of Spent Fuel/High Level Waste (SF/HLW) and Low/Intermediate Level Waste (L/ILW) in the "Nördlich Lägern" region. The proposal for the repository location is justified based on dedicated laboratory and field studies conducted in the period 2019-2024. The detailed documentation of geological and hydrological data, including diffusion and sorption measurements on the samples extracted from the site-specific drill cores, was completed in 2023-2024. These studies provide a reliable basis for site- and formation-specific databases of diffusion and sorption parameters used for the performance assessment calculations and demonstration of repository safety at the proposed repository location.

The datasets for the safety assessment were derived based on mechanistic sorption models, and laboratory measurements served for model benchmarking and validation. This is a unique and holistic approach in which scientific results are directly integrated in the safety assessment. Most remarkable is the self-consistent use of the thermodynamic data and model for consideration of pore water chemistry, solubility limits, sorption and diffusion data for radionuclides.

Following the period of very intensive site-specific exploration leading to the submission of the RBG, the focus of the LES research programme is now shifting towards the development and application of model-based tools for the optimisation of the repository design. By the time of repository construction, some building materials currently considered as the basis for the repository design might not be conveniently available, for economical or technological reasons, and so it is important to future-proof the design concept through assessment of emerging materials.

Accordingly, LES maintains knowhow and continues research on the main pillars of repository safety, namely the mechanistic description of radionuclide interaction with repository barriers and the processes in the repository near field. Present and future research activities focus on the chemical evolution of the repository near field, sorption competition phenomena, the behaviour of redox-sensitive radionuclides, the role of organic matter, and mineral surface-induced redox reactions. For the period of the post-RBG phase, LES puts strong emphasis on the further improvement of advanced modelling capabilities for reactive transport simulations. These capabilities are particularly important for understanding the long-term evolution of *in situ* repository conditions, and the interaction between repository barriers causing an alteration of their retention and transport properties. Such expertise is the essential for the optimisation of repository design.

Significant progress has been made in development of high-fidelity simulations and the process-based multiscale modelling of complex physical phenomena in repository systems. Particularly challenging in this context is the parameter transfer between models at different scales, and efficient process coupling in complex 3D models. Internationally, LES is taking a leading role in the development of so-called data driven surrogate models based on modern algorithms developed in the field of artificial intelligence and machine learning. In this context Deep Neural Networks (DNN) are applied for improvement of numerical performance of coupled codes, by use of surrogate models for the simulation of repository nearfield and material evolution. These developments are fostered through international collaboration supported by web-based collaborative tools (https://www.geoml.ai) maintained by the LES team. Several demonstrations of surrogate model development and digital twins are provided at (https://www.geoml.eu).

Among 52 mandated actors (European research entities (RE), waste management organisations (WMO) and technical safety organisations (TSO)), LES made a significant contribution to the successful completion of the Joint European Research program COFUND-EJP NFRP-2018-6: *"European Joint Research Programme in the management and disposal of radioactive waste Eurad"*. The project started on June 1st, 2019 and has

been successfully completed on May 31st 2024. Within the EURAD programme, LES contributed to eight individual work packages (WPs):

FUTURE: Fundamental understanding of radionuclide retention (WP Lead and Task lead)

DONUT: Modelling of process couplings and numerical tools applied to performance assessment (Task co-Lead)

ACED: Assessment of chemical evolution of ILW and HLW disposal cells (Task Lead)

GAS: Mechanistic understanding of gas transport in clay materials (Contributor)

CORI: Cement organics radionuclide interactions (Contributor)

UMAN I+II: Uncertainty management multi-actor network (Contributor)

MAGIC: Chemo-Mechanical AGIng of Cementitious materials (Task Lead)

MODATS: Monitoring equipment and data treatment for safe repository (Contributor)

Within the EURATOM NFRP-2019-2020-10 RIA call, LES participates in the project *"Pre-disposal management of radioactive waste, PREDIS".* This 4-year EU project started on September 1st, 2020 and was successfully completed on August 31st 2024. In this project, LES has been working on the development of a model-based digital twin for the evolution of cementitious waste packages under various scenarios for extended intermediate storage.

Building on the success of the Eurad-I and PREDIS projects, a follow up pan-European partnership Eurad-II has started in October 2024. The project spans the 5-year period 2024-2029, and comprises overarching topics of Waste Management Policies, Predisposal, Engineered Barrier System (EBS), Geoscience, Optimisation, and Safety Case. Due to the political decision of the European Commission to exclude Switzerland from the Horizon research programme, Swiss research entities currently participate as associated partners with no funding provided by the EC. Instead, the participation of Swiss partners in the call is directly co-funded by the State Secretariat for Education, Research, and Innovation SERI.

LES participates in 15 individual work packages, in some of which LES takes a leading scientific role:

HERMES: High fidelity numerical simulations of coupled processes (WP Lead and Task Lead).

DITOCO2030: Next generation digital twins to support optimisation, construction and operation of surface and subsurface radioactive waste management facilities (Task Co-Lead).

DITUSC: Development and improvement of quality assured thermodynamic understanding for use in nuclear waste disposal safety case (Task-Lead).

ASTRA: Alternatives radioactive waste management strategies (Task-Lead).

RAMPEC: Radionuclide mobility under perturbed conditions (Task-Lead).

KM: Knowledge Management (Task Co-Lead).

ICARUS: Innovative characterisation techniques for large volumes (Contributor).

STREAM: Sustainable treatment and immobilisation for challenging waste (Contributor).

L'OPERA: Long-term performance of waste matrices (Contributor).

SAREC: Release of safety relevant radionuclides from spent nuclear fuel under deep disposal conditions (Contributor).

InCoManD: Innovative and new container/canister materials under disposal fields conditions: manufacturing feasibility and improved durability (Contributor).

ANCHORS: Hydraulic mechanical chemical evolution of bentonite for barriers optimisation (Contributor).

OPTI: HLW repository optimisation including closure (Contributor).

SUDOKU: Near-surface disposal optimisation based on knowledge and understanding (Contributor).

The project PRINCE: PRocesses at the INterface of iron and Cement, supported by the Sinergia program of the Swiss National Science Foundation, has been launched in 2024 to investigate the corrosion of steel in reinforced concrete. PRINCE is a 4-year project comprising 7 PhDs and 2 Postdoctoral fellows working within the research consortium of PSI-EMPA-UniBern and ETHZ. It seeks to make a breakthrough in the fundamental understanding of the processes that occur at the interface between steel and cementitious environment to elucidate 1) the kinetics of the electrochemical iron dissolution, which is coupled to 2) transport of ferrous and ferric ions in pore water solution through the liquid phase held within a porous medium, and the simultaneously occurring 3) chemical reactions (complexation, oxidation, …) and 4) interactions with solid phases (e.g. sorption in calcium silicate hydrates (C-S-H)) as well as 5) nucleation and precipitation of solids (see section 4.8).

The reactive transport codes developed at LES are versatile and applicable in broad cross-disciplinary

applications. Complementary to geochemical applications, the codes are also used in collaborative research projects including thermohydraulic applications for nuclear reactors, desalination membranes, and pharmaceutical applications. With the support of Swissnuclear, further development of multiscale simulation codes for the modelling of boiling phenomena and crud formation in nuclear reactors is ongoing.

Several LES scientists have retired recently. To retain the core expertise of LES, and to more fully align the LES research portfolio to future oriented research questions, a number of both junior and senior experts have been recruited.

Dr. Anke Neumann has taken the Group Leader position for the Clay Sorption Mechanisms group in January 2024. She is a well-known expert in redox geochemistry of phyllosilicates and pollutant dynamics in near-surface environmental systems.

Dr. Yaana Bruneel has joined the diffusion group in December 2024. She has several years of experience in experimental studies of radionuclide transport and retention in cement and clay systems.

Scientific exchange is an essential component of research and development programmes. Particularly important in this context is the cross dissemination of knowledge in neighbouring fields. LES actively maintains collaborations with national and international research institutes in the field of waste management and environmental research. The main multi- and bi-lateral cooperations with external institutions and universities are summarised in Table 1.1.

Participation in international research projects and independent acquisition of project funding for PhD and postdoc projects is an essential driving force for developing state-of-the-art research capabilities, knowledge transfer and education of young generation scientists. Ongoing MSc/BSc/PhD projects and postdoc fellowships approved or started in 2024 at PSI and at the University of Bern are listed below, along with ongoing ones.

M. Alisher (PhD student/EMPA): "*Nucleation and precipitation kinetics of Fe(II)/Fe(III) containing hydrates* Start date: July 2024 (Collaboration with EMPA; Funding SNSF-Sinergia).

J. Ban (PhD student): *"Fe-doped hydrotalcites in Mg-cements".* Start date: September 2023 (Funding: SNSF).

M. Baur (PhD student/UBern): *"Reactive transport modelling of Fe transport in cement at pore scale"*. Start date: August 2024 (Funding SNSF-Sinergia).

E. Bayram (PhD student): *"Synthesis and characterisation of metal-doped C-S-H phases"*. Start date: February 2023 (Funding: PSI-Research Grant).

M. Delekta (PhD student): "*Formation, synthesis, chemical structure, and thermodynamic properties of Fe-hydrotalcite in Mg-rich cement"*. Start date: January 2024 (Funding: SNSF)

A. Ermanni (PhD student): *"Fe diffusion in cement phases"*. Start date: October 2024 (Funding SNSF-Sinergia).

P. Hänggi (PhD student/UBern): *"Incorporation of heavy metals in waste incineration residuals".* Start date: September, 2024 (Funding: Industry).

A. Katheras (PhD student/UBern): "*Molecular scale understanding of Tc and Pu sorption by magnetite*". Start date: October 2020 (Funding: BMBF, Germany).

L. Khait (PhD student): *"Se-uptake by zeolites"*. Start date: December 2024 (Funding SNSF).

S. Khiari (PhD student EMPA): "*Thermodynamic data for Fe(II) and Fe(III) containing hydrates".* Start date: July 2024 (Collaboration with EMPA; Funding SNSF-Sinergia).

J. Lu (PhD student): *"Fe speciation in cementitious pore water"*. Start date: December 2024 (Funding SNSF-Sinergia).

S. Mingione (PhD student/EMPA/UBern): "*Impact of process conditions on xonotlite quality and different components in xonotlite-based products on the high-T properties of these materials"*. Start date: October 2021 (Collaboration with EMPA; Funding: Industry).

H. Peng (PhD student): *"In situ chemical tomography and modelling of reactive transport processes in porous media".* Start date: November 2021 (Funding: PSI-Cross).

N. Shaik (PhD student): *"Fe speciation in cement phases by XAS"*. Start date: July 2024 (Funding SNSF-Sinergia).

V. Stotskyi (PhD student): *"Molecular scale understanding of competitive cation adsorption on swelling clay minerals"*. Start date: May 2021 (Funding: SNSF).

R. Yang (PhD student/UBern): *"Atomistic modelling of Fe uptake by cement phases"*. Start date: July 2024 (Funding SNSF-Sinergia).

Dr. G. Hu (postdoc): "*Data driven and physics-based TH-model for repository near-field*". Start date: February 2022 (Funding: HORIZON 2020, Eurad).

Tab. 1.1: National and international co-operations.

Co-operations
National Nagra* (Major financial contribution, various technical working groups) Swissnuclear* (Reactor safety, material aging)
Multinational NEA Thermodynamic Database Project EURATOM HORIZON2020 (Eurad) EURATOM HORIZON2020 (PREDIS) Mont Terri Projects* (diffusion retardation, clay-cement interaction)
Universities University of Bern*, Switzerland (mineralogy, petrography, water chemistry, C-14 AMS, circular economy & environmental remediation) EPFL, Switzerland (cement systems) Université de Bourgogne, Dijon, France (molecular modelling) ETH*, Zurich, Switzerland (GEMS; redox phenomena in cements) Hiroshima University, Japan (clay-cement interaction) University of Luxembourg* (porous media) Lanzhou University, School of Nuclear Engineering and Technology; Sino-French Institute of Nuclear Engineering and Technology; China Institute for Radiation Protection China (diffusion, retention) University of Leeds, UK (materials analysis) Luleå University of Technology (cements) Newcastle University, UK (clay mineral redox) University of Sheffield, UK (cements)
Research Centres CEA*, France (chemistry of near and far field) Eawag, Switzerland (Gas MS analytics) EMPA*, Switzerland (cements) IRE, HZDR*, Germany (XAS, TRLFS, atomistic modelling, reactive transport) INE, KIT*, Germany (near and far field; TRLFS) FZJ, Germany (sorption/diffusion of Ra, reactive transport, thermodynamics of solid solutions) SCK/CEN, Belgium (clay and cement systems) UFZ*, Germany (reactive transport, clay systems)
Industrial Partners GlaxoSmithKline* Nanocem Congineer Cosylab

**formal co-operation agreements*

Dr. A. Mokos (postdoc): *"Boiling crisis in nuclear reactor"* and "*Microstructural changes in cementitious materials*". Start date: March 2021 (Funding: Swissnuclear, EURAD-MAGIC).

Dr. A. Rajyaguru (postdoc): *"In situ chemical tomography and modelling of reactive transport processes in porous Media".* Start date: August 2021 (Funding: PSI-Cross).

Dr. D. Wang (postdoc): *"Atomic-scale understanding of redox behaviors of Fe-doped hydrotalcites in Mg-cements".* Start date: July 2023 (Funding: PSI-Fellow, EU).

Dr. X. Wei (visiting postdoc): *"Co-migration of clay colloids and radionuclides"*. Duration: September 2022 - August 2023 (Funding: Sino-Swiss-NNSFC exchange program).

Several PhD projects have successfully been completed in 2024:

P. Luraschi (PhD student): *Evolution and transport properties of cement clay interfaces*. Defence date: June 24th, 2024, (Funding: Nagra).

M. Mahrous (PhD student): *"Resolving dissolution-precipitation processes in porous media: Pore-scale Lattice Boltzmann modelling combined with synchrotron-based X-ray characterisation"*. Defence date January 29th , 2024 (Funding: SNSF).

Y. Qian (PhD student): *"Adsorption of redox sensitive radionuclides on Fe-bearing clay minerals"*. Defence date January 2nd, 2024 (Funding: HORIZON 2020, Eurad).

P. Ingold (PhD student/UBern): *"Pollutant dynamics of bottom ash landfills".* Defence date January 2nd, 2024 (Funding: Industry).

The organisational chart of LES comprises four research groups located at PSI (Fig. 1.1). A fifth research group is located at the Institute of Geological Sciences (IfG) at the University of Bern. The mineralogy group at IfG is provides complementary expertise in the field of mineral dissolution kinetics, structural studies of highly porous materials, X-ray diffraction-based structure refinement, and the geochemistry of conventional waste disposal. In particular, the mineralogy group hosts the Competence Centre for Secondary Raw Materials, conducting applied research in the field of environmental geochemistry and secondary raw materials.

The LES annual report 2024 is organised in six thematic research projects addressing specific aspects of repository geochemistry and radionuclide transport:

Chapter 2: Geochemical evolution of repository systems

Chapter 3: Retention and transport in clay systems

Chapter 4: Cement science and engineering

Chapter 5: Thermodynamic models and databases

Chapter 6: Landfills geochemistry and secondary raw materials

Chapter 7: Fundamental aspects of mineral reactivity and structural transformations

The following section provides an overview of LES activities contributing to the Sectoral Plan for Deep Geological Disposal, repository near and far field, reactivity of barrier systems and code benchmarking.

1.3 Sectoral plan for deep geological disposal

The safety assessment for the general licence application relies on site-specific state-of-the-art sorption (SDBs) and diffusion (DDBs) databases tailored to relevant radionuclides and the specific geological barriers, including the Opalinus Clay, confining units and bentonite buffer in the near field. Distribution coefficients (R_d values) for radionuclides were computed based on the clay mineralogy (illite, smectite, and illite/smectite mixed layers) and site-specific porewater chemistry. This was achieved in a single, consistent, fully coupled thermodynamic equilibrium calculation that included models for sorption on illite and montmorillonite, aqueous speciation, and solubility-limiting solid phases. For radionuclides with established sorption models, R_d values were derived for site-specific conditions, with 95% confidence intervals reflecting parameter uncertainties. Considering mineralogical data across the drilling intervals, high-resolution continuous profiles of sorption and diffusion properties along borehole or stratigraphic columns were provided.

The diffusion data for dose-relevant radionuclides are predicted using a generic model considering electrostatic effects on diffusion of ions in charged porous media. Such effects are described using the so-called «Mean-Potential Donnan Layer» (MPDL) approach to quantify the equilibrium distribution of charged species between the bulk porewater and the Donnan phase (a defined volume of charged solution near the charged rock surfaces). The empirical geometrical relationships and the MPDL approach are implemented in the so-called ClaySorDif model, which is a further development of the in-house ClaySor sorption model. The model calibration relies on an extensive series of diffusion measurements on rock samples obtained from Nagra's deep drilling campaign in Northern Switzerland.

The modelling methodology, developed by LES for the sorption and diffusion database formulation, has been extensively validated tested and improved based on laboratory measurements and sophisticated geochemical modelling tools. The underlying mathematical model and software allow characterisation of model uncertainties and model-based sensitivity studies for evaluation of sorption and diffusion parameters beyond the reference scenarios. The methodological framework represents the most sophisticated and accurate approach available in sorption and diffusion database development for safety assessment. Using the models for sorption and diffusion, together with mineralogical data from the drilling campaign, high-resolution continuous profiles of sorption and diffusion properties along the borehole mineralogical profiles have been generated. These profiles were used by Nagra in radionuclide transport models, upscaling, and for statistical approaches to provide reference, upper and lower bounding values of stratigraphic units identified in the models of the geological underground (see sections 5.2 and 5.3).

Extracted drill cores provide a unique opportunity for in depth characterisation of underground rocks with respect to their chemical mineralogical and hydraulic properties. Such data are obtained in laboratory tests which are expensive and time consuming. To support and accelerate the data processing, a Machine Learning based framework was developed for the analysis of drill cores and extraction of mineralogical information from the drill core images. The developed model has been shown to provide accuracy competitive with the most advanced regression models such as the MultiMin tool (see section 2.5).

The drilling campaign and analysis of the cores provided detailed information about the petrophysical variation in rock properties at the drilling locations in the underground. The key challenge lies in deriving up-scaled (i.e. effective) transport or mechanical parameters for a simplified geological model of the underground. Specifically, the rock models need to account for the spatial scale and spatial variation in the desired material properties of the rocks. A geostatistical workflow was developed to estimate the effect of heterogeneities in the Opalinus Clay formation on the transport of tracers through the host rocks, and corresponding dose curves. The workflow takes into account lithostratigraphic units (as rock facies) and mineralogical data derived from the analysis of drill cores (see section 2.2).

Profiles of a natural tracer (e.g., ^{2}H, ^{18}O, ^{37}Cl) across low-permeability formations represent a natural analogue for the system considered for deep geological waste disposal. The evolution of the profiles was modelled with separate 1-D approaches for each borehole. Overall, reasonable matches with the data could be obtained by using the measured (or interpolated) diffusion coefficients considering pure

diffusion, and assuming changes in the aquifers confining the Opalinus clay formation (see section 2.3).

Anhydrite-rich rocks are present in the lithological profiles of potential siting regions. The diffusive properties of these rocks are needed for interpretation of natural isotope profiles obtained in the framework of the site exploration campaign. A series of diffusion measurements with the anhydrite samples from different drill cores of the siting regions were conducted under elevated temperature conditions (50 °C, the expected in situ temperature). The obtained data indicate anion exclusion effects, whereas no sorption of $^{22}Na^{+}$ tracer was observed. This unique dataset thus provides a basis for the interpretation of natural tracer profiles and the radionuclide transport in the repository far field (see section 3.4).

1.4 Repository near field

1.4.1 Repository chemistry and thermodynamic databases

Thermodynamic data are the basis for geochemical modelling of repository *in situ* conditions, for pore waters, radionuclide solubility, sorption, and transport used in the safety assessments. The latest update of the PSI/Nagra chemical thermodynamic database was released in 2023. The database was used to update the solubility limits calculations, sorption, diffusion, pore water models and host rock mineralogy for repository performance assessment. The thermodynamic database and the integral modelling tools are further extended via participation in an internally consistent thermodynamic database Thereda, that focuses on the solubility of radionuclides and other radioactive waste disposal relevant processes in highly saline systems. Both databases share the core datasets of standard state thermodynamic properties for elements and species related to low solubility solids. A Pitzer model for Al-Si speciation was developed to extend its applicability to model cement materials in saline systems (see section 5.6).

Thanks to the support of the Open Research Data Program of the ETH Board, a workflow for curating and importing thermodynamic data in a standardised format, ensuring they are accessible and traceable to their original bibliographic sources, has been implemented within the THRACE project (see section 5.5).

1.4.2 Clay systems

Sorption and diffusion properties of the host rocks are among the most important pillars for the long-term safety of deep geological repository. Experimental quantifications of these parameters are time consuming and expensive. Considerable effort is taken to assess these parameters using a model-based approach. To account for the local geochemical and mineralogical variations in the host rock geochemistry, the site-specific porewater chemistry of Opalinus Clay was modelled and physico-chemical data of host rocks were derived the for the three study areas, ZNO, NL, and JO. For the sake of comparison, several well-established methods for the determination of the Cation Exchange Capacity CEC (e.g., Ni-CEC, Cs-CEC) were benchmarked. Using the mineralogical and physico-chemical data, the modelled porewater chemistries for the three regions agree well with the data derived from laboratory experiments, including squeezing and advective displacement methods. The developed modelling approach is generic and applicable to a broad range of argillaceous rocks with significant clay content, and should be considered as a reference methodology for deriving the host rock parameters for the safety assessment models (see section 3.2.1).

To support the further development of the sorption database for the safety assessment, sorption isotherms of Cs(I), Ni(II), Eu(III), Th(IV), and U(VI) were measured on representative drill core samples from Bözberg-1-1 in JO, Bülach-1-1 in NL, and Trüllikon-1-1 in ZNO. These data were further used to evaluate the predictive capability of the newly developed sorption model ClaySor for blind predictions of radionuclide distribution coefficients. This model integrates the generalised Cs sorption (GCS) model and the 2-site protolysis non-electrostatic surface complexation and cation exchange (2SPNE SC/CE) model, and has been parametrised consistently with the PSI/Nagra thermodynamic database (TDB 2020, see section 3.2.2).

Further collaboration in the Soreda project is aimed to develop a sorption database of radionuclides, relevant for the safety case of a deep geological repository, taking into account the minerals of argillaceous host rocks and buffer materials, such as clay minerals, quartz, carbonates and iron-bearing minerals. The most important and distinctive feature of the database is the physicochemical feasibility of its constituent sorption models due to the consideration of spectroscopically confirmed surface complexes. A careful review of potentiometric titration data available in literature revealed strong correlation between sorption model parameters and protolysis constants, which are used together in sorption modelling on montmorillonite, illite and kaolinite. To improve the sorption model and to evaluate the uncertainties of the model parameters, the protolysis constants were re-fitted to the existing potentiometric titration data using the GEMSFITS package. The updated protolysis constants were used to refit the surface complexation constants, which were adjusted in response to the changes in protolysis

constants. In some cases, this resulted in reduced uncertainty in the surface complexation constants (see section 5.4).

Diffusion parallel to the bedding occurs faster than in the perpendicular direction. To evaluate the diffusion anisotropy of selected rock specimens from the recent deep drilling campaign, diffusion measurement on twin samples we conducted parallel and perpendicular to the bedding using the same tracers. Further, the samples were selected from different depths to evaluate possible changes in anisotropy as a function of compaction. All samples originate from the clay-rich members of the Opalinus Clay. The diffusion parameters obtained for HTO are in very good quantitative agreement with the expected trends. In contrast, the derived diffusion coefficients for $^{36}Cl^-$ tracers show significant scatter for some values of diffusivity and porosity. The likely reasons for the uncertainties could be related to the relaxation of stresses in the confined samples and are being investigated further (see section 3.4).

Several studies of radionuclide retention and transport in clays and argillaceous materials were finalised within the framework of the EURAD programme WP FUTURE. The selenium isotope ^{79}Se, with a half-life of more than 100'000 years, belongs to the group of safety relevant radionuclides. Under oxic conditions, Se is predominantly present as selenate (SeO_4^{2-}) and selenite (SeO_3^{2-}), which are both soluble and highly mobile, and can become protonated at lower pH values. Under reducing conditions, both oxyanions are reduced to elemental selenium in amorphous (red) and grey crystalline (grey) forms. Building on previous studies demonstrating that Fe(II)-bearing minerals are capable of reducing selenate and selenite to elemental Se and even selenides, the ability of structural Fe in clay minerals to reduce selenite species was investigated. The Fe in two montmorillonites (SWy-2, STx-1) and one nontronite (NAu-2) was reduced to different extents and the combined sorption and reduction of selenite monitored over time, using both aqueous phase measurements of selenite and XAS-characterization of the solid phase-associated Se. Kinetically controlled reduction of Se(0) was confirmed by EXAFS measurements. The extent of reaction and Se(0) speciation were found to depend on Fe content and its reduction state (see section 3.5.1).

Combined experimental and theoretical studies of $Zn^{2+}/Ni^{2+}/Lu^{3+}$ uptake on synthetic saponite were conducted to improve the molecular scale understanding of cation adsorption on trioctahedral clay minerals. The innovative combination of ab initio molecular simulations and XAS spectroscopy provides structural insight into the mechanism of the surface complexation process and the thermodynamic affinity of the surface complexes. One of the central aspects of the study deals with the question of whether the models developed for di-octahedral clay minerals are transferable to trioctahedral phyllosilicates (see section 3.3).

Due to the large surface area, high reactivity and presence of redox active iron in the structure, clay minerals can take an active role in surface mediated redox reaction or acting as catalysts in complex chemical synthesis. Several proof-of-concept studies, conducted in collaboration with colleagues from Newcastle University, UK, have demonstrated that clay minerals can be applied for water and wastewater treatment and remediation in novel, mineral-based advanced oxidation processes targeting micropollutants and other emerging contaminants (see section 3.5.2 and 3.5.3).

1.4.3 Cement systems

Corrosion of activated steel is a potentially important ^{14}C release mechanism in a repository. The ^{14}C mobility and retention depend strongly on the chemical properties of its carrier. Compound-specific release of ^{14}C species due to corrosion of activated steel under anoxic conditions in aged cement pore water (pH=12.5) has been investigated in the LOMIR experiment supported by a consortium of waste management organisations. Nearly 8 years of observations of ^{14}C containing species in gas phase have indicated a long term corrosion rate of 1 nm/a, also supported by H_2 release measurements, which is within the range of corrosion rates expected for steel under anoxic alkaline conditions. The ^{14}C that is released from irradiated steel disposed under reducing conditions in a L/ILW DGR is expected to be released as $^{14}CH_4$ into the gas phase during the course of corrosion (see section 4.2).

In the framework of the EURAD project MAGIC, mechanical and structural degradation of cement under ingress of Opalinus clay pore water has been investigated. The pore-scale microstructure evolution was modelled using a 3D multi-component lattice Boltzmann (LB) approach. The chemical processes considered in the model are the kinetic dissolution of portlandite and recrystallisation of the calcium silicate hydrates. The simulated geometries were used to evaluate the mechanical properties of degrading cement paste and upscale the results for application in continuum scale codes (see section 2.9).

Sorption of radionuclides can be strongly affected by the presence of compexing ligands. Ethylenediaminetetraacetic acid (EDTA) is considered to be the one of the most important complexing ligands for cationic radionuclides in a cement-based repository. In particular, EDTA may form strong complexes with (III)- and (IV)-valent actinides. To evaluate the effect

of EDTA on sorption of actinides in a cement matrix, laboratory investigations of Th sorption on oxide surfaces have been conducted in an alkaline environment. The preliminary results suggest that the quaternary Ca-An(IV)-(OH)-EDTA complexes do not lead to reduction of sorption of An(IV) due to the anionic nature of such complexes and the positive surface charge of minerals in alkaline environments at significant Ca^{2+} concentration. A follow-up study has been initiated to confirm the results in the C-S-H system (see section 4.3).

Recently, a number of projects have been launched at LES focusing on innovative non-Portland cements, seeking materials that will serve as a high-quality and reliable basis for durable engineering structures and contribute to the global decarbonisation of industrial processes. Working in collaboration with the University of Sheffield (UK) and Sumitomo Mitsui Construction Co. (Japan), the mechanisms controlling the long-term strength development and nano- and microstructural evolution in some high-performance concretes have been revealed. These cements were produced and formulated without Portland cement, and at exceptionally low water content, gaining their initial fluidity and setting from an innovative combination of chemical activation and pH-triggered release of superplasticisers (see section 4.6).

Magnesium-rich cements have been considered as potential substitutes for conventional Ca-rich cements, intending to reduce the CO_2 emissions due to clinker production. However, thermodynamic stability of cement phases in the M-S-H system is poorly known. To fill the existing knowledge gaps several PhD projects in collaboration with Empa are focusing on the structural investigation of M-S-H and related phases, and their thermodynamic stability (see section 4.5).

Within the SCENE (Swiss Center of Excellence for Net zero Emissions) project, supported by a joint initiative in the ETH Domain, a novel approach is developed for AI-assisted discovery of cementitious blends, minimising the environmental impact while maintaining material performance. The optimisation yields a series of optimal cement recipes on a Pareto front, showcasing optimal tradeoffs between bulk modulus (ranging from 21 to 28 GPa) and CO_2 emissions (0.48 to 0.57 kg CO_2 per kg of cement paste) for the considered constraints. This methodology demonstrates significant potential to reduce CO_2 emissions while maintaining or even enhancing the mechanical properties of cementitious materials used in construction (see section 4.7)

1.4.4 Interfacial processes

Dissolution and precipitation reactions lead to the changes in porosity and connectivity in porous media, and thus effect their transport properties. These processes are best described by 2D/3D reactive transport simulations at a pore scale. Conventional reactive transport simulations for such systems are prohibitively expensive due to small integration timestep and complexity of geochemical calculations. An innovative algorithm for adaptive time-stepping has been developed and applied for the pore scale simulation of cement-clay interactions. Additional computational efficiency was obtained by replacing the geochemical code with a computationally efficient surrogate model (see section 2.4).

Corrosion of steel under the reducing conditions typical for underground repository leads to formation of nanoparticulate magnetite (Fe_3O_4). Such magnetite nanoparticles can provide an important contribution to redox-mediated uptake of redox sensitive radionuclides in the repository near field. Particularly important for such processes is information on redox active iron of the mineral surface. So, surface structure and stability of magnetite nanoparticles were investigated by ab initio simulations. The modelling reveals stability fields for various surface speciation and the surface charge as a function of pH and Eh conditions. In particular, nanoparticles show stronger interaction with water compared to macroscopic surfaces. The obtained surface stability phase diagrams are the basis for further investigations of radionuclide absorption on the magnetite surface (see section 7.3).

1.5 Model development and code benchmarking, thermodynamic databases, and Digital Twins

In the framework of the PSI-funded CROSS project *"In situ 4D micro X-ray chemical imaging and a digital twin of miniaturized counter-diffusion experiments: co-precipitation of metals with carbonates in porous media"*, digital twins of laboratory experiments with increased realism are developed to accompany and augment the experimental observations as well as to measure specific quantities of interest via inverse modelling. The model was extended to integrate the major processes occurring in the counter-diffusion calcium carbonate precipitation experiments. The classical nucleation theory, a model for predicting the formation of amorphous calcium carbonate phase (ACC), and a neural network surrogate model for the chemical speciation have been implemented in the parallel GPU lattice Boltzmann code. Initial scoping calculations have been set up to predict the nucleation positions of calcium carbonate polymorphs, and provide fair agreement with experimental results. (see section 2.7).

Within the EURAD WP MODATS the development of the digital twin of the Full-Scale Experiment (FE) at Mont Terri has been finalized. A simulation workflow includes a physics based model and a data-driven model allowing improvement of the predictions of the temperature evolution of the experiment. At the same time it was possible to conduct a sensitivity analysis on repository-relevant parameters such as the thermal conductivity of the involved materials. Such considerations can be used in the repository design optimization (see section 2.10).

Within the PREDIS project, a digital twin of waste packages has been developed based on the mixing tank approach and GEMS calculations. To accelerate the subsequent sensitivity analysis, simulations rely on a machine learning based model for geochemical systems (see section 2.11).

The application of artificial intelligence (AI) and machine learning (ML) in geochemical and reactive transport simulations is rapidly advancing, hand in hand with the improvements in numerical algorithms and computational hardware. A dedicated benchmarking effort has been setup within the EURAD WP DONUT "Geochemistry and machine learning: methods and benchmarking", to test, analyse, and standardise the most important aspects of the ML techniques, and to reveal the benefits and limitations of the method, with a specific focus on geochemical systems relevant to radioactive waste management. The results of the benchmarking conducted provide confidence in the accuracy and computational performance of ML models in reactive transport simulations. The future applications of ML models might be boosted by the development of automated workflows and user-friendly interfaces for model setup, training and validation (see section 2.6).

In the project "Boiling flow simulation in fuel-assembly affected by CRUD" (BoilCRUD) under the Swissnuclear funding agency and in collaboration with the Laboratory for Scientific Computing and Modelling at PSI (LSM-PSI), a new thermal LB model has been implemented into the existing multi-GPU 3D LB code, suitable for high performance computing simulations. The new model uses the Multi-Relaxation-Time (MRT) collision scheme for mass transport, and a second order central finite difference scheme for the energy equation. The model was used to simulate the nucleation and growth of bubbles in algorithmically generated porous domains representing CRUD deposited on the cladding of the nuclear fuel. The simulations provide the average nucleation site density (NSD), which is a key parameter in macroscopic simulation of boiling in nuclear reactor simulations (see section 2.8).

1.6 Environmental impact of conventional waste disposal, secondary raw material recycling and fundamental aspects of mineral reactivity

In collaboration with the Wyss Academy for Nature, an inventory of material qualities of various mineral wastes in Switzerland was carried out. Over 220 samples of different material categories were sampled and analysed for their chemical and mineralogical composition. The partial replacement of primary resources with secondary raw materials in cement production represents a major environmental benefit due to an improved CO_2 balance. One approach can rely on decarbonisation of limestone in clinker production. Another can reduce the proportion of clinker in cement by increasing the use of supplementary cementitious materials (SCMs) (see section 6.2-6.4).

The Swiss waste disposal ordinance defines an aftercare period of 50 years for the monitoring of landfill sites for bottom ash. A large body of field characterisation and monitoring data has been collected and used to develop hydro-geochemical model of landfill site evolution. The model takes into account chemical equilibrium between domains with distinct hydrodynamic transport properties, and semi-quantitatively explains the chemical and hydraulic behaviour of landfill discharge systems. (see section 6.5).

Conventionally, column leaching tests are used to evaluate the hydraulic properties of materials disposed in landfills, their reactivity, and metal concentrations in the leachate. These tests are time-consuming and need to run over several weeks to months to give a glimpse into processes taking place over several decades in the natural environment. To obtain an estimate for long term bottom ash leaching behaviour, a machine learning approach has been applied to the data delivered by the early-stage measurements. For selected elements, this study could successfully demonstrate the potential of machine learning to streamline environmental monitoring of long-term landfill management (see section 6.6).

1.7 Fundamental aspect of structural transformations in minerals

Zeolites are a class of porous crystalline materials which are exploited in a widespread range of technological and industrial applications. In the last decades, particular attention was paid to their gas-sorption and separation capacity, with a special focus on CO_2 removal. Zeolites are particularly competitive because of their tunable structure, faster adsorption kinetics, high selectivity for CO_2, and extended thermal stability. In collaboration with colleagues from

University of Urbino Carlo Bo, Italy, the structural transformation and reactivity of temperature-activated CHA zeolites has been investigated. The structural characterisation reveals that despite their low Si content, CHA zeolites do not lose crystallinity up to 350 °C and can be a good candidate for selective gas-sorption (see section 7.2).

Xonotlite is an industrially important calcium silicate mineral, which is considered as a possible alternative to more common calcium silicate hydrates. The solubility of xonotlite remains poorly constrained experimentally. In a collaborative PhD project with EMPA, the thermodynamic properties of xonotlite were investigated by combining wet chemistry studies and ab initio thermodynamic modelling. Based on ab initio simulations, the structure of the most stable polymorphs was revealed and used for the Rietveld refinement of the synthesised samples. The study explains the origin of discrepancies between the solubility data reported for natural and synthetic xonotlite. The thermodynamic data obtained provide reliable predictions of xonotlite performance in construction materials, and reactive transport modelling of cement evolution at elevated temperatures (see section 7.4).

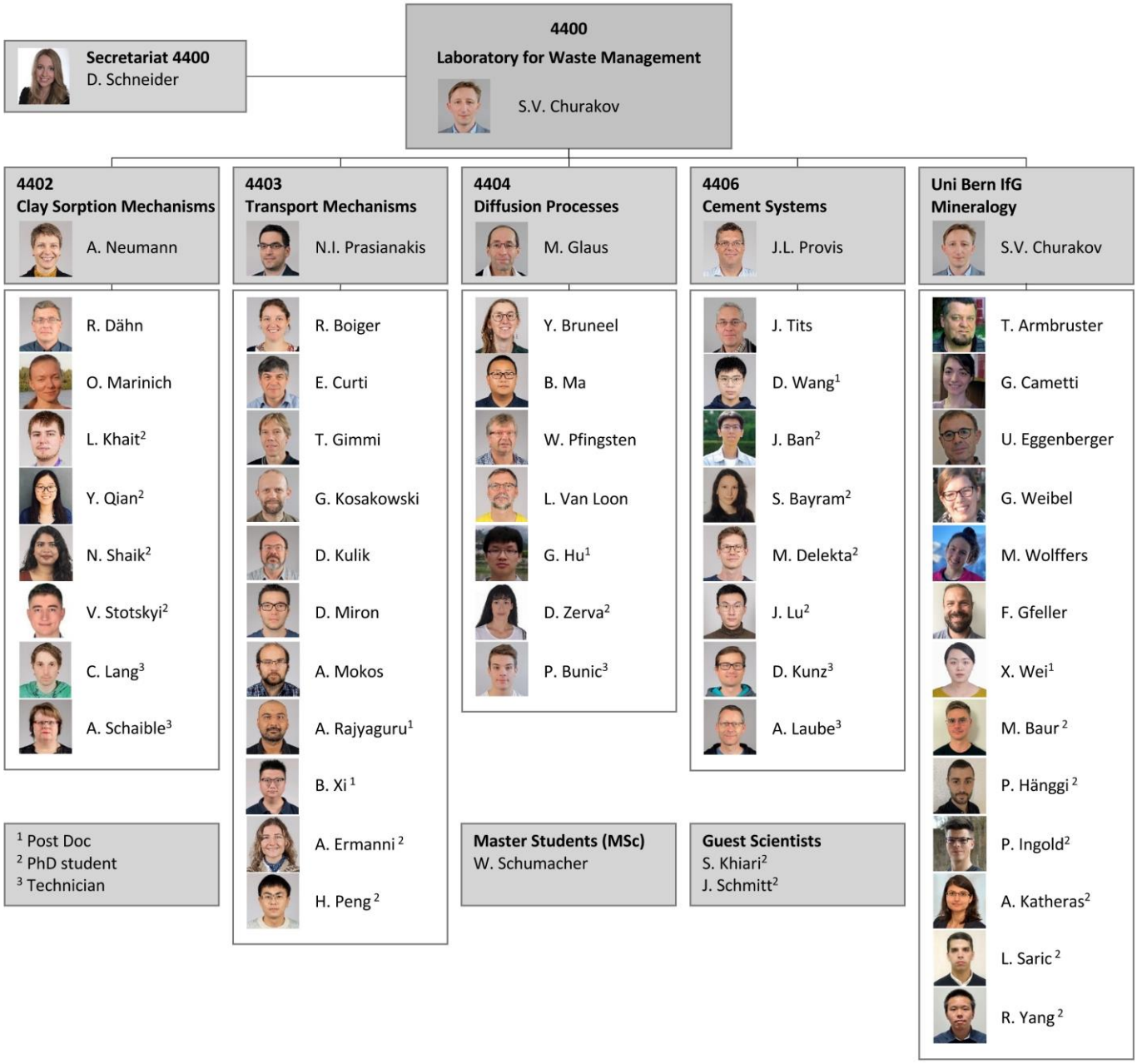

Fig. 1.1: Organisational chart of LES.

2 GEOCHEMICAL EVOLUTION OF REPOSITORY SYSTEMS

Prasianakis N.I., Churakov S.V., Gimmi T., Kosakowski G., Boiger R., Miron G.D., Mokos A., Xi B. (postdoc), Rajyaguru A. (postdoc), Peng H. (PhD student)

2.1 Introduction

Cross scale thermal-hydraulic-mechanics-chemistry (THMC) models and simulation tools are essential for describing the long-term evolution of multi-barrier repository systems and geotechnical engineering. Such models provide the basis for the safety assessment and optimisation of repository designs. The next major milestone following the submission of the General License Application (RGB) in November 2024, will be the construction licence. Whereas the general licence operates to a large extent with generic concepts of repository design and define limiting dimensions of the repository system, the construction licence must contain specific description of repository system including exact dimensions and the material specifications. These will come as result of multiparameter optimisation in which THMC modelling is expected to play a central role.

The research activities described in this chapter cover three main topics relevant to the repository engineered barrier systems: 1) numerical modelling of the formation scale transport by accounting for the heterogeneity and the anisotropy of the diffusivity; 2) fundamental understanding of the reactive transport processes within porous materials through multiscale modelling and upscaling techniques; 3) the benchmarking of coupled codes as well as the development and coupling of state-of-the-art reactive transport codes with thermodynamic modelling tools and databases.

With respect to the pore-scale reactive transport simulations a combination of machine learning tools and of a smart adaptive time-stepping algorithm resulted in an acceleration of several orders of magnitude for a specific type of problems, related to cement-clay interactions. The methodology allows to simulate the microstructural evolution of materials at diffusive conditions over long time periods.

LES has been strongly involved in several EURAD-I Work Packages (WP) and plays an important role in the implementation of newly started EURAD-2 project. Within the EURAD-I WP DONUT several multiscale codes and their couplings have been developed. An international benchmarking exercise was set up to test a variety of ML techniques relevant to geochemical and reactive transport simulations in the framework of radioactive waste disposal, aiming at providing basic guidelines about the benefits and limitations of using ML techniques (Prasianakis et al., 2025). As the main outcome, a concise framework with guidelines for producing training datasets as well as for measuring the accuracy of the ML methods has been developed. Within the EURAD-I WP MAGIC the chemo-mechanical aging of cementitious materials was investigated by combining reactive transport simulation at the pore-scale level, including dissolution and precipitation reactions. The predicted morphology of cement paste was used subsequently by the partners of the project to estimate the elastic properties of the aging cement paste.

The PSI-CROSS project "*In situ* 4D micro-X-ray chemical imaging and a digital twin of miniaturized counter-diffusion experiments: co-precipitation of metals with carbonates in porous media" has continued in 2024. The overarching research goal of the project is to elucidate the role of trace metals (Ni, Zn, Pb) in polymorph stabilisation and growth kinetics of calcium carbonate in porous media (silica gel, mineral powders). The experimental characterisation has been completed in 2024. The numerical models have been extended to include the nucleation and precipitation of carbonate polymorphs as well as the formation of the amorphous calcium carbonate phase (ACC).

Artificial intelligence (AI) is implemented to accelerate the processing of drill core data from Nagra drilling campaigns and to support the upscaling of core data to the field scale. A numerical framework was developed and tested allowing to predict the mineral content and effective diffusion parameters directly from core images.

Several ongoing projects on multiscale multiphysics computational fluid dynamics (CFD) extend the advanced modelling tools actively developed in LES. Two new Swissnuclear projects have been initiated in 2024. The project "Resolving CRUD growth mechanisms" (RESCUE), which is conducted in collaboration with the Laboratory for Nuclear Materials (LNM) and the Hot Laboratory (AHL) at PSI, will combine numerical simulations and experimental studies to investigate and understand the conditions which result in CRUD formation. The project "Boiling flow in realistic fuel assemblies: modelling and validation of advanced CFD codes" (BRAVA), is in collaboration with the Laboratory for Scientific Computing and Modelling (LSM) at PSI. The project aims at using machine learning and advanced numerical models to simulate the boiling flow within fuel assemblies.

2.2 Modelling formation scale radionuclide transport in Opalinus Clay taking into account heterogeneity and anisotropy of clay rocks

Exploitation of the geological underground, for example, for oil and gas exploration, or for geological repositories, relies at the development of reservoir models. In this project, the term reservoir model refers to the stratigraphic representation of the geological underground with assigned physical and chemical properties of the rocks in 2D and 3D space (e.g. Pyrcz et al., 2015). These models are used for simulating elemental transport or gas migration. In a generic workflow, a conceptual geological model is established first, then rock (facies) models are built, and finally are populated with rock materials (i.e. rock properties). The challenge lies in deriving up-scaled (i.e. effective) transport or mechanical parameters for a simplified geological model of the underground. Specifically, the rock models need to account for the spatial scale and spatial variation in the desired material properties of the rocks.

In Switzerland the Opalinus Clay (OPA) is foreseen as the host rock for the Swiss deep geological repositories for radioactive waste. The OPA resembles a stratified low permeability porous medium. The correlation length of layers/units in the vertical direction (perpendicular to bedding) is relatively simple to estimate from borehole/core analysis. Correlation in the horizontal direction (parallel to bedding) is uncertain, but by comparison of borehole data and based on knowledge about formation/sedimentation it can be estimated that correlation length parallel to bedding should be high, possibly even up to km scale. In previous experiments it was observed that the diffusion coefficient in Opalinus Clay is by a factor of 4-6 higher in the direction parallel to the bedding compared to the direction perpendicular to bedding (Van Loon et al., 2004). The corresponding through-diffusion measurements were conducted at lab-sample scale (cm – dm). For the performance/safety assessment of radioactive waste repositories in Opalinus Clay the radionuclide transport in the vertical direction (perpendicular to bedding) is of major interest, while the effect of anisotropic diffusion is mostly ignored.

In this project we developed a geostatistical workflow to simulate the mineralogical heterogenieties in the Opalinus Clay formation at the siting region “Nördlich Lägern”. The workflow takes into account lithostratigraphic units (as rock facies) and data measured in boreholes, the so called “MultiMin” data included in Dossier III of the data reports for boreholes Bülach (Nagra, 2021), Stadel-2 (Nagra, 2022a) and Stadel-2 (Nagra, 2022b). The geostatistical workflow combines spatial cross-correlations between mineral amounts, specifically clays, silicates and carbonates, into a linear model of coregionalization (Marcotte, 2012). The linear model of coregionalization was used to drive unconditional and conditional Gaussian sequential co-simulations of clay, calcite, and silicates on 2D vertical cross-sections of Opalinus Clay formation imported from a transport simulator.

For the solution of the diffusive transport equation utilizing an anisotropic diffusion tensor, the Discontinuous Galerkin (DG) symmetric interior weighted penalty (SWIP) method was implemented in the DOLFINx software (Baratta et al., 2023). The DG-SWIP method is well suited for calculation of diffusion in mildly heterogeneous anisotropic media (Ern et al., 2008).

For the setup of transport models, the simulated mineralogical composition was used to estimate the local effective diffusion coefficients with help of the diffusion to clay content correlation described by Van Loon et al. (2023). The generated 2D anisotropic diffusivity fields, with a resolution of about 8 triangles per 1 m^2, are the base for calculations of the diffusion of a conservative non-decaying tracer in a 55 m long (vertical z-direction) and 100 m wide (x-direction) vertical 2D cross section of Opalinus Clay formation (Fig. 2.1). Independent from the clearly layered (anisotropic) spatial structure of the diffusivity field in Fig. 2.1, a 5 times higher effective diffusion coefficient in the horizontal direction (parallel to layering) was used for the diffusion tensor. This anisotropy factor accounts for the sub-grid anisotropy of diffusion caused by microscopic arrangement of clay platelets.

The tracer is injected along the surface of a tunnel segment with radius of 1.9 m at the lower “left” corner of the cross section with a constant flux for 1000 years. In line with performance assessment models for radionuclide transport, the top boundary of the Opalinus Clay formation is assumed to be a zero-concentration boundary. The model setup further assumes that the repository consists of many very long parallel emplacement tunnels that are spaced 200 m apart. This allows treatment of the left and right model boundaries as zero-flux boundaries for symmetry reasons. Fluxes across the top Opalinus Clay boundary at z=55.0 m are modelled for up to 10^7 years.

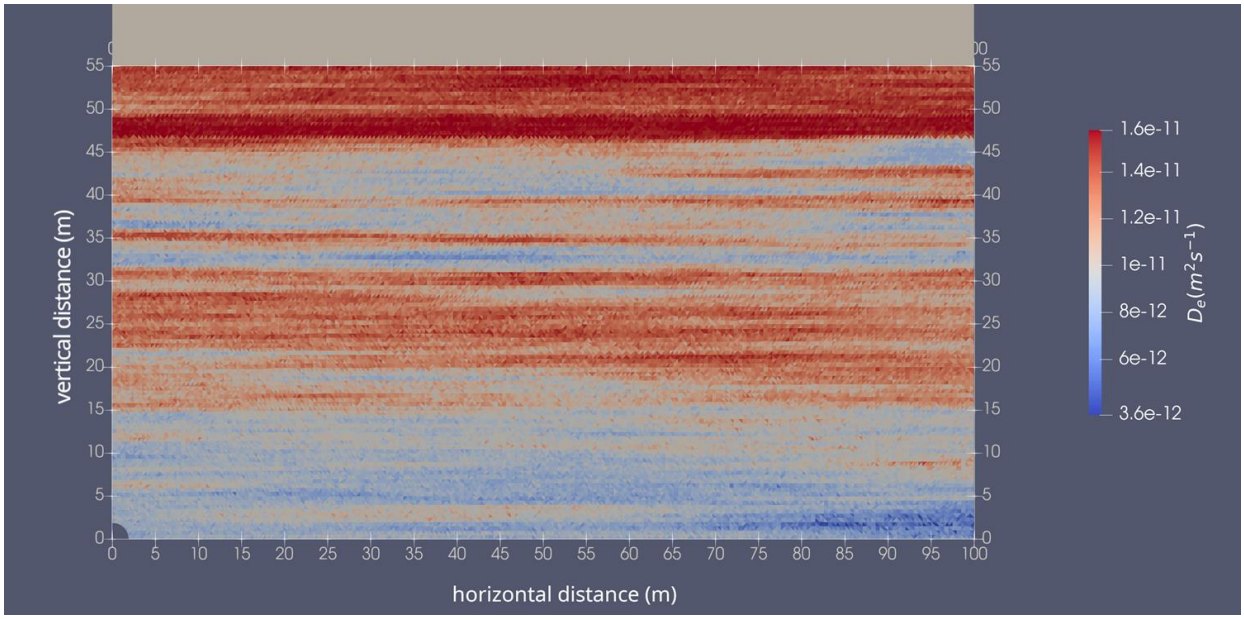

Fig. 2.1: Spatial distribution of effective diffusivity based on a simulation of clay content conditioned to the data from borehole Stadel-2 at horizontal distance of 50 m.

Fig. 2.2 shows an example of the spreading of the tracer with time. For up to about 10'000 years, the (sub-grid) anisotropic diffusivity dominates the spatial spreading of tracer. At later times the gradients near the upper boundary dominate the tracer flux. The heterogeneity of effective diffusivity from Fig. 2.1 is not reflected in the concentration fronts. A similar observation is done for the integral tracer flux across the top Opalinus Clay boundary. Fig. 2.3 (left) shows a comparison of the fluxes calculated from the heterogenous isotropic (without sub-scale anisotropy factor) calculation case, a "homogeneous" isotropic realization that uses the harmonic mean of the effective diffusion coefficient (in vertical direction) in the whole domain, and an 1D analytical solution using the harmonic mean of effective diffusion coefficient. The right part of Fig. 2.3 shows the same calculations using the anisotropy factor in the numerical models, and for comparison the same 1D analytical solution using the harmonic mean of effective diffusion coefficient.

The three flux curves in both simulations agree very well and show only minimal differences. The results suggest that the heterogeneity of the diffusivity field is not strong enough to significantly influence the tracer breakthrough and cause early breakthrough or anomalous long tailing. The anisotropy seems to have little effect, because vertical tracer fluxes are not strongly influenced by horizontal transport. Tracer fluxes are integrated along the upper boundary, which averages out any local variation in vertical fluxes. The good agreement between the different models in Fig. 2.3 is a strong indication that the simplified 1D models, typically used for performance assessment calculations, are well suited to calculate the integral fluxes for conservative tracers in the Opalinus Clay.

2.3 Natural tracer diffusive transport at the formation scale

A profile of a natural tracer (e.g., ^{2}H, ^{18}O, ^{37}Cl) across low-permeability formations represents a natural-analogue for the system considered for deep geological waste disposal. The profile developed over very long time scales and across the formations of interest. Data from eight new Nagra deep drillholes were gathered in the last years, and these data provide a powerful basis to determine main transport processes and to check parameters (e.g., diffusion coefficients, porosities) obtained at the lab scale. The profiles of each of the water tracers at the different boreholes have some similarities, notably similar values in the center. Their further evolution was then obviously triggered by changing boundary conditions in the embedding aquifers (Malm at the top, only in some boreholes Keuper in the lower part, and Muschelkalk at the bottom). The evolution of the profiles was modelled presently with separate 1-D approaches for each borehole. Overall, reasonable matches with the data could be obtained by using the measured (or interpolated) diffusion coefficients considering pure diffusion, and assuming changes of the boundary conditions in the Malm, the Keuper (if present) and the Muschelkalk at different times (Gimmi et al., 2024; Wersin et al., 2024).

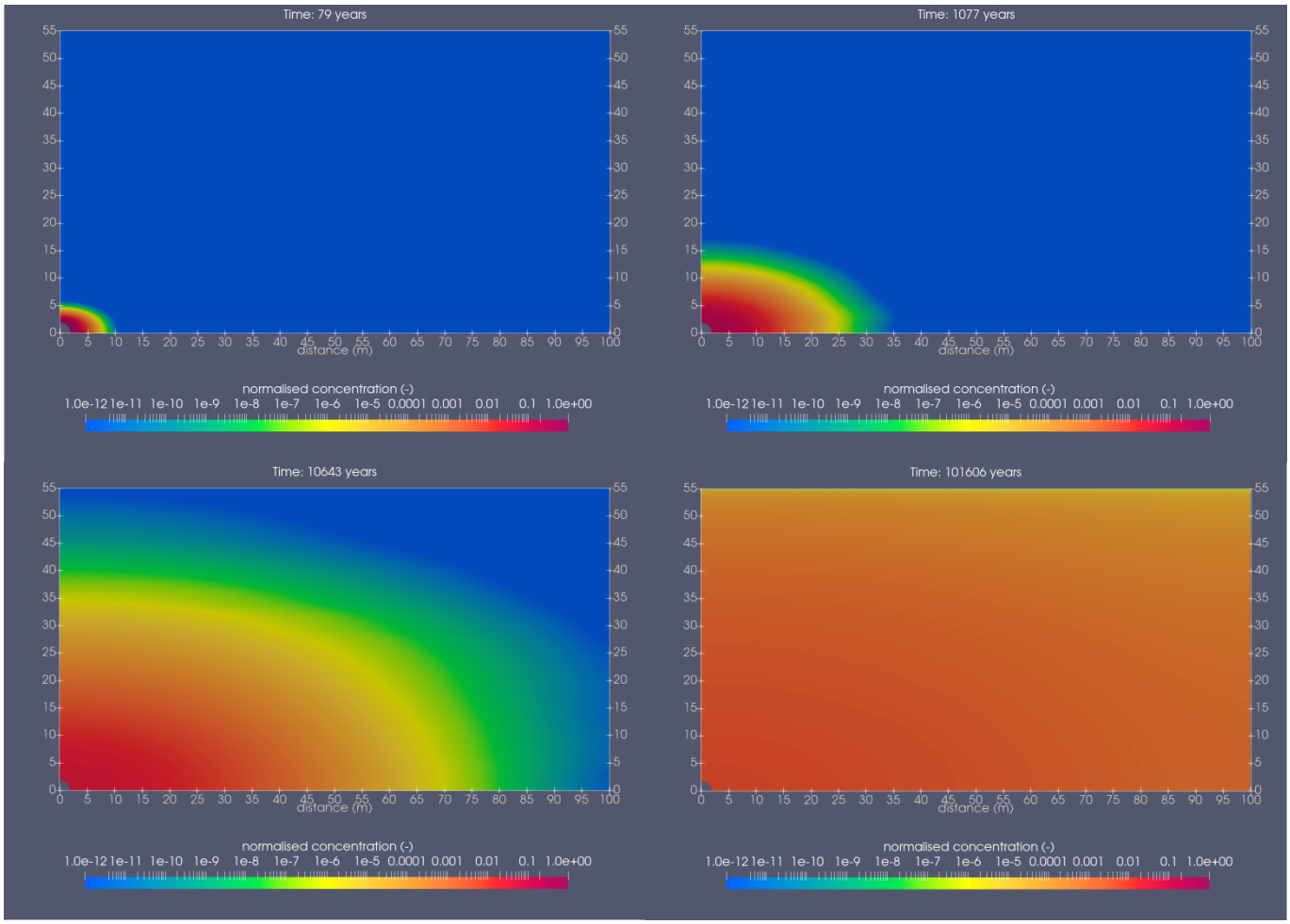

Fig. 2.2: Plot of normalised concentrations calculated in heterogeneous diffusivity field after 79, 1'077, 10'643 and 101'606 years. At the bottom left corner of the plots is the considered tunnel. Tunnels are assumed to be 200 m apart and the simulation is set up by considering the symmetry.

2.4 High performance reactive transport model for cement-claystone interface simulations

The chemical interaction at the cement-claystone interface plays an important role in the long term evolution of underground repositories for radioactive waste in argillaceous host rocks (Kosakowksi, 2013). Interactions between cementitious materials and the claystone are triggered from the geochemical gradient which exists between the materials and is manifested in the vicinity of their interface. Typically, the portlandite and calcium silicate hydrate (C-S-H) are leaching at the cement side of the interface resulting in a porosity increase, while at the claystone side precipitation of different solid phases, mainly C-S-H phases, is observed leading to porosity decrease. Of importance is to be able to predict the evolution of the diffusive mass fluxes as a function of the decrease in porosity. Reactive transport models (RTM) at the pore scale can support the understanding of the complex feedback mechanism between solute transport and chemical reactions occurring at this interface. However, such simulations are computationally very expensive for practical applications.

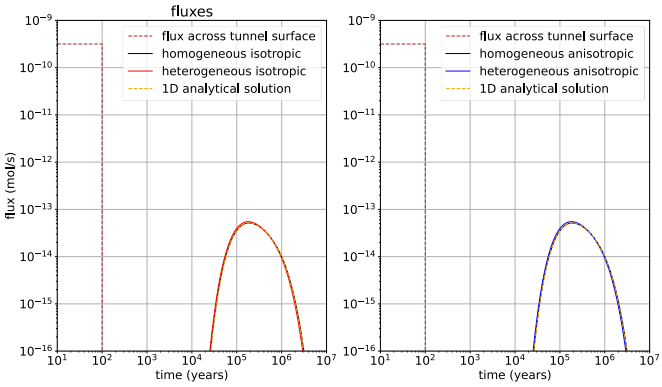

Fig. 2.3: Temporal evolution of integral tracer fluxes across the top of the Opalinus Clay versus time with 1D analytical solution for simulation cases with homogeneous diffusivity (left) and heterogeneous diffusivity (right).

A combination of machine learning techniques and a smart adaptive time-stepping algorithm allowed significant acceleration of the calculations. The first accelerator is a neural network based surrogate model that replaces the geochemical solver during the simulations (Prasianakis, 2020). It takes the aqueous concentrations of $Ca(OH)_2$ [aq] and SiO_2 [aq] as an input and relates it to the precipitation of the four C-S-H endmembers tobermorite-D, tobermorite-H, jennite-D and jennite-H as an output. The consideration of the quaternary C--S--H solid solution with four endmembers allows the tracing of the Ca/Si ratio and the computation of the gel porosity during the simulation (Kulik, 2011). This further accelerates the total simulation time by at least two orders of magnitude (>100 times). The second accelerator is a smart adaptive time-stepping algorithm. It takes advantage of the temporal multi-scale nature of the processes described in RTMs, namely the diffusion (very fast process), the precipitation reactions (fast process) and the solid growth which can fill-up one computational voxel (slow process). The algorithm monitors the solute flux and the precipitation rates during the simulation to detect temporal quasi steady-states while an acceptance criterion is also implemented (threshold values). After a positive detection, the algorithm dynamically adapts the time-step for the solid growth until the pore space is significantly altered to affect the transport properties of the media.

This new algorithm was benchmarked and tested on different geometries and boundary conditions. The overall acceleration by combining the aforementioned techniques resulted in acceleration factors of 5'000 to 900'000 depending on the chemical gradients, while maintaining errors of the resulting effective diffusivity below 2%, as shown in Fig. 2.4. Applying this algorithm, the simulations are able to address longer evolution time not accessible with conventional approaches in realistic time spans.

2.5 AI assisted drill-core image analysis

Underground exploration is routine in various industries, including mining, energy, and the safe disposal of radioactive waste. In Switzerland, Nagra's deep drilling campaign contributes to national efforts to identify suitable sites for geological disposal, generating a substantial amount of data, including drill core images. Extracted drill cores provide a unique opportunity for in depth characterization of underground rocks with respect to their chemical mineralogical and hydraulic properties. Such data are obtained by in laboratory tests which are expensive and time consuming.

The goal of the study published in (Boiger et al., 2024) was to extract valuable information such as mineral content directly from drill core images using AI and machine learning techniques, specifically convolutional neural networks. Initially, a limited dataset from the Trüllikon 1-1 borehole was available to develop proof-of-concept models for classifying the geological formations and predicting the mineral content. Given the limited size dataset for mineral content regression, a transfer learning approach was adopted, based on the knowledge gained from the training of the formation classification model. To further advance these methods the study was expanded to include a larger dataset comprising core images from the Trüllikon 1-1 borehole and two additional boreholes: Bözberg 1-1, Bözberg 2-1. All new images were processed using the standardized image preprocessing pipeline outlined in (Boiger et al., 2024) which ensured consistent color correction, crack detection and core segmentation.

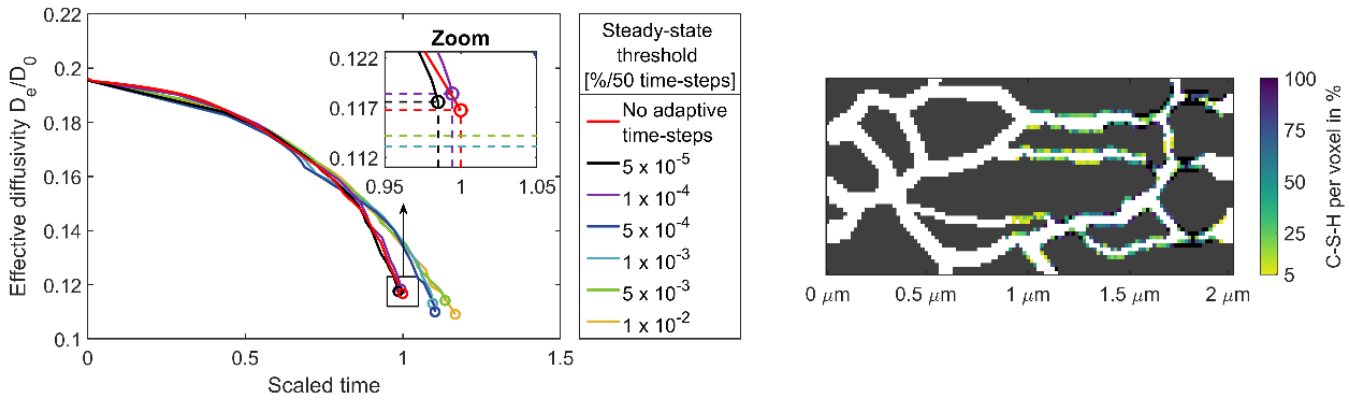

Fig. 2.4: Left: Time-evolution of the effective diffusivity for simulations with different steady-state thresholds compared to a simulation without the adaptive time-stepping algorithm (red). Steady-state thresholds of 10^{-4} % / 50 time-steps have a good accuracy which decreases with larger steady-state thresholds. Right: End of the simulation (clogged by C-S-H precipitates) with a steady-state threshold of 10^{-4} % / 50 time-steps.

Two transfer learning strategies were employed for model training: one using a pretrained ResNet50 architecture as the backbone and another utilizing the pretrained formation classification model. The results indicated in this case that the formation classification model provided only marginal improvements in performance, if any. In contrast, increasing the training dataset size and incorporating data from two boreholes significantly enhanced model performance. Models trained on data from both boreholes demonstrated the highest accuracy overall, as evidenced by the mean squared error metrics summarized in Tab. 2.1.

While the first results are promising, further improvements in model architecture and refinement of training methods are recommended. These enhancements could make the models more robust and reliable for subsequent applications, such as predicting petrophysical properties based on the outputs of the image regression.

2.6 Machine learning Benchmark within the EURAD-DONUT framework

The application of artificial intelligence (AI) and machine learning (ML) in geochemical and reactive transport simulations is rapidly advancing, hand in hand with the improvements in numerical algorithms and computational hardware technology. Within the EURAD community, ML techniques are being actively used to accelerate numerical simulations, to enhance multiscale and multiphysics couplings, and to efficiently conduct uncertainty quantification and sensitivity analysis. Several case studies have highlighted that ML-based approaches can achieve overall acceleration rates of one to three orders of magnitude without loss in accuracy. A dedicated benchmarking effort within the EURAD-I WP DONUT "Geochemistry and machine learning: methods and benchmarking", has been conducted to test, analyze and standardize the most important aspects of the ML techniques, and to provide an understanding of the benefits and limitations, with specific focus on geochemical systems relevant to the radioactive waste management (Prasianakis et al., 2025).

A systematic approach has been applied to generate high-quality training datasets and to evaluate ML techniques in two geochemical scenarios relevant to cement chemistry and uranium sorption in clays. The performance, accuracy, and computational efficiency of various ML models, across different hardware architectures was demonstrated with the results confirming the potential of ML methods to reduce the computational cost of the geochemical calculations by several orders of magnitude. Several systems of increasing complexity were tested. The most basic example addressing the chemical speciation in cement is shown in Fig. 2.5.

The results of conducted benchmarking provide confidence in the accuracy and computational performance of ML models in reactive transport simulations. The future applications of ML models might be boosted by the development of automated workflows and user-friendly interfaces for model setup, training, validation, and testing. Future efforts within the EURAD-2 HERMES project will also address coupling efficiency with flow solvers and evaluate performance gains in realistic reactive transport scenarios.

Tab. 2.1: Mean squared error of the mineral content regression (clay, carbonate, silicate) for machine learning models trained with different datasets. "Small" refers to the dataset available for the pilot study, "all data (6 formations)" includes all available data covering the six geological formations used in the pilot study, and "data OPA" uses only data from the Opalinus clay formation. "Resnet" and "formation" refer to the different backbone architectures, while "TRU1" and "TRU1-BOEZ2" indicate, whether the models were trained using data from a single borehole or two boreholes.

MSE	carbonates	total clay	silicate	mean
TRU1 – small dataset - formation	0.045294	0.021597	0.005512	0.024135
TRU1 – all data (6 formations) - resnet	0.015266	0.010999	0.003151	0.009806
TRU1 – all data (6 formations) -formation	0.011865	0.009566	0.003006	0.008146
TRU1 – data OPA - resnet	0.006156	0.008821	0.002967	0.005982
TRU1 – data OPA - formation	0.009334	0.008632	0.002987	0.006984
TRU1-BOEZ2 – data OPA - resnet	0.003972	0.007649	0.003815	0.005146
TRU1-BOEZ2 – data OPA - formation	0.005083	0.007473	0.003535	0.005363

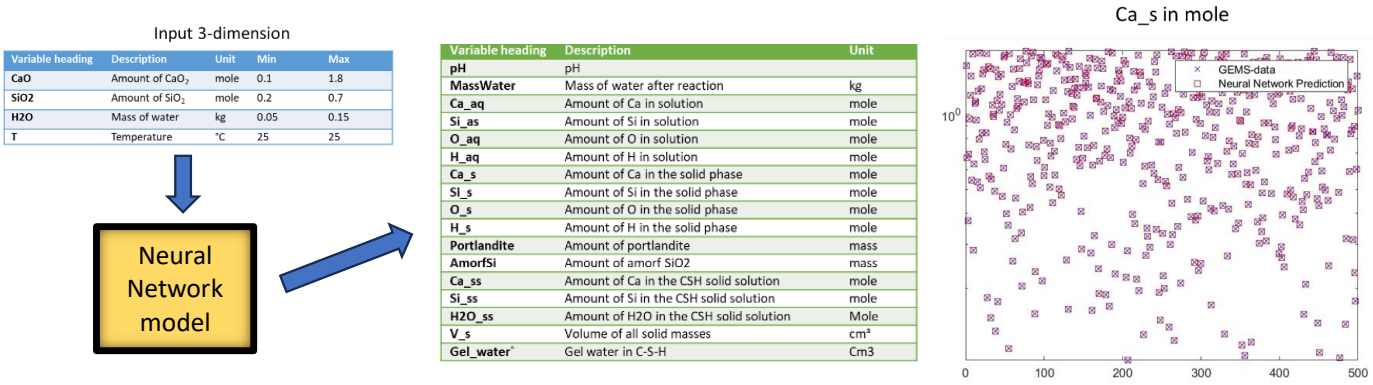

Fig. 2.5: The reference surrogate model for chemical equilibrium in cementitious system, with the definition of input and output parameters. From left to right: input, surrogate neural network models, output and visualisation of results. The surrogate model predictions (example of PSI-team using neural networks) for the amount of Ca in the solid phase after equilibration, is compared with the geochemical solver GEMS on the right. The y-axis is the molar concentration of Ca in the solid phase, while the x-axis signifies the test case under consideration. A total of 500 random 3-dimensional input test is shown. Accuracy and speed up of calculations are maintained at very high levels.

2.7 Towards digital twins of lab experiments: an integrated physics-based machine-learning framework for inverse modelling of microfluidic mass transport processes

In the framework of the PSI-funded CROSS project, titled 'In-situ 4D Micro-X-ray Chemical Imaging and a Digital Twin of Miniaturized Counter-Diffusion Experiments: Co-precipitation of Metals with Carbonates in Porous Media,' a digital twin framework of the laboratory experiments has been developed. The experimental part of the project activities, including metal co-precipitation has been completed in 2024. The numerical framework was extended to integrate the major processes occurring at the counter-diffusion calcium carbonate precipitation experiments. The classical nucleation theory, a model for predicting the formation of amorphous calcium carbonate phase (ACC) and a neural network surrogate model for the chemical speciation have been implemented in the parallel GPU lattice Boltzmann code. Initial scoping calculations have been set up to predict the nucleation positions of calcium carbonate polymorphs and provide fair agreement with experimental results. Fine tuning of the models is expected to further improve the accuracy of the framework. In Fig. 2.6, the comparison of the predictions of the first vaterite crystal with the experiments are shown. The simulations include also the induction time, which is the time needed for the solution at supersaturation to produce the first crystal. The total time of the experiment and simulation is reported, with the model currently predicting an earlier onset of precipitation, however with a reasonable accuracy for such processes, as well as a location of first precipitate close to the experimentally observed one.

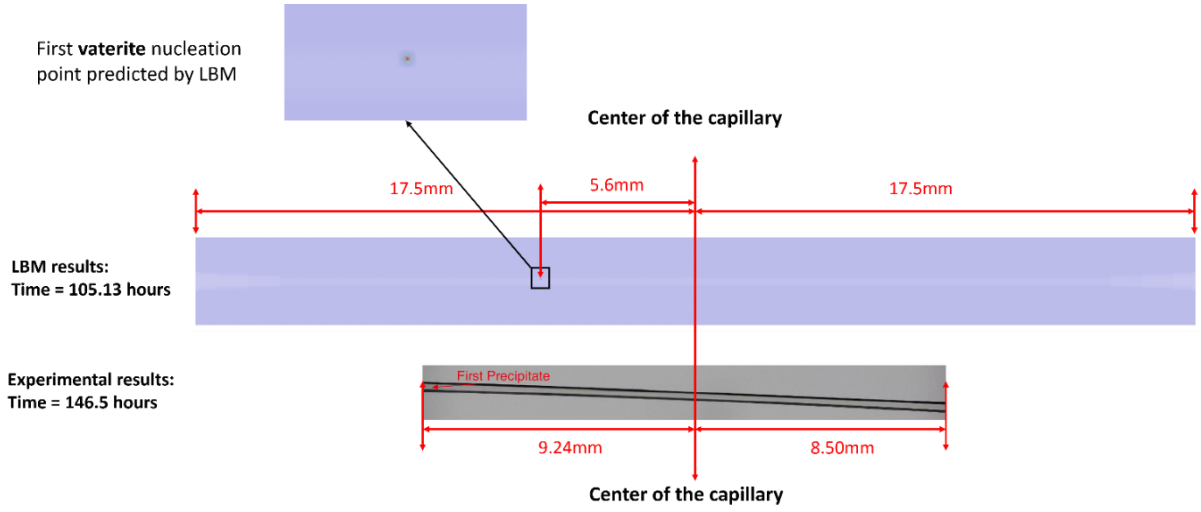

Fig. 2.6: 3D Lattice Boltzmann model for prediction of calcium carbonate precipitation in porous media. The model includes elements of the nucleation theory, while the chemical speciation is obtained by a surrogate neural network model.

2.8 Multiscale boiling flow simulations in nuclear reactor fuel assembly considering CRUD

The project "Boiling flow simulation in fuel-assembly affected by CRUD" (BoilCRUD) under the Swissnuclear funding agency and in collaboration with the Laboratory for Scientific Computing and Modelling at PSI (LSM-PSI) has been successfully completed. The project incorporates a new thermal LB model into the inhouse developed multi-GPU 3D LB code, suitable for high performance computing simulations. The new model uses the Multi-Relaxation-Time (MRT) collision scheme for mass transport and a second order central finite difference scheme for the energy equation. The model was used to simulate the nucleation and growth of bubbles in numerically generated porous domains representing CRUD deposited on the cladding of the nuclear fuel.

Fig. 2.7 illustrates nucleation and growth of low density fluid bubbles (vapor) on the surface of porous media, in a small part of the 3D computational domain represented by more than 1 billion voxels. The bubbles number density emerging on the surface was subsequently measured to evaluate the average nucleation site density (NSD), which is a key parameter in macroscopic simulation of boiling in nuclear reactor simulations. For this specific geometry the NSD was measured as $6.15 \cdot 10^8$ bubbles per m^2. The simulations were conducted at the Piz Daint supercomputer in CSCS utilizing efficiently in parallel 40 GPUs. The simulation allocated at the first 10 GPU's is shown in Fig. 2.8, illustrating a 2D slice of a 3D simulation of a different CRUD domain with a cylindrical steam chimney placed in the middle where a nucleated bubble preferentially propagates much faster than within the porous domain.

The results were disseminated in two conferences: the 33rd Discrete Simulation of Fluid Dynamics conference (Mokos et al., 2024a), where the presentation and work were distinguished by receiving the Gold Medal in the Fluids section and the Supercomputing in Nuclear Applications + Monte Carlo conference (Mokos et al., 2024b). A journal paper with results investigating the nucleation of bubbles in the ZrO_2 cladding was also published (Mokos et al., 2024c).

The project "Resolving CRUD growth mechanisms" (RESCUE) under the Swissnuclear funding was initiated in 2024. This project is conducted in collaboration with the Laboratory for Nuclear Materials (LNM) and the Hot Laboratory (AHL) and will combine an experimental study of the chemical composition and porosity of CRUD with a modelling study. So far, the work has focused on the implementation of a generalized contact angle in the multi-GPU LB code that allows for modelling multiple materials in contact with the liquid, and an initial coupling with neural networks is pursued for the inclusion of chemical reactions.

The project "Boiling flow in realistic fuel assemblies: modelling and validation of advanced CFD codes" (BRAVA) under the Swissnuclear funding agency and in collaboration with the Laboratory for Scientific Computing and Modelling (LSM) was initiated in 2024. This project aims to simulate an entire nuclear reactor fuel assembly using an Eulerian model that tracks the presence of bubbles via population balance equations rather than resolving the interfaces of each vapor bubble. Such models are described by a large number of empirical correlations and parameters which have to be tuned for specific flow setups. To facilitate the model parameter optimization a surrogate model of the fluid dynamics model using neural networks was created.

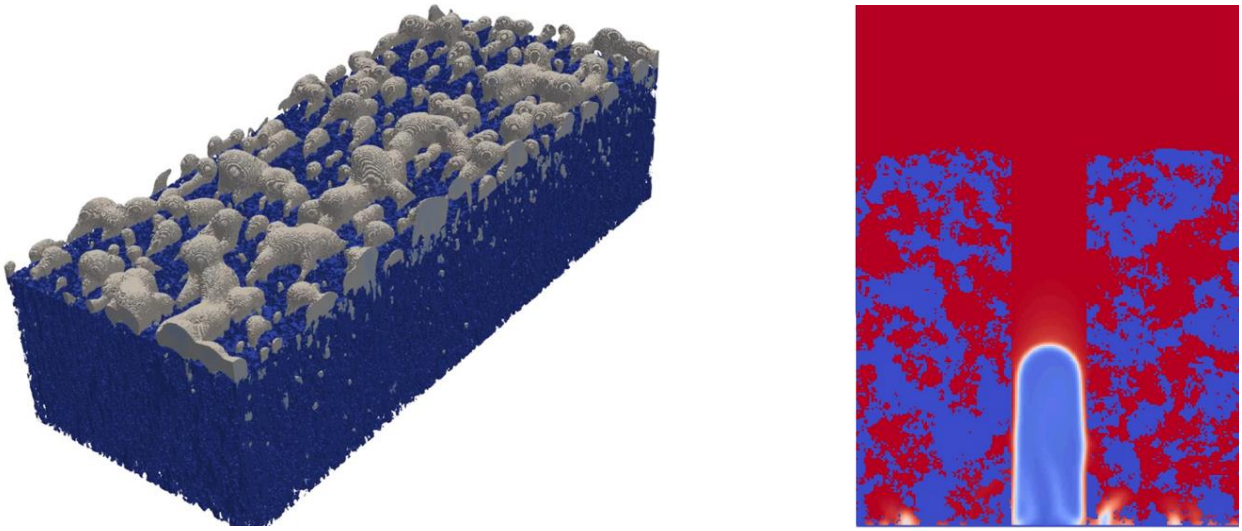

Fig. 2.7: (left) Bubbles emerging from a 3D CRUD porous domain at boiling nuclear reactor conditions (CRUD is blue, water vapor in white, water phase is not plotted for better visibility). (right) Acceleration of bubble nucleation within a steam chimney (CRUD is blue, vapor is light blue and red is the water phase).

The resulting model was used to fit the fluid dynamics models to the experimental results by inverse modelling based on genetic algorithms. On the inverse problem, the algorithm looks to derive the empirical parameters of the CFD model to minimize the error to the experimental results. Fig. 2.8 shows results obtained by using the parameters derived through the inverse modelling workflow. Compared to the results of the original model (Vlcek & Sato, 2023), the simulation with the new parameters achieves lower errors for 3 of the 4 experimental results. Work is ongoing to improve the quality of the inverse results as well as the underlying population balance models.

2.9 Microstructural evolution of cementitious materials

Mechanical and structural degradation of cement under ingress of Opalinus clay pore water has been investigated in EURAD-I WP MAGIC. The study is aimed at the pore-scale microstructure evolution using a 3D multi-component LB approach and numerical modelling of elastic properties of evolved material. The chemical processes considered in the model are the kinetic dissolution of portlandite (CH) and recrystallization of the calcium silicate hydrates (C-S-H).

The simulation code keeps track of the concentrations of calcium and silica in the different CH and C-S-H solid phases, as well as in the pore solution. The diffusion of the ions and the dissolution of calcium by considering the subgrid nanoscale porosity of the C-S-H phase.

Fig. 2.9 shows three representative 2D slices through the 3D computational domain, showing a gradual dissolution of CH and C-S-H. The project is run in collaboration with SCK-CEN and the LAMCUBE laboratory from the University of Lille, who simulate the mechanical properties (elasticity) of the simulated evolved geometries and upscale the results for cement paste to take into account the presence of nonreactive aggregates in mortar and concrete.

2.10 Digital Twin of Mont-Terri experiment within the EURAD-MODATS framework

In the final phase of the "Monitoring Equipment and Data Treatment for Safe Repository Operation and Staged Closure" (MODATS) project, digital twins were developed to simulate temperature evolution in the Full-Scale Emplacement (FE) experiment at Mont Terri. A physics-based model (PBM) and a data-driven model (DDM) were constructed, compared, and integrated into a digital twin model. The workflow started with an initial calibration phase using data from the first 1.5 years of the experiment (548 days). Both models were tested, optimized, and then applied in a temporal loop, sequentially incorporating new sensor data (temperature and humidity) to refine predictions (Fig. 2.10). For the PBM, the thermal conductivity parameter was updated via a surrogate model for humidity in the granular bentonite (GBM). At the same time, the DDM utilized new temperature and heater

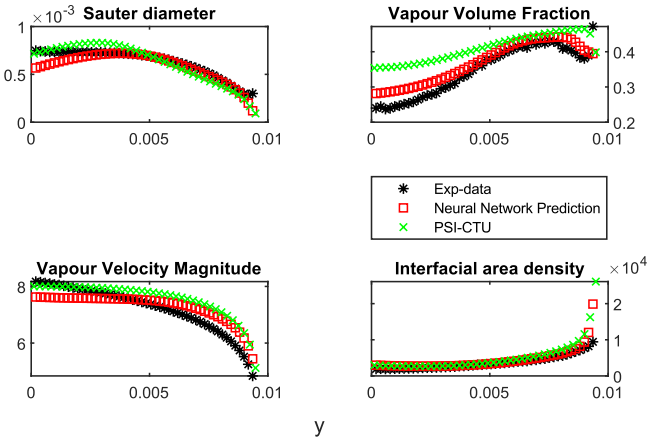

Fig. 2.8: Neural network predictions of the optimized model compared to experimental results (Exp-data) and CFD simulations with default parametrization (PSI-CTU) (Vlcek & Sato, 2023).

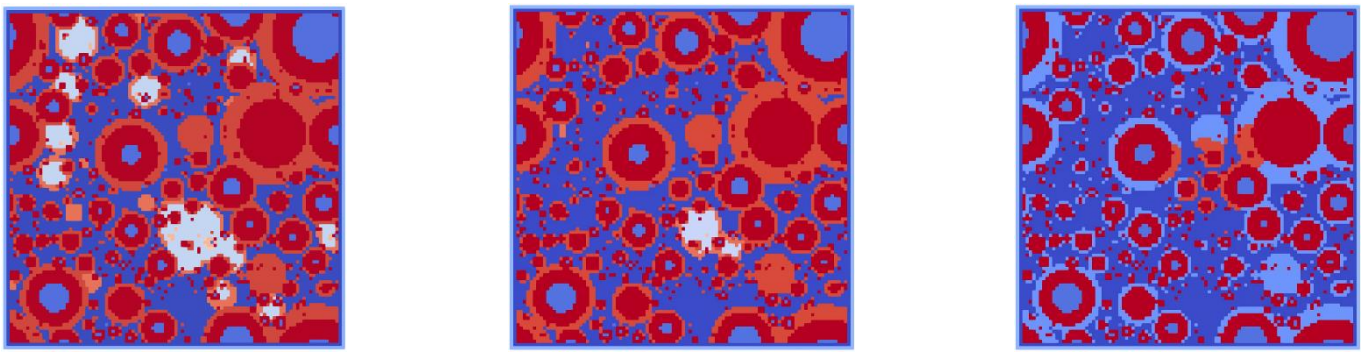

Fig. 2.9: Snapshots of slices within the domain as the CH (light blue and orange nodes, with the latter currently dissolving) and C-S-H (light red for low density and red for high density) solid nodes gradually dissolve. (left) is the beginning of the simulation, (centre) after the majority of CH has dissolved and (right) after most of the low density C-S-H has also dissolved.

power data to expand and improve its learning and testing dataset. This iterative process mimicked real-time data acquisition from the FE sensors database in increments of 500 days, extending up to 3000 days. The resulting PBM and DDM digital twins provided temporally updated temperature distributions in the FE experiment's near-field, incorporating new incoming data to enhance the temperature evolution predictions.

The PBM DT allows mechanistic insights into thermal processes, and a sensitivity analysis was performed on the repository design relevant parameters, for example heater powers and thermal conductivities of different barrier materials (granular bentonite, bentonite blocks, container material). Additionally, both the PBM and DDM digital twins demonstrated the ability to detect sensor failures. The DDM, in particular, proved highly efficient for real-time temperature prediction. The predicted temperature evolution highlights the potential of digital twin approaches to enhance repository monitoring, improve safety analysis strategies in the early repository phase, and optimize repository design and operational efficiency.

2.11 Digital Twin of waste packages within the PREDIS framework

Within the PREDIS project, subtask 7.4 the primary objective of developing a proof of concept aspect of digital twin technology in the pre-disposal management of radioactive waste packages was achieved. The use of ML algorithms to predict the geochemical and mechanical evolution of waste packages over time was demonstrated (Hu, et al, (2024)). The study presents an advance in predicting long-term stability in waste containment systems. Employing a surrogate model based on 25 GEMS Python scripts, the geochemical interactions within waste degradation processes over 100 years were simulated. The model simplified the complex full-scale geochemical models by using a mixing tank approach, primarily examining the evolution of material properties influenced by uncertain surface characteristics and reaction kinetics.

To achieve this, 1 million cases were generated using the neural network-based surrogate model, drastically reducing computational time (~1.9 seconds) compared to traditional methods (~78.4 days). The model evaluates the deterioration mechanisms of various materials like iron, aluminium, zinc, and brass, in cementitious waste packages, crucial for assessing their impact on the integrity of waste containment over extended periods. The findings with the neural network-based surrogate model, including ion concentrations and mass changes in materials like iron, brass, aluminium, and copper, offer detailed insights into chemical changes in the system. Incorporating a sensitivity analysis with 1 million cases generated by the surrogate model, the study underscores the interplay between chemical reactions and material properties, establishing a digital twin that links reaction rates to the stability of nuclear waste repositories. This study presents key indicators of potential integrity concerns due to material expansion, contraction, or gas-induced pressure variations.

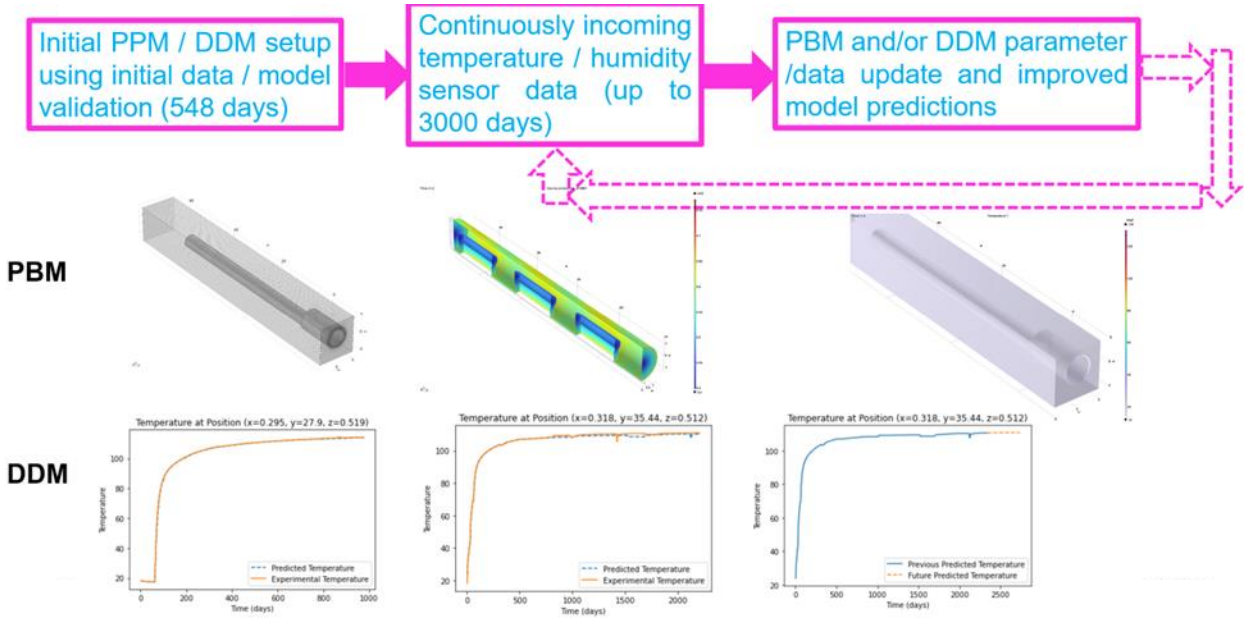

Fig. 2.10: Physics Based model (PBM) and Data-Driven model (DDM) Digital Twin workflow. After the initial calibration both the physics-based model and the data-driven model can be updated in order to improve future predictions. Both models are in very close agreement with the experimental observations. In the lower set of plots, a comparison of the simulation and experimentally measured temperature profiles for three specific locations during the evolution of the experiment is plotted.

2.12 References

Boiger, R., Churakov, S. V., Llagaria, I. B., Kosakowski, G., Wüst, R., & Prasianakis, N. I. (2024) Direct mineral content prediction from drill core images via transfer learning. *Swiss Journal of Geosciences*, *117*(1), 8. https://doi.org/10.1186/s00015-024-00458-3

Gimmi, T., Aschwanden, L., Waber, H.N., Gaucher, E.C., Ma, J., & Traber, D. (2024) Profiles of $\delta^{18}O$ and $\delta^{2}H$ in porewater of a Mesozoic rock sequence: Regional variability and relation to large-scale transport regimes. *Applied Geochemistry, 160*, 105846. https://doi.org/10.1016/j.apgeochem.2023.105846

Jenni, A., Gimmi, T., & Mäder, U. (2024) Coupling of porosity and diffusive transport in highly reactive systems: Open issues of reactive transport modelling. *Applied Geochemistry, 170*, 106076. https://doi.org/10.1016/j.apgeochem.2024.106076

Kosakowski, G., & Berner, U. (2013) The evolution of clay rock/cement interfaces in a cementitious repository for low- and intermediate level radioactive waste. *Physics and Chemistry of the Earth Parts A/B/C, 64*, 65–86. https://doi.org/10.1016/j.pce.2013.01.003

Kulik, D. A. (2011) Improving the structural consistency of C-S-H solid solution thermodynamic models. *Cement and Concrete Research, 41*(5), 477–495. https://doi.org/10.1016/j.cemconres.2011.01.012

Luraschi, P, (2024) *Evolution of porosity, diffusivity and mineralogy of different cement-clay interfaces* (PhD thesis). Supervisor: Gimmi, T.; Co-supervisors: Churakov, S. V., Van Loon, L. R.; External referee: Fernández Martin, R. Defence on June 24, 2024, Bern, Switzerland.

Luraschi, P., Gimmi, T., Van Loon, L. R., Shafizadeh, A., & Churakov, S. V. (2020) Evolution of HTO and 36Cl- diffusion through a reacting cement-clay interface (OPC paste-Na montmorillonite) over a time of six years. *Applied Geochemistry, 119*, 104581. https://doi.org/10.1016/j.apgeochem.2020.104581

Mokos, A., Churakov, S. V., & Prasianakis, N. I. (2024a) Pore-scale nucleate boiling simulations using a 3D multiphase Lattice-Boltzmann approach. In *Discrete Simulation of Fluid Dynamics* (p. 50). Zurich, Switzerland.

Mokos, A., Patel, R., Karalis, K., Churakov, S., & Prasianakis, N. (2024c) Surface controlled mechanism of water boiling for nuclear reactor fuel assembly. *International Journal of Heat and Mass Transfer*, *230*, 125747. https://doi.org/10.1016/j.ijheatmasstransfer.2024.125747

Mokos, A., Sato, Y., Niceno, B., Churakov, S. V., & Prasianakis, N. I. (2024b) Nucleate boiling within a fuel assembly affected by CRUD. *EPJ Web of Conferences*, *302*, 03003. https://doi.org/10.1051/epjconf/202430203003

Prasianakis, N. I., Haller, R., Mahrous, M., Poonoosamy, J., Pfingsten, W., & Churakov, S. V. (2020) Neural network based process coupling and parameter upscaling in reactive transport simulations. *Geochimica et Cosmochimica Acta*, *291*, 126–143. https://doi.org/10.1016/j.gca.2020.07.019

Prasianakis, N. I., Laloy, E., Jacques, D., Meeussen, J. C. L., Miron, G. D., Kulik, D. A., Idiart, A., Demirer, E., Coene, E., Cochepin, B., Leconte, M., Savino, M. E., Samper-Pilar, J., De Lucia, M., Churakov, S. V, Kolditz, O., Yang, C., Samper, J., & Claret, F. (2025) Geochemistry and machine learning: methods and benchmarking. *Environmental Earth Sciences*, *84*(5), 121. https://doi.org/10.1007/s12665-024-12066-3

Shafizadeh, Amir (2019) *Neutron imaging study of evolution of structural and transport properties of cement-clay interfaces* (PhD thesis). University of Jena, Germany. Supervisor: Mäder, U.; Co-supervisors: Gimmi, T., Van Loon, L. R., Churakov, S. V.; External referee: Schäfer, T. Defence on July 30, 2019, Bern, Switzerland.

Shafizadeh, A., Gimmi, T., Van Loon, L., Kaestner, A., Mäder, U., & Churakov, S. (2020) Time-resolved porosity changes at cement-clay interfaces derived from neutron imaging. *Cement and Concrete Research, 127*, 105924. https://doi.org/10.1016/j.cemconres.2019.105924

Vlček, D., & Sato, Y. (2023) Sensitivity analysis for subcooled flow boiling using Eulerian CFD approach. *Nuclear Engineering and Design, 405*, 112194. https://doi.org/10.1016/j.nucengdes.2023.112194

Wersin, P., Gimmi, T., Ma, J., Mazurek, M., Zwahlen, C., Aschwanden, L., Gaucher, E., & Traber, D. (2023) Porewater profiles of Cl and Br in boreholes penetrating the Mesozoic sequence in northern Switzerland. *Applied Geochemistry*, *159*, 105845. https://doi.org/10.1016/j.apgeochem.2023.105845

3 RETENTION AND TRANSPORT IN CLAY SYSTEMS

Glaus M.A., Neumann A., Marques Fernandes M., Churakov S.V., Adamou P. (PhD student), White M.L. (PhD student), Stotskyi V. (PhD student), Di Lorenzo F. (postdoc)

3.1 Introduction

Clay minerals are a major contributor to the retention of cations in natural environments due to their high surface area and significant structural excess charge. The very small particle size of clay minerals composing argillaceous rocks is responsible for the high tortuosity of transport pathways and, accordingly, small sized – a few nm – pores limit possible transport mechanisms to essentially diffusion only. These properties make clay formations suitable host rocks for the geological disposal of radioactive waste. To better constrain the retention and transport phenomena in natural systems, LES experimental studies supported by modelling focus on clay systems and how solutes interact with mineral surfaces, leading to differential retention, species transformation and changes in clay system composition and properties. The examples included here demonstrate the breadth and depth of the work being carried out.

One major focus has been the characterisation of rock properties linked to radionuclide retention in the designated host rock for the deep geological repository for radioactive waste in Switzerland. In collaboration with Nagra and the University of Bern, cation exchange and sorption properties of exemplary radionuclides were determined in samples of both the host rock, Opalinus Clay, and the Confining Units. This practical work is being supported by investigations of sorption at a fundamental level, using molecular modelling tools, and was recently extended from divalent transition metals to trivalent lanthanides. To complement sorption studies, experiments have focussed on how rock properties such as bed orientation (in clay-rich TBO samples) or the presence of anhydrite affect diffusion of selected tracers.

Finally, we have been translating our expertise to investigating redox properties of clay systems and have contributed to an improved understanding of interfacial electron transfer reactions. Our work in this area has included investigating interfacial electron transfer between aqueous ferrous iron and ferric iron in the structure of clay minerals with different total Fe contents (Neumann et al., 2013; Soltermann et al., 2014; Latta et al., 2017), exploring the electron transfer properties of Fe-bearing clay minerals using mediated electrochemical approaches (Gorski et al., 2012) and organic probe compounds and kinetic modelling (Neumann et al., 2008), and the dependence of clay mineral Fe(II) reactivity on the pathway by which the clay mineral Fe had been reduced (Rothwell et al., 2023). In one of our more recent studies, we have been applying this knowledge to better understand the retention of redox-sensitive radionuclides such as Se in repositories and their mobility in near-surface environments.

Moreover, we have been exploring new research directions in waste management in a broader sense, focussing on emerging topics in water and wastewater treatment and remediation. In several proof-of-concept studies, we have demonstrated the potential of clay mineral redox reactions to be used in novel, mineral-based advanced oxidation processes targeting mostly organic contaminants of emerging concern (short: emerging contaminants). Most current daily use chemical products, including pharmaceuticals, household chemicals and personal care products, are man-made organic compounds, and new classes of organic compounds are added constantly, with some emerging to display adverse effects. For these emerging contaminants, one major pathway to the environment is via the effluents of conventional wastewater treatment (WWT) plants, which were designed in the later part of the 19th century to remove major contaminants such as faecal bacteria and macronutrients for the benefit of both human and environmental health, but not with the – then unknown – diversity of man-made organic compounds in mind. Most of these anthropogenic chemicals are present at (very) low concentrations, often below µg/L and in the ng/l to pg/L range, and are hence also called micropollutants. Despite their low concentrations, micropollutants exert adverse effects on human and environmental health and are thus increasingly legislated. However, due to their chemical diversity, removal and degradation approaches must be sufficiently unspecific and simultaneously circumvent the formation of harmful degradation byproducts. In this research space, redox reactions of naturally occurring minerals such as clay minerals could potentially be harnessed for the removal and degradation of emerging contaminants, and more generally, treatment and remediation.

3.2 Characterisation of the retention properties of the Mesozoic sedimentary sequence of Northern Switzerland

In Stage 2 of the Sectoral Plan for Deep Geological Repositories (SGT), three regions – Jura Ost (JO), Nördlich Lägern (NL), and Zürich Nordost (ZNO) – were identified as potential sites for a deep geological repository for radioactive waste. To assess radionuclide retention and support safety analyses in Stage 3 of the SGT, a comprehensive laboratory programme was conducted to characterise the retention properties of the Mesozoic sedimentary sequence in Northern Switzerland.

3.2.1 Cation-exchange properties and modelling of the Opalinus Clay porewater

We collected site-specific physico-chemical data and modelled the porewater chemistry of Opalinus Clay for the three study areas, ZNO, NL and JO. Rock samples from seven boreholes, representing various lithologies, were analysed for cation exchange capacities (CEC) and exchangeable cation occupancies (Marques Fernandes et al., 2024b).

To benchmark the accuracy of our methods and select the most reliable approach, we tested four different methods of CEC measurements, which all gave consistent results (Fig. 3.1). Cs-CEC values were generally higher than the sum of other cations or Ni-CEC values, reflecting the stronger ability of Cs^+ to displace low-hydration cations (e.g., K^+ and NH_4^+) in illite-rich samples. This trend underscores the role of 2:1 phyllosilicate minerals like illite in governing cation exchange and retention. Furthermore, cation occupancies were similar across lithologies with clay contents exceeding 20 wt% (Fig. 3.2).

Using the mineralogical and physico-chemical data, we modelled porewater chemistries for the three regions. The results aligned well with compositions derived from laboratory experiments, including squeezing and advective displacement methods (Fig. 3.3). The developed approach is generic and applicable to a broad range of argillaceous rocks with significant clay content and should be considered as reference methodology for deriving host rock parameters for the safety assessment models.

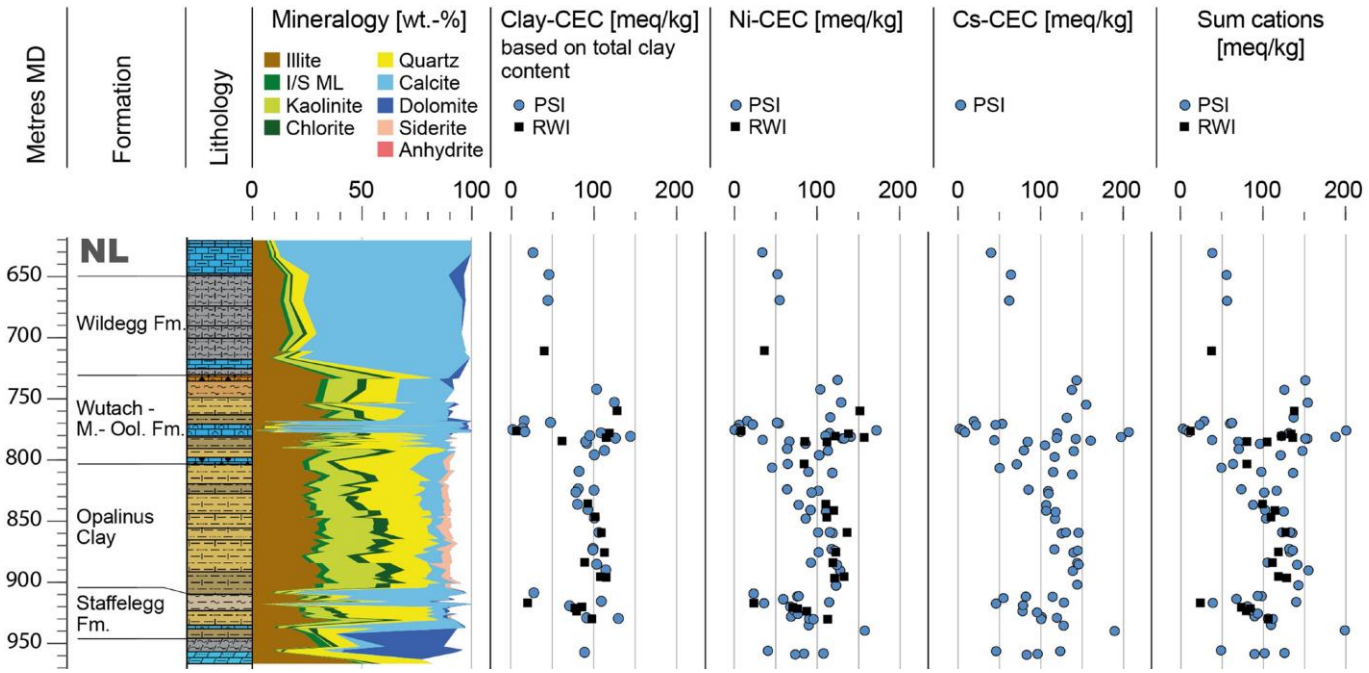

Fig. 3.1: Profile of NL showing representative stratigraphic sections and the mineralogical data. The formation depths are adjusted to the profiles of BOZ1-1 (JO), STA2-1 (NL) and TRU1-1 (ZNO). Clay minerals, quartz and calcite dominate the composition of these Mesozoic rocks. The cation data include results from the Clay-CEC$_{calc}$, Ni-CEC, Cs-CEC and $\Sigma_{cations}$ methods. Figure modified from Marques Fernandes et al. (2024b).

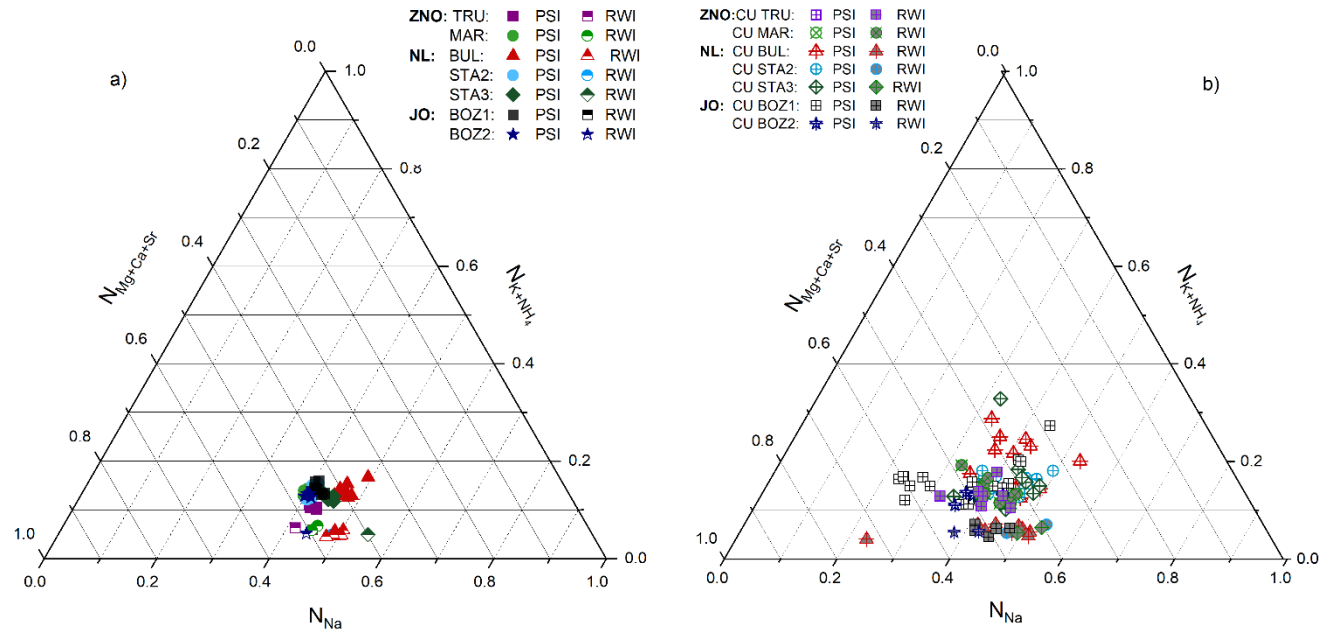

Fig. 3.2: Ternary representation of N_{Na} , N_{K+NH4} and $N_{Mg+Ca+Sr}$ determined for the samples from (a) Opalinus Clay and (b) the formations above and below the Opalinus Clay for ZNO, NL and JO. Figure from Marques Fernandes et al. (2024b).

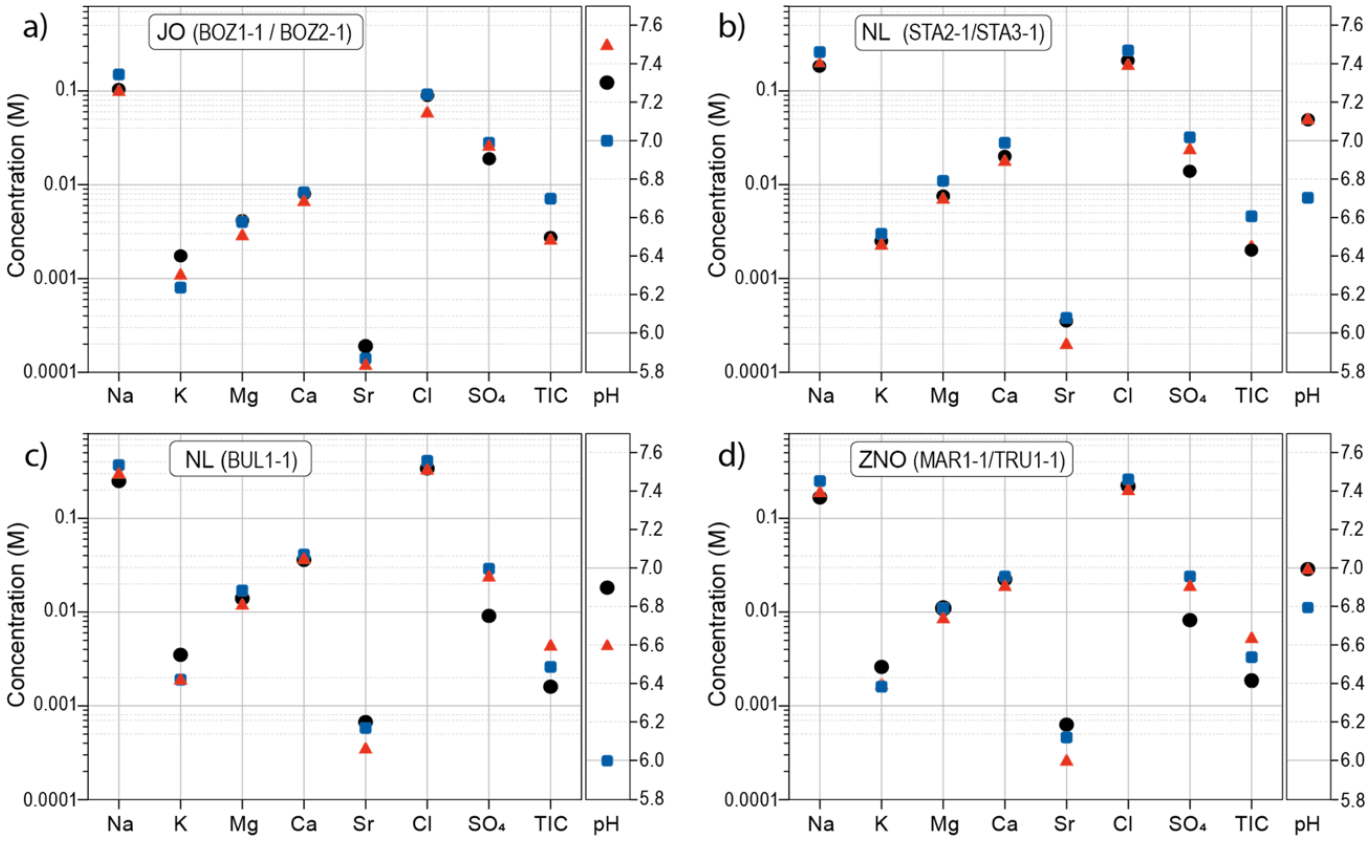

Fig. 3.3: Comparison of Opalinus Clay porewater compositions obtained from geochemical modelling (●: Model), squeezing (▲: SQ) and advective displacement (■: AD) for (a) JO (BOZ1-1/BOZ2-1), (b) NL (STA2-1/STA3-1), (c) NL (BUL1-1) and (d) ZNO (MAR1-1/TRU1-1). Figure from Marques Fernandes et al. (2024b).

3.2.2 Sorption of Cs, Ni, Eu, Th and U on rock samples of Opalinus Clay and confining geological units

Sorption isotherms of Cs(I), Ni(II), Eu(III), Th(IV) and U(VI) were measured on representative drill core samples from Bözberg-1-1 in JO, Bülach-1-1 in NL and Trüllikon-1-1 in ZNO, to validate the sorption database for the safety assessment (NTB 23-01: Marques Fernandes et al. (2024a)). These data were used to evaluate the predictive capability of the "bottom-up" approach to sorption modelling.

The ClaySor model (Kulik et al., 2018; Marinich et al., 2024) was employed for blind predictions of radionuclide distribution coefficients (R_d values). This model integrates the generalised Cs sorption (GCS) model and the 2-site protolysis non-electrostatic surface complexation and cation exchange (2SPNE SC/CE) model, designed specifically for illite. Using the PSI/Nagra thermodynamic database (TDB 2020: Hummel & Thoenen, 2023), the model predictions accounted for aqueous speciation and were scaled to the 2:1 clay mineral content of the rocks.

The experimental results showed good agreement with model predictions for Cs, Eu and Th in clay-rich samples (Fig. 3.4). However, Ni sorption was consistently overestimated at equilibrium concentrations below $10^{-5.5}$ M, likely due to unaccounted competing cations such as Fe(II) or Mn(II). Conversely, U sorption was systematically underestimated, potentially due to updates in the formation constant for $Ca_2UO_2(CO_3)_3(aq)$ in TDB 2020 or the reduction of U(VI) to U(IV) by Fe(II)-bearing minerals, which enhances retention. In clay-mineral-poor rocks, sorption appeared influenced by other minerals, such as calcite.

The methodology developed by LES for the sorption database formulation has been extensively validated and improved based on laboratory measurements and sophisticated geochemical modelling tools. The derived approach allows characterisation of model uncertainties and model-based sensitivity studies for the evaluation of sorption parameters beyond the reference scenarios. The methodological framework described in NTB 23-01 represents the most sophisticated and accurate approach in the sorption database development for the safety assessment.

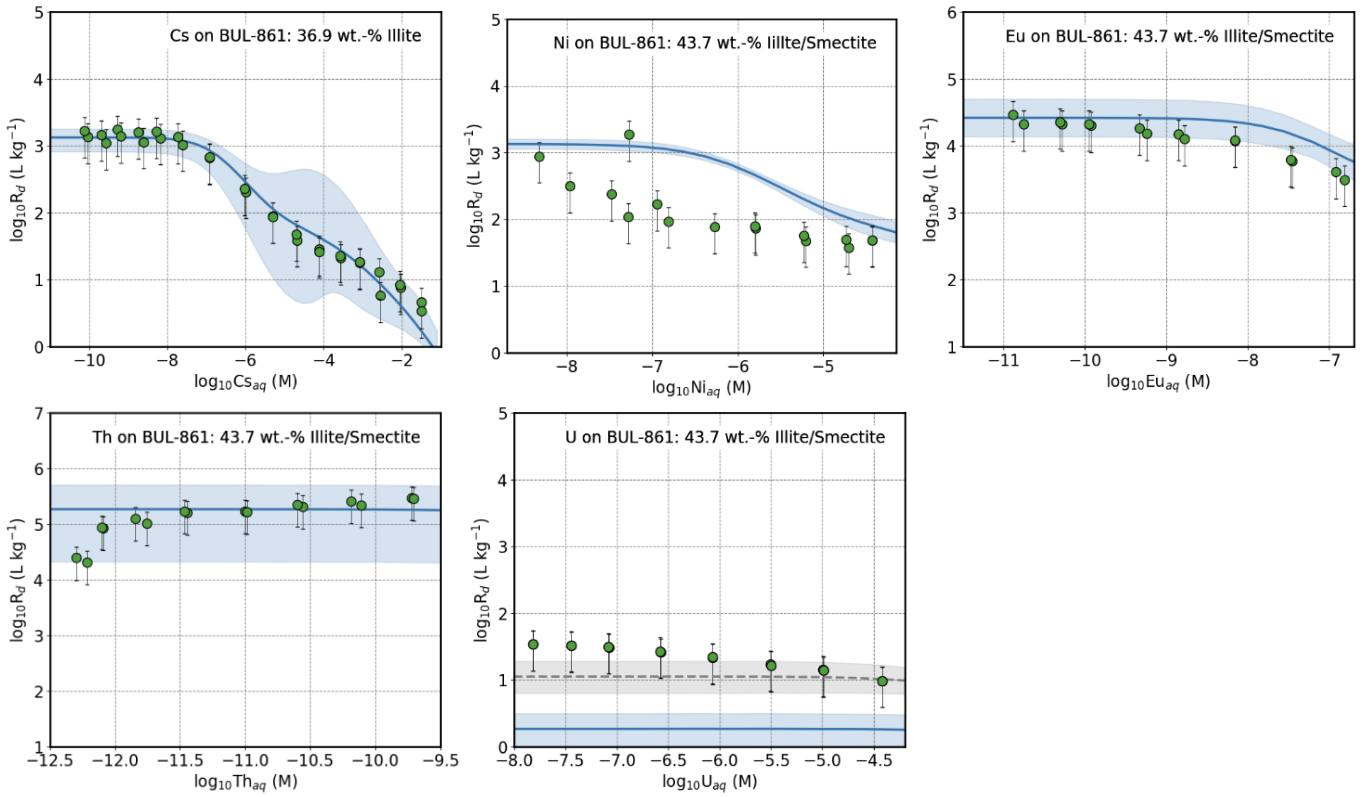

Fig. 3.4: Comparison of measured (green markers) and modelled (blue line) sorption isotherms of Cs, Ni, Eu, Th and U determined for a selected sample from the drill core Bülach-1-1 in NL, demonstrating excellent agreement for Cs, Eu and Th and deviations for Ni and U. Figure taken from Marques Fernandes et al. (2024a).

3.3 Molecular scale understanding of competitive cation adsorption on swelling clay minerals

To complement the work on polymineral argilaceous rocks, we have been investigating the sorption of cations in model systems, such as the sorption of divalent (Zn, Ni) and trivalent cations (Lu) to the synthetic trioctahedral clay mineral saponite. Within the SNSF funded project "*Molecular scale understanding of competitive cation adsorption on swelling clay minerals*" (SNSF Nr. 200021-129947), spectroscopic methods and molecular simulations are combined to study the surface complexation of these cations.

In this project, saponite samples were synthesised in the presence of Ni and Zn, leading to their incorporation into the clay mineral structure. These samples were used to produce reference EXAFS spectra of incorporated Ni and Zn for testing the accuracy of theoretical results obtained from ab initio molecular dynamics (MD) simulations. Our study builds on previous work that employed ab initio methods to reproduce measured EXAFS of trioctahedral clay minerals and demonstrates, for the first time, that this approach can be successfully expanded to polarised EXAFS. Our model results for trioctahedral clay minerals display a significant dependence on polarisation angle, with a higher sensitivity than observed for dioctahedral clay minerals (Dähn et al., 2002). By including the polarisation correction, we were able to correctly describe single and multiple scattering paths of Mg atoms in trioctahedral binding arrangements, which have previously been unaccounted for, leading to significant discrepancies between measured and modelled spectra at larger distances (~6 Å). Our results strongly suggest that polarisation effects on the EXAFS of trioctahedral clay minerals need to be considered for an improved mechanistic understanding of cation binding in and at these clay minerals.

In contrast to strong sorption and incorporation of divalent metals Ni and Zn to and in clay minerals, trivalent lanthanides (or Rare Earth Elements, REEs) show loose binding to clay mineral surface, as EXAFS spectra do not contain signal from the second and third coordination shell, and show negligible dependence on the polarisation angle. Typically, such behaviour has been explained by weaker sorption and/or sorption in an out-of-plane position (Schlegel, 2008; Finck et. al, 2012; Finck et. al, 2015). To delineate these different sorption mechanisms for trivalent REEs, we made use of the synthetic – and structurally well defined – saponite and investigated the sorption of the lanthanides Lu, Ce, Dy, Nd and Tb in batch experiments and characterised the samples with polarised EXAFS at the ESRF in collaboration with HZDR. Although all REEs exhibited sorption coefficients that were higher than for Ni, the EXAFS spectra do not show any backscattering contributions from clay mineral octahedral and tetrahedral sites. Moreover, REEs also displayed no angular dependence in the polarised EXAFS. Shell fitting of the EXAFS spectra showed that lanthanides likely formed an inner-sphere sorption complex, yet its exact structure could not be resolved as fitting was limited to the first oxygen shell.

To identify possible structural candidates, we complemented our spectroscopic work with metadynamics simulations of Lu sorbing to the clay mineral octahedral sheet in the classical weak edge sorption site geometry. Because these simulations did not reproduce our experimental results, additional ab initio MD simulations were performed for Lu sorbing to each of the two saponite surfaces ((010) and (110)), while constraining the bonds and coordination of Lu to experimentally obtained values. One of the trajectories showed Lu sorbed aligned with the octahedral Mg sheet (similar to Ni), whereas in the second trajectory Lu also shared oxygen bonds with the tetrahedral Si sheet. Both sorption complexes have been reported independently for different REEs and RNs (Schlegel, 2008; Finck et. al, 2012; Finck et. al, 2015), and we calculated the polarised EXAFS spectra of these two alternative Lu sorption complexes, using the FEFF code in conjunction with its POLARIZATION function (Fig. 3.5). Our results revealed that the EXAFS spectra for neither complex depended on the polarisation angle, which was expected for the out-of-plane complex, but not for the in-plane sorption position. Moreover, binding to the electron-denser Si compared to Mg did not significantly affect the simulated spectra, which all matched the experimentally obtained EXAFS spectra equally well. As our approach was unable to clearly distinguish the location and mechanism of Lu sorption, we suggest that an alternative approach is required.

3.4 Understanding the effect of rock properties on diffusion

3.4.1 Anisotropy of diffusion in rock samples from the deep borehole drilling campaign

During the past years, a comprehensive set of diffusion data for tritiated water tracer (HTO), $^{36}Cl^{-}$ and $^{22}Na^{+}$ was measured at LES on more than 120 rock samples from Nagra's deep borehole drilling campaign (Van Loon et al., 2023). All these measurements were performed with the direction of diffusion perpendicular to the bedding of the rock samples. It is well known from previous studies (Van Loon & Soler, 2003) that diffusion parallel to the bedding occurs faster than in the perpendicular direction. However, no such

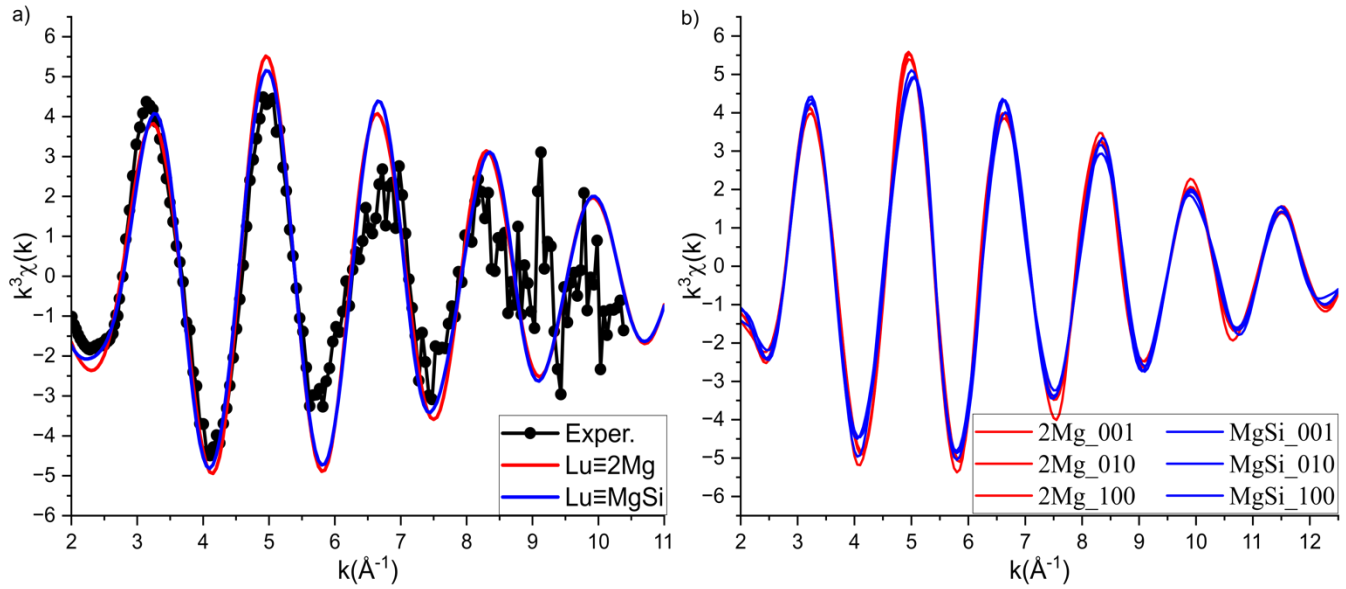

Fig. 3.5: (a) Experimentally measured Lu L3-edge EXAFS spectra at 35° polarisation angle (black) vs the theoretical EXAFS spectra of two possible Lu inner-sphere sorption complexes on saponite edge surfaces (red, blue). (b) Theoretical Lu L3-edge polarised EXAFS as a function of the polarisation vector. Red lines represent Lu bound exclusively to Mg atoms along the octahedral sheet; blue lines show Lu sharing oxygen bonds between Mg in the octahedral sheet and Si in the tetrahedral sheets.

measurements were carried out so far with samples from the recent deep drilling campaign. To test the diffusion anisotropy of selected rock specimens, diffusion measurements on twin samples were conducted parallel and perpendicular to the bedding, further denoted as 'anisotropy measurements'. In contrast to conventional measurements in cells to study diffusion perpendicular to the bedding, the anisotropy measurements were carried out using a rigid steel confinement for the rock samples. In these experiments, the in-situ overburden pressure could be adjusted using screws with disk springs and the axial pressure load was measured (Van Loon et al., 2004). A secondary purpose of the measurement campaign was to evaluate possible variations in anisotropy as a function of sample depth. Because the vertical position of the Opalinus Clay formation differs by several hundreds of meters between the Jura Ost and the Nördlich Lägern siting areas, samples from those drillings were chosen for the anisotropy experiments. All samples originate from the clay-rich members of the Opalinus Clay.

The experimental setup is very challenging and requires fine-tuning of sample dimensions to the diffusion cell geometry. A first series of anisotropy measurements carried out in 2023 failed, owing to the presence of bypasses in the sample assemblies, leading to advective artefacts. A second series of samples was therefore set up with rock samples precisely machined to match the exact dimension of the confining porous filters. The results for the diffusion of HTO and $^{36}Cl^-$ tracers, effective diffusion coefficients (D_e) and diffusion-accessible porosities (ε), have recently become available and are presented in Tab. 3.1.

Tab. 3.1: Results of diffusion measurements for HTO and $^{36}Cl^-$ perpendicular and parallel to the bedding.

		HTO				**$^{36}Cl^-$**			
		perpendicular		**parallel**		**perpendicular**		**parallel**	
	Ionic strength	D_e × 10^{-12}	ε	D_e × 10^{-11}	ε	D_e × 10^{-13}	ε	D_e × 10^{-13}	ε
Sample name [a]	[M]	[$m^2\,s^{-1}$]	[–]	[$m^2\,s^{-1}$]	[–]	[$m^2\,s^{-1}$]	[–]	[$m^2\,s^{-1}$]	[–]
STA3-1-872.74 A	0.190	3.21±0.06	0.136±0.006	2.96±0.20	0.135±0.008	No breakthrough		15.9±0.6	0.062±0.004
STA3-1-872.74 B	0.505	3.42±0.21	0.140±0.014			0.15±0.09	0.001±0.004		
BAC1-1-903.41	0.190	5.72±0.16	0.147±0.009	3.09±0.24	0.115±0.009	5.01±0.11	0.056±0.002	1.97±0.24	0.016±0.003
BOZ1-1-641.60	0.190	5.78±0.18	0.149±0.008	2.67±0.21	0.106±0.009	4.13±0.13	0.049±0.003	1.72±0.46	0.011±0.006
BOZ1-1-650.33	0.190	7.24±0.23	0.145±0.008	2.98±0.20	0.145±0.008	5.98±0.23	0.062±0.004	3.19±0.18	0.019±0.002

[a] Abbreviations: STA = Stadel, BAC = Bachs, BOZ = Bözberg

All experiments were carried out with the same synthetic porewater previously used for the samples from the Bözberg1-1 drilling (pH 7.90, ionic strength 0.190 M). Sample STA3-1-872.74 with perpendicular orientation was used to explore the effect of ionic strength, and a twin sample was run with the synthetic porewater previously used for the samples from the Bülach1-1 drilling (pH 7.56, ionic strength 0.505 M).

The diffusion parameters obtained for HTO are in very good quantitative agreement with expected trends. In contrast, the results for $^{36}Cl^-$ tracers are highly inconsistent, with some values of D_e and ε being substantially lower than expected and other values falling within the expected range. The reasons for this unexpected inconsistency are currently unclear. A likely explanation could be related to the variable adjustment of the diffusion cells' external pressure, although such effects were not observed in the past (Van Loon et al., 2004). The anisotropy factors for HTO, i.e., the ratio of D_e values for measurements parallel to the bedding relative to those perpendicular to the bedding, are in the order of 5 ± 1 for the Bachs and Bözberg samples, and higher (~9) for the samples from Stadel. For the $^{36}Cl^-$ tracer, the anisotropy factors are again inconsistent, with some values less than 1 and others substantially larger than 1. Clearly, anisotropy effects are strongly superimposed by unexpected strong effects of anion exclusion in these cases. The results of ongoing $^{22}Na^+$ diffusion experiments may aid in clarifying the current interpretation. In any case, it will be important to investigate the relative diffusion behaviour of HTO and $^{36}Cl^-$ by targeted variation of the external pressure on one of the current samples.

3.4.2 Diffusion measurements on rock samples from Triassic formations rich in anhydrite

The diffusion properties of anhydrite-rich rock present in the lithological profiles at potential siting regions for the deep geological repository are of great interest for the interpretation of natural isotope profiles. These profiles exhibit rather large concentration changes indicating low diffusive mass transfer rates. However, no experimental confirmation of such properties has been attained so far from laboratory experiments. The reason is: on one hand, the large content of anhydrite, and on the other hand, the low diffusivity that can readily be masked by experimental artefacts such as advection or diffusion properties related to minor short circuiting / bypasses. Further, it must be assumed that the anhydrite will be converted to gypsum during a classical diffusion experiment at ambient temperature. Indeed, no breakthrough of tracers was measured in a sample originating from the Bänkerjoch formation of the Trüllikon1-1 borehole (Van Loon et al., 2024). After various attempts to carry out diffusion experiments at a temperature of 50 °C, reliable data could be obtained during the past reporting year. Information on the samples is available in Tab. 3.2, and the results of the diffusion measurements are shown in Tab. 3.3. The experiments were carried out in laboratory atmosphere using a simple electrolyte mixture consisting of 0.2 M NaCl and 0.023 M $CaSO_4$, with diffusion cells placed in a thermo-controlled compartment and solution reservoirs outside the oven at ambient temperature. It was demonstrated earlier that such a setup is sufficient to maintain the target temperature in the solutions pumped through the diffusion cells.

All results were obtained by manual fitting of breakthrough curves, and uncertainties were rather subjectively estimated from sensitivity analysis. Despite the uncertainties related to potential artefacts, the results obtained appear reliable and consistent.

Tab. 3.2: Information on samples used for diffusion measurements.

Sample name [a]	Formation	Anhydrite [wt.%]	Clay [wt.%]	Water loss porosity, 105 °C [–]
BAC1-1-1033.60	Bänkerjoch	95	0	0.002
STA2-1-1126.66	Zeglingen	97	0	0.002
MAR1-1-862.35	Bänkerjoch	93	0	0.004
BOZ1-1-743.10	Bänkerjoch	99	0	0.001

[a] Abbreviations: STA = Stadel, BAC = Bachs, BOZ = Bözberg, MAR = Marthalen

Tab. 3.3: Results of diffusion measurements carried out at 50 °C. No significant sorption of $^{22}Na^+$ tracer was measured in any sample.

	HTO		$^{36}Cl^-$		$^{22}Na^+$
	D_e	ε	D_e	ε	D_e
Sample name [a]	[m² s⁻¹]	[–]	[m² s⁻¹]	[–]	[m² s⁻¹]
BAC1-1-1033.60	$(1.3\pm0.5)\times10^{-13}$	0.0035±0.002	$(4.0\pm1.0)\times10^{-14}$	0.00035±0.0001	$(4.2\pm1)\times10^{-14}$
STA2-1-1126.66	$(2.0\pm1.0)\times10^{-13}$	0.0036±0.002	$(4.0\pm2.0)\times10^{-14}$	0.00036±0.0002	n.a.
MAR1-1-862.35	$(2.1\pm1.0)\times10^{-12}$	0.0073±0.003	$(1.7\pm1.0)\times10^{-12}$	0.0036±0.002	$(1.3\pm0.3)\times10^{-12}$
BOZ1-1-743.10	$(1.6\pm0.5)\times10^{-12}$	0.0036±0.002	$(1.6\pm0.5)\times10^{-12}$	0.0029±0.002	$(2.1\pm0.6)\times10^{-12}$

[a] Abbreviations: STA = Stadel, BAC = Bachs, BOZ = Bözberg, MAR = Marthalen

In all experiments rather short breakthrough times were observed. The agreement of the diffusion-accessible porosities of HTO with the water-loss porosities is remarkable. In view of these low porosity values, thicker rock samples could be more appropriate for such measurements. The results indicate some anion exclusion effects, whereas no sorption of the $^{22}Na^{+}$ tracer was observed. However, as clay minerals are mostly absent in these rock samples, the electrostatic diffusion model used in previous measuring campaigns to describe the behaviour of charged tracers is not the appropriate model here (Glaus et al., 2024).

3.5 Investigating the redox properties of clay systems

In addition to effectively sorbing cations and radionuclides, clay minerals can also contribute to redox transformations of dissolved and sorbed inorganic and organic compounds. Here, the presence of redox active Fe in the structure of clay minerals is the key to either direct electron transfer from structural Fe(II) to the species under investigation – such as redox-sensitive elements such as selenium here – or to the indirect formation of oxidising species from the reduction of dissolved oxygen by clay mineral Fe(II) and subsequent oxidative degradation of compounds – examples included here are organic contaminants and antimicrobial resistance genes. The results reported on the oxidative transformation of contaminants originate from, and utilise outcomes of, the project "*Cleaning water with mud: clay minerals producing reactive oxidizing species*", which was funded by the UK's Engineering and Physical Sciences Research Council's (EPSRC) "*Bright Ideas Award*".

3.5.1 Influence of structural Fe content in clay minerals on selenite redox reactions

Selenium is an element relevant in a general environmental context due to its toxicity if present at elevated concentrations (daily intake exceeding 400 µg) and, as the isotope ^{79}Se with a half-life of more than 100'000 years, also forms a substantial part of the radioactive waste inventory. In the latter case, its speciation as anionic species presents an additional challenge, whereas its redox reactivity provides potential for its sequestration. Under oxic conditions, Se is predominantly present as selenate (SeO_4^{2-}) and selenite (SeO_3^{2-}), which are both soluble and highly mobile, and can become protonated at lower pH values. Under reducing conditions both oxyanions are reduced to elemental selenium, which can be present as red amorphous Se(0) and grey crystalline Se(0). At even more reducing conditions, selenides (Se(-I), Se(-II)) prevail, which have a high affinity to form low solubility metal compounds (see also Fig. 3.6 for a Pourbaix diagram of Se).

Building on previous studies demonstrating that Fe(II)-bearing minerals are capable of reducing selenate and selenite to elemental Se and even selenides, this study investigated the role of clay mineral structural Fe for the reduction mechanism of selenite. The Fe in two montmorillonites (SWy-2, STx-1) and one nontronite (NAu-2) was reduced to different extents and the combined sorption and reduction of selenite monitored over time, using both aqueous phase measurements of selenite and XAS-characterization of the solid phase-associated Se. For experiments carried out at low pH values of 5, XAS analyses show extensive reduction of selenite to red amorphous Se(0) for all clay minerals and reduction extents. For both montmorillonite SWy-2 and the high-reduced nontronite NAu-2, this amorphous Se(0) transformed into the more crystalline grey Se(0) over extended reaction times (Fig. 3.7), suggesting that there is a kinetic constraint on the formation of crystalline Se(0). Neither further reduction to selenides nor formation of FeSe or $FeSe_2$ was observed, which may have been limited by the low aqueous Fe(II) concentrations in the experiments and/or the insufficiently low reduction potential.

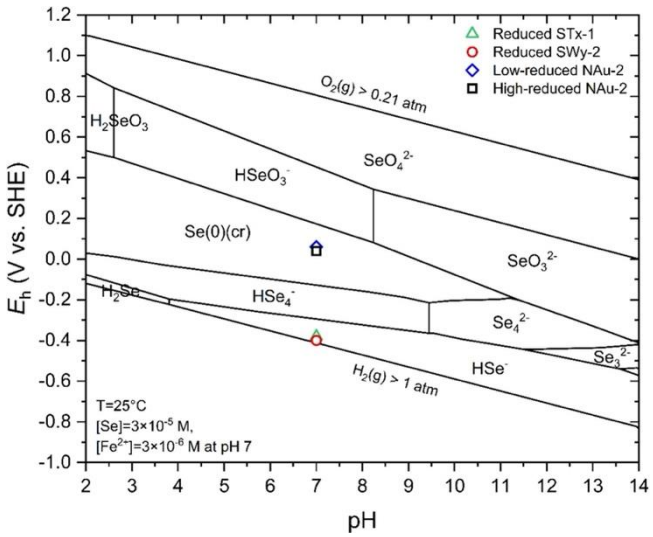

Fig. 3.6: Pourbaix diagram of Se for the experiments carried out at pH 7 and 25 °C, with total selenium concentrations of $3{\cdot}10^{-5}$ M and aqueous Fe(II) concentrations of $3{\cdot}10^{-6}$ M. For comparison, the reduction potentials of the reduced clays measured at pH 7 are also displayed: reduced STx-1 (green triangle), reduced SWy-2 (red circle), low-reduced and high-reduced NAu-2 (blue diamond and black square). Figure from Qian et al. (2024).

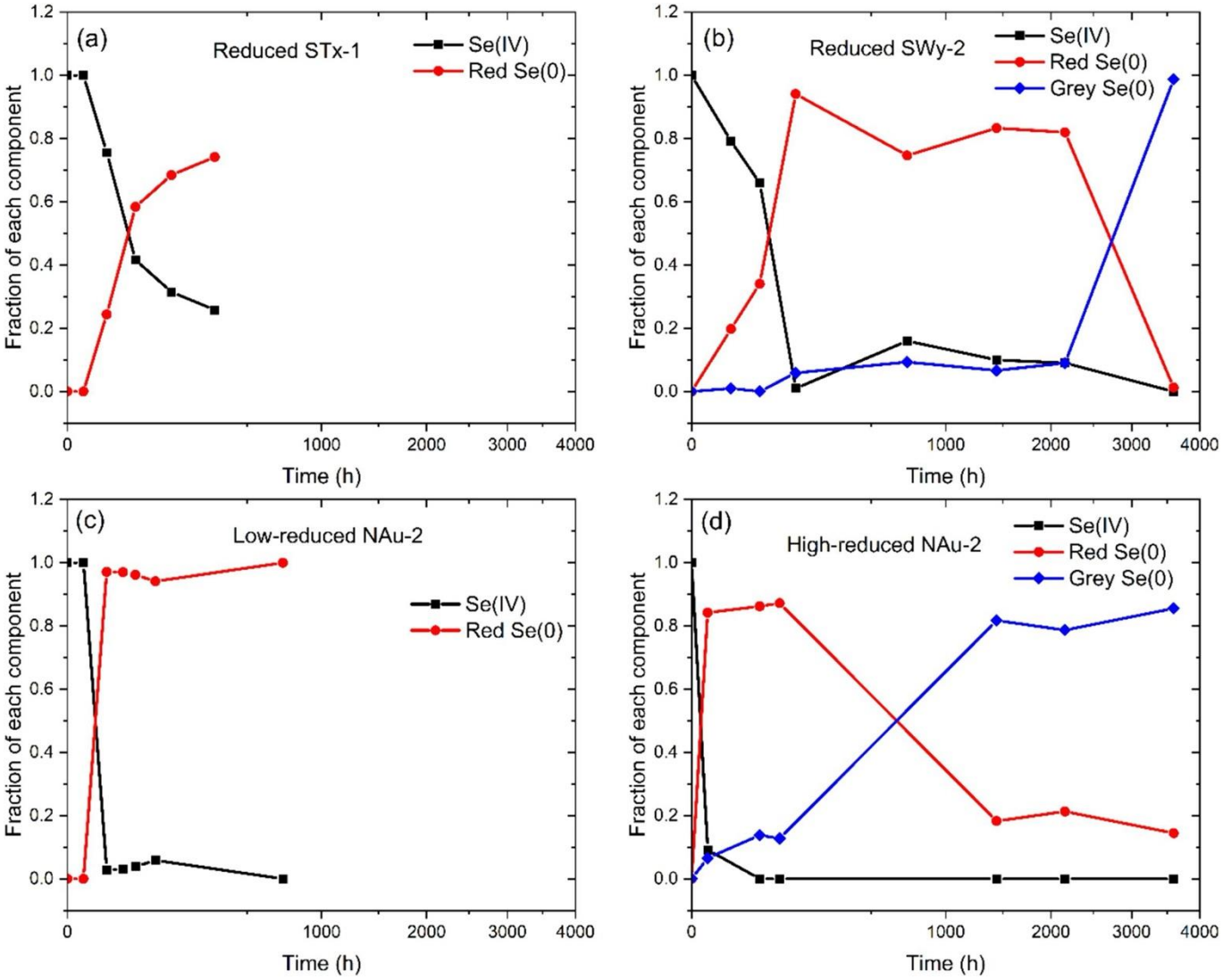

Fig. 3.7: Reduction of selenite (Se(IV): black squares) to elemental selenium (Se(0)) in either amorphous red form (red dots) or crystalline grey form (blue diamonds) in the presence of reduced montmorillonites STx-1 and SWy-2, and low-reduced and high-reduced nontronite NAu-2. Note that the y-axis is in a logarithmic scale. Figure from Qian et al. (2024).

Additional experiments at the higher pH value of 7 were used to investigate the effect of selenite reduction potential on the overall reaction kinetics and product distribution. Consistent with the expected decrease in selenite reduction potential with increasing pH value (Fig. 3.6), less extensive and much slower selenite reduction occurred with all reduced clays. The most surprising finding, though, was that high-reduced NAu-2 was the fastest to reduce selenite to crystalline Se(0) at pH 5 (Fig. 3.7) but was less reactive than the other clays at pH 7. Measured reduction potentials of the reduced clays can, however, explain this result: reduced STx-1 and SWy-2 have much lower reduction potentials compared to the reduced NAu-2 samples, which provide a higher potential difference (ΔE) for the electron transfer process to selenite at pH 7 (Fig. 3.6). At pH 5, less reducing conditions suffice for the reduction of selenite to elemental selenium, and the total available amounts of electrons, which are present as Fe(II) in the clay minerals, determine the kinetics and extent of selenite reduction.

3.5.2 Clay mineral-based advanced oxidation of micropollutants

In a recently concluded PhD research project hosted at Newcastle University, UK (viva took place on 5 November 2024), we provided proof-of-concept evidence for how to *"Harness[ing] Microbially-mediated Redox Processes for Sustainable Water Treatment"*. Here, the targets were micropollutants, which can be degraded effectively in so-called advanced oxidation processes (AOPs), which rely on the in-situ formation of highly reactive oxidising species such as hydroxyl radicals (•OH). These same species are also formed when clay mineral Fe(II) reacts with dissolved oxygen in water (Tong et al., 2016), and the regeneration of clay mineral Fe(II) can be realised

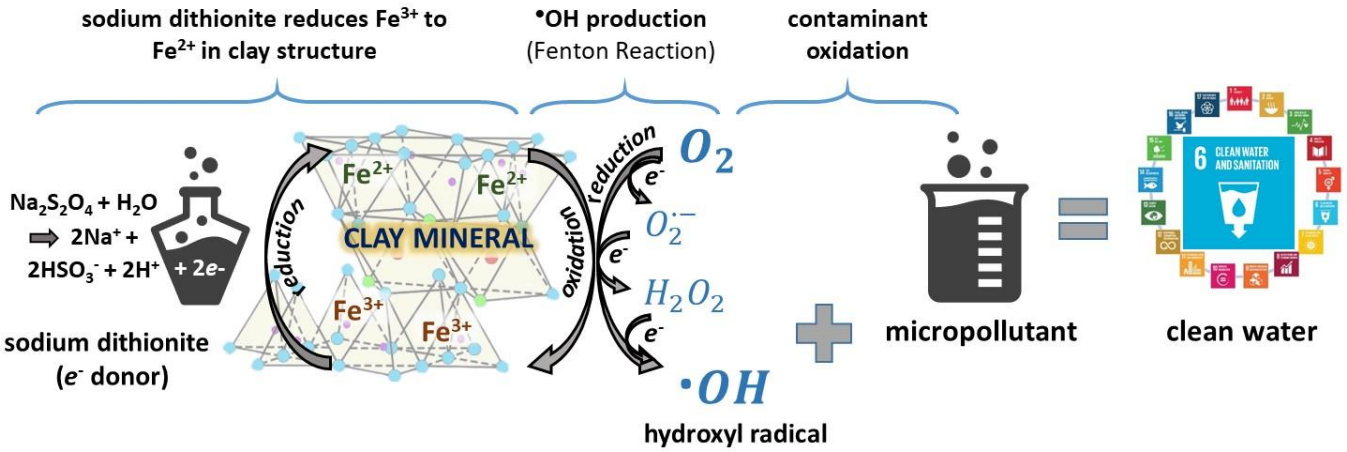

Fig. 3.8: Conceptual scheme of the simplified micropollutant treatment process for water and wastewater using the redox reactivity of clay mineral Fe(II). Indicated are the 'activation step', using dithionite to reduce clay mineral Fe(III) to Fe(II), and the 'treatment step' that utilises the hydroxyl radicals (•OH) formed by the reduction of dissolved oxygen by clay mineral Fe(II) for the oxidative degradation of micropollutants. Figure from White (2024).

by microbial activity in anoxic conditions, making this approach a potentially sustainable AOP. However, the direct coupling of several sequences of (microbial) iron reduction ('activation') and oxygenation for micropollutant degradation ('treatment') in one contained filter assembly has not been demonstrated before.

In the project, clay minerals with different Fe content were used in column experiments and the activation process was implemented in a first simplified setup with the chemical reductant dithionite (Fig. 3.8). This provided a proof of concept that (a) water flow through a clay-based filter can be maintained, (b) clay mineral Fe activation and •OH production can be sustained in repeated treatment cycles, and (c) clay mineral Fe can repeatedly be reduced and re-oxidised without being lost from the column via either reductive dissolution or colloidal transport.

3.5.3 Removing antibiotic resistance genes with novel mineral-based advanced oxidation processes

Another class of emerging contaminants that are mainly released to aqueous environments via WWT effluents are antimicrobial resistant bacteria (ARB) and antimicrobial resistant genes (ARGs). Antimicrobial resistance (AMR) is a major emerging threat around the world, and to better control the spread of ARB and ARGs, their major dissemination pathways are targeted in treatment. Tertiary/quaternary treatment of WWTP effluents can be an option, and disinfection technologies, such as chlorination, ozonation and UV irradiation, can remove some ARB and ARGs from WWTP effluents. Among tertiary treatment options, AOPs have the greatest potential for reducing AMR levels in pretreated wastewater, yet most of these technologies are costly and have high energy and chemical demands. Again, we suggest that clay minerals may be used in a more sustainable, alternative AOP, either efficiently converting H_2O_2 to •OH in a Fenton-like process (Pham et al., 2012) or producing •OH during the oxygenation of clay mineral Fe(II) (Tong et al., 2016). We hypothesised that •OH produced in these mineral-based AOPs could oxidatively degrade ARGs. To assess the potential for ARG removal, we used real effluent from a local WWTP and monitored selected ARGs present as part of the native bacterial communities in these effluents.

First, we benchmarked ARG removal in conventional disinfection (UV irradiation), commonly used AOPs (UV/H_2O_2), and our novel AOP that combined Fe-bearing clay mineral NAu-1 with H_2O_2 (H_2O_2/NAu-1). Our results demonstrate that selected ARG (*tet*M – coding for resistance to tetracycline antibiotics), total bacteria (16S rRNA gene), and an example mobile genetic element cassette, MGE (*int*1), were removed to similar or even higher extents with the H_2O_2/NAu-1 treatment compared to conventional AOP and disinfection treatment (Fig. 3.9). Additional experiments investigated the effect of treatment parameters H_2O_2 dose and contact time to establish pseudo-optimal treatment conditions that could be trialled in pilot scale experiments in the future. Importantly, contact times of 4-8 hours and H_2O_2 doses of 0.26 mM are within the ranges that are feasible for use in conventional WWTPs, for example operating the activated sludge process, and water quality parameters important for effluent discharge (e.g., pH, COD, TP, TSS and TOC) meet the required standards (for the UK). These results suggest that this mineral-based AOP has potential for ARG removal in tertiary wastewater treatment.

Secondly, we tested the effectiveness of gene removal by reduced NAu-1 (rNAu-1) upon contact with oxygen. Stirring deoxygenated effluent with rNAu-1 in the laboratory atmosphere allowed diffusion of oxygen from air into the wastewater. This treatment succeeded in removing all ARGs (*tet*M, *tet*Q, and bla_{OXA-10}), the mobile genetic element *int*1, and bacteria (16S rRNA) by almost three orders of magnitude, which is the highest removal observed in our study (Fig. 3.9). Measured metal release was negligible, the suspension pH remained constant or increased, and net oxidation of clay mineral Fe(II) was quantified. This combined evidence confirmed that gene removal was due to the in-situ formation of reactive oxidising species such as •OH. Surprisingly, also treatment with rNAu-1 under anoxic conditions within the anoxic glovebox resulted in substantial and comparable gene removal. In this case, release of Fe(II) from the reduced clay mineral was significant, although the suspension pH remained similarly high, and suggests a different mechanism for gene destruction compared to treatment with rNAu-1 under oxic conditions. Because dissolved oxygen concentrations remained low (<2 ppm) and no net oxidation of clay mineral Fe(II) occurred, we suspect that increased bacterial uptake of aqueous Fe(II) led to subsequent intracellular production of •OH (oxidative stress), which then resulted in gene destruction. Overall, gene and bacteria removal by rNAu-1 was rapid (within 30 minutes) and non-selective, and bacterial regrowth was suppressed over 24 h in the presence of rNAu-1. While operationalising "rNAu-1 tertiary treatment" from the lab to pilot to full scale will require additional research, this mineral-based oxidation reaction may also play a significant role in natural sedimentary environments and could be promoted for in-situ remediation and nature-inspired treatment systems, such as riverbank filtration or wetlands.

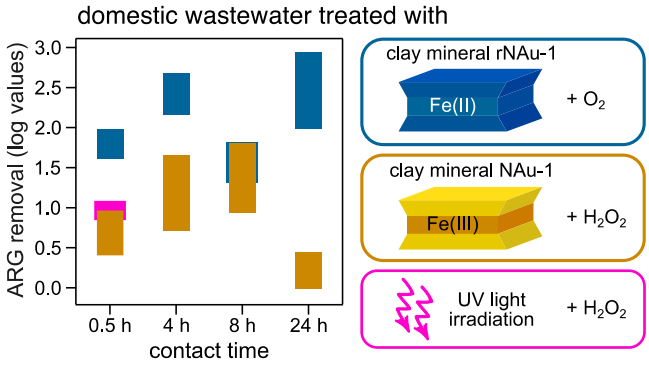

Fig. 3.9: Removal of antimicrobial resistance genes (ARG) are significantly higher with the novel clay mineral-based advanced oxidation processes (AOPs) rNAu-1 (blue) and NAu-1/ H_2O_2 (brown) compared to the conventional AOP UV/H_2O_2 (pink). Figure from Adamou et al. (2024).

3.6 References

Adamou, P., Entwistle, J., Graham, D. W., & Neumann, A. (2024)
Novel mineral-based advanced oxidation processes for enhancing the removal of antibiotic resistance genes from domestic wastewater *[Manuscript submitted for publication], LES, PSI.*

Baeyens, B., & Bradbury, M. H. (1997)
A mechanistic description of Ni and Zn sorption on montmorillonite. Part I: Titration and sorption measurements. *Journal of Contaminant Hydrology*, *27*(3-4), 199-222.
https://doi.org/10.1016/S0169-7722(97)00008-9

Finck, N., Bouby, M., Dardenne, K., & Geckeis, H. (2012)
Characterization of Eu(III) co-precipitated with and adsorbed on hectorite: from macroscopic crystallites to nanoparticles. *Mineralogical Magazine*, *76*(7), 2723-2740.
https://doi.org/10.1180/minmag.2012.076.7.07

Finck, N., Dardenne, K., & Geckeis, H. (2015)
Am(III) coprecipitation with and adsorption on the smectite hectorite. *Chemical Geology*, *409*, 12-19.
https://doi.org/10.1016/j.chemgeo.2015.04.020

Glaus, M. A., Van Loon, L. R., & Wüst, R. A. J. (2024)
Diffusion of HTO, ^{36}Cl and ^{22}Na in the Mesozoic rocks of northern Switzerland: II. Data interpretation in terms of an electrical double layer model. *Applied Geochemistry*, *162*, 105842.
https://doi.org/10.1016/j.apgeochem.2023.105842

Gorski, C. A., Aeschbacher, M., Soltermann, D., Voegelin, A., Baeyens, B., Marques Fernandes, M., Hofstetter, T. B., & Sander, M. (2012)
Redox properties of structural Fe in clay minerals. 1. Electrochemical quantification of electron-donating and -accepting capacities of smectites. *Environmental Science and Technology*, *46*, 9360−9368.
https://doi.org/10.1021/es3020138

Hummel, W. & Thoenen, T. (2023)
The PSI Chemical Thermodynamic Database 2020. *Nagra Technical Report NTB 21-03.*
https://nagra.ch/downloads/technical-report-21-03/

Juillot, F., Morin, G., Ildefonse, P., Calas, G., & Brown, G. E. (2006)
EXAFS signature of structural Zn at trace levels in natural and synthetic trioctahedral 2:1 phyllosilicates. *American Mineralogist*, *91*(8-9), 1432-1441.
https://doi.org/10.2138/am.2006.1923

Kulik, D. A., Marques Fernandes, M., & Baeyens, B. (2018)
The 2SPNE SC/CE sorption model in GEM-Selektor v.3.4 code package (ClaySor): Implementation, tests, and user guide. *Nagra Arbeitsbericht NAB 18-27*.

Laboratory for Waste Management (2023)
Progress Report 2023. *Paul Scherrer Institut, Nuclear Energy and Safety Department.*
https://www.psi.ch/en/les/annual-reports

Latta, D. E., Neumann, A., Premaratne, W. A. P. J., & Scherer, M. M. (2017)
Fe(II)–Fe(III) electron transfer in a clay mineral with low Fe content. *ACS Earth and Space Chemistry*, *1*, 197-208.
https://doi.org/10.1021/acsearthspacechem.7b00013

Marinich, O., Marques Fernandes, M., Miron, G. D., & Kulik, D. A. (2024)
ClaySor 2023: Update of 2SPNE SC/CE sorption model for illite and montmorillonite in GEMS implementation. *Nagra Technical Report NTB 23-05.*

Marques Fernandes, M., Marinich, O., Miron, G. D., & Baeyens, B. (2024a)
Sorption of Cs, Ni, Eu, Th and U on drill core samples of Opalinus Clay and confining geological units from deep boreholes in the potential siting regions Nördlich Lägern, Zürich Nordost and Jura Ost: Measurements and predictive sorption modelling. *Nagra Technical Report NTB 23-01.*

Marques Fernandes, M., Mazurek, M., Wersin, P., Wüst, R., & Baeyens, B. (2024b)
Cation-exchange properties of the Mesozoic sedimentary sequence of Northern Switzerland and modelling of the Opalinus Clay porewater. *Applied Geochemistry*, *162*, 105852.
https://doi.org/10.1016/j.apgeochem.2023.105852

Neumann, A., Hofstetter, T. B., Lüssi, M., Cirpka, O. A., Petit, S., & Schwarzenbach, R. P. (2008)
Assessing the redox reactivity of structural iron in smectites using nitroaromatic compounds as kinetic probes. *Environmental Science and Technology*, *42*, 8381–8387.
https://doi.org/10.1021/es801840x

Neumann, A., Olson, T. L., & Scherer, M. M. (2013)
Spectroscopic evidence for Fe(II)–Fe(III) electron transfer at clay mineral edge and basal sites. *Environmental Science and Technology*, *47*, 6969–6977.
https://doi.org/10.1021/es304744v

Pham, A. L.-T., Doyle, F. M., & Sedlak, D. L. (2012)
Kinetics and efficiency of H_2O_2 activation by iron-containing minerals and aquifer materials. *Water Research*, *46*(19), 6454-6462.
https://doi.org/10.1016/j.watres.2012.09.020

Qian, Y. T., Scheinost, A. C., Grangeon, S., Hoving, A., Churakov, S. V., & Marques Fernandes, M. (2024) Influence of structural Fe content in clay minerals on selenite redox reactions: Kinetics and structural transformations. *Geochimica et Cosmochimica Acta*, *377*, 19-33.
https://doi.org/10.1016/j.gca.2024.05.012

Rothwell, K. A., Pentrák, M., Pentrakova, L. Stucki, J. W., & Neumann, A. (2023)
Reduction pathway-dependent formation of reactive Fe(II) sites in clay mineral. *Environmental Science and Technology*, *57*, 10231-10241.
https://doi.org/10.1021/acs.est.3c01655

Schlegel, M. (2008)
Polarized EXAFS characterization of the sorption mechanism of yttrium on hectorite. *Radiochimica Acta*, *96*(9-11), 667-672.
https://doi.org/10.1524/ract.2008.1551

Soltermann, D., Marques Fernandes, M., Baeyens, B., Dähn, R., Joshi, P. A., Scheinost, A. C., & Gorski, C. A. (2014)
Fe(II) uptake on natural montmorillonites. I. Macroscopic and spectroscopic characterization. *Environmental Science and Technology*, *48*, 8688−8697.
https://doi.org/10.1021/es501887q

Tong, M., Yuan, S., Ma, S., Jin, M., Liu, D., Cheng, D., Liu, X., Gan, Y., & Wang, Y. (2016)
Production of abundant hydroxyl radicals from oxygenation of subsurface sediments. *Environmental Science and Technology*, *50*(1), 214-221.
https://doi.org/10.1021/acs.est.5b04323

Van Loon, L. R., & Soler, J. M. (2003)
Diffusion of HTO, $^{36}Cl^{-}$, $^{125}I^{-}$ and $^{22}Na^{+}$ in Opalinus Clay: Effect of confining pressure, sample orientation, sample depth and temperature (PSI Bericht 04-03). *Paul Scherrer Institut, Nuclear Energy and Safety Department; and (NTB 03-07). Nagra.*
https://nagra.ch/downloads/technical-report-ntb-03-07/

Van Loon, L. R., Bunic, P., Frick, S., Glaus, M. A., & Wüst, R. A. J. (2023)
Diffusion of HTO, ^{36}Cl and ^{22}Na in the Mesozoic rocks of northern Switzerland. I: Effective diffusion coefficients and capacity factors across the heterogeneous sediment sequences. *Applied Geochemistry*, *159*, 105843.
https://doi.org/10.1016/j.apgeochem.2023.105843

Van Loon, L. R., Bunic, P., Frick, S., Glaus, M. A. & Wüst, R. A. J. (2024)
Diffusion Measurements of HTO, $^{36}Cl^{-}$ and $^{22}Na^{+}$ on Rock Samples of Opalinus Clay and Confining Units from Deep Bore Holes at the Potential Siting Regions for a Deep Geological Repository for Radioactive Waste in Switzerland: Jura Ost, Nördlich Lägern and Zürich Nordost. *Nagra Arbeitsbericht NAB 23-26.*

Van Loon, L. R., Soler, J. M., Müller, W., & Bradbury, M. H. (2004)
Anisotropic diffusion in layered argillaceous rocks: a case study with Opalinus Clay. *Environmental Science and Technology*, *38*, 5721-5728.
https://doi.org/10.1021/es049937g

White, M. L. (2024)
Harnessing Microbially-mediated Redox Processes for Sustainable Water Treatment *[Unpublished Doctoral Thesis], Newcastle University.*

4 CEMENT SCIENCE AND ENGINEERING

Provis J.L., Tits J., Wang D. (postdoc), Laube A., Kunz D., Boiger R., Prasianakis N.I., Miron G.D., Xi B., Churakov S.V., Ma B., Bayram S.E. (PhD student), Ban J. (PhD student), Delekta M. (PhD student), Bonvin M. (master student), Schmitt J. (Guest researcher)

4.1 Introduction

This chapter describes some highlights of the LES research in cement science in 2024. The ongoing projects in this topic span a wide variety of areas of interest, from steel corrosion to fundamental cement science to concrete design and testing. LES cement science activities involve extensive collaborations within and beyond the nuclear sector, including participation in major European consortia, beamline-based research, and industrial connections; the result of this high degree of connectivity is that we can ensure the relevance and quality of our research, while delivering answers to important questions in cement science and geodisposal of nuclear wastes. The following sections provide snapshots of some ongoing projects.

The project “LOMIR” was established with the aim to gain insight in the fate of ^{14}C released during anoxic corrosion of irradiated steel under the hyperalkaline conditions existing in the cementitious near field of a deep geological repository for low and intermediate level radioactive waste (L/ILW DGR). In 2024, the last sampling campaign of this project has been carried out, and this report gives a brief summary of the outcomes of the project.

The role of complexing ligands in Th(IV) sorption on calcium silicate hydrate (C-S-H) is a fundamental question that underpins how we describe actinide sorption and mobility in the complex chemical environment of an underground repository. The understanding of the interactions between actinides, dissolved calcium, and complexing ligands has evolved significantly in recent years, and our recent work has applied this new knowledge to investigate and update the descriptions of how dissolved actinides interact with oxide surfaces.

The description of the thermodynamic stability and structure of cement phases is essential in understanding and predicting their evolution during cement hydration, and in service in applications including waste disposal and civil construction. LES has longstanding interests and expertise in this area, and our work in synthesising cementitious hydrate phases for detailed analysis, and also in understanding fundamental phase chemistry, is highlighted.

Machine learning and Artificial Intelligence (AI) have been widely used for material discovery and process optimisation. Within the SCENE project (Swiss Center of Excellence for Net zero Emissions) research has been initiated in the direction of reducing the carbon emissions of cementitious materials. A numerical workflow based on a combination of AI and physical modelling techniques has allowed us to explore the space of possible cement recipes which can result in cements with significantly reduced CO_2 emissions, and at the same time maintain high levels of elastic properties.

Within the 4-year SNSF-Sinergia project PRINCE, a consortium of researchers from LES/PSI, EMPA, University of Berne and ETHZ seeks to make breakthroughs in the fundamental understanding of the processes that occur at the interface between steel and a porous medium, in particular in a cementitious environment. The project comprises 7 PhD students and 2 postdoctoral fellows working jointly on fundamental aspects of steel-concrete interface, namely the kinetics of the electrochemical iron dissolution, transport of ferrous and ferric ions in pore water solution, redox and complexation reaction in the aqueous phase, interactions with solids, as well as nucleation and precipitation phenomena.

4.2 LOng-term Monitoring of ^{14}C compounds released during corrosion of Irradiated steel (LOMIR)

The project “LOMIR” was established with the aim to gain insight into the fate of ^{14}C released during anoxic corrosion of irradiated steel under the hyperalkaline conditions existing in the cementitious near field of a deep geological repository for low and intermediate level radioactive waste (L/ILW DGR). To achieve this goal, in 2016 PSI established a long-term corrosion experiment with an irradiated stainless-steel nut from the Gösgen nuclear power plant (Switzerland), to monitor the speciation and concentration of ^{14}C released under conditions relevant for a L/ILW DGR. In 2024, the last sampling campaign of this project has been carried out and this report gives a brief summary of the outcomes of the project. Detailed information can be found in the final report of the project (Tits et al., 2024). In 2025 and 2026, the experiment will be decommissioned, and it is planned that as part of this process, the slices of the corroded irradiated steel nut will be examined.

Briefly, two 2 mm thick slices of an irradiated steel

guide tube nut from the Gösgen nuclear power plant (Switzerland) were immersed in 300 mL of a synthetic, highly alkaline, aged cement pore water (ACW, pH = 12.5) in a 550 mL gas-tight stainless steel pressure reactor, under 5 bar of N_2. Both the solution and the gas phase were sampled at regular time intervals during the corrosion experiment using an in-house developed sampling system allowing sampling without opening the reactor. To ensure similar conditions over the entire duration of the corrosion experiment, 7 mL of fresh O_2-free ACW was re-injected and the pressure was re-adjusted to 5 bar with N_2 after each sampling campaign. $^{12/13}C$ organic compounds in solution and in the gas phase were measured by high performance ion exchange chromatography coupled to mass spectrometry (HPIEC-MS) and gas chromatography coupled to mass spectrometry (GC-MS). Furthermore, the H_2 concentration was monitored by GC-MS. Identification and quantification of individual ^{14}C-compounds in both solution and gas phases are performed using compound-specific radiocarbon analysis (CSRA) based on chromatographic separation techniques (HPIEC and GC) combined with accelerator mass spectrometry (AMS) measurements (Cvetković et al., 2018a; Cvetković et al., 2018b; Guillemot et al., 2020).

The vast majority of the release of stable $^{12/13}C$ was during the initial phase of the experiment within the first 30 days, whern the amounts released to the solution are 2 – 4 times larger than those released to the gas phase. After 7.7 years, LMW $^{12/13}C$-carboxylic acids (CAs) make up approximately 26 % of the non-purgeable stable organic carbon (NPOC) in solution. The CAs include ~16.4 % formic acid (FA), ~56.4 % acetic acid (AA), and ~16.1 % lactic acid (LA), 1.5 % oxalic acid (OA) and 1.4 % glycolic acid (GA). The gaseous $^{12/13}C$ compounds identified after 7.7 years were mainly CH_4 (~84.5% C), C_2H_6 (~13.2% C) and C_3H_8 (~2.3% C). At the end of the experiment after 7.7 years, the total amounts of $^{12/13}C$ released exceeded the calculated stable carbon inventory of the steel nut slices. Both this latter observation and the observed temporal evolution of the $^{12/13}C$ release led to the conclusion that a significant part of this $^{12/13}C$ originates from organic contaminants sorbed on the surface of the steel nut slices and reactor surfaces.

The temporal evolution of the ^{14}C release during the corrosion of the irradiated steel nut segments is characterised by a fast initial release in solution of dissolved oxidised ^{14}C-bearing compounds, mainly low molecular weight carboxylic acids identical to the $^{12/13}C$ CAs found in solution, and carbonate. In the long term the concentrations of dissolved ^{14}C compounds are constant over time. It is speculated that this instantaneously released aqueous ^{14}C fraction was accumulated in an oxic corrosion layer formed on the irradiated steel nut surfaces before the start of the anoxic corrosion experiment.

^{14}C concentrations were measured in the gas phase (mainly $^{14}CH_4$ together with tiny amounts of $^{14}C_2H_6$ and ^{14}CO); the measured ^{14}C content is consistent with a predicted corrosion rate of 1 nm/a after an initial period of fast release. This release rate is similar to the H_2 production rate and within the range of corrosion rates expected for steel under anoxic alkaline conditions. The observed ^{14}C-hydrocarbon distribution in the gas phase could be an indication that a Fischer-Tropsch-like process might play a role in the formation of hydrocarbon species.

The overall conclusion of this study is that among the ^{14}C present in irradiated steel disposed under reducing conditions in a L/ILW DGR, the fraction not being instantaneously released (around 99.997% of the inventory in this case), is expected to be released as $^{14}CH_4$ into the gas phase during the course of corrosion.

4.3 Influence of EDTA on thorium(IV) sorption by TiO_2 and C-S-H phases under cement pore water conditions

Ethylenediaminetetraacetic acid (EDTA) is considered to be one of the most important complexing ligands of radionuclides in a cement-based L/ILW repository as is planned in Switzerland (Nagra, 2023). Maximum concentrations in the near-field cement pore waters (CPW) are estimated to reach values up to 0.025 M (Nagra, 2023). Thermodynamic speciation calculations reported by Hummel et al. (2022) show EDTA to exist nearly exclusively in the form of a $CaEDTA^{2-}$ complex under strongly alkaline conditions and in the presence of Ca (≥ 1 mM). Under these conditions, no major influence of EDTA complex formation on the adsorption of actinides onto cement phases is expected to occur. Recent studies (DiBlasi et al., 2021; DiBlasi et al., 2022) report the existence of very stable Ca-An(III/IV)-OH-EDTA complexes in CPW.

In the absence of further evidence from the literature, it was assumed in the most recent PSI-Nagra cement sorption database (Tits & Wieland, 2024) that the formation of such strong quaternary complexes is possible for all tri- and quaternary actinides, and so that database assigned EDTA sorption reduction factors ranging between 1000 and 33’000 depending on the type of actinide. The aim of the current study was to determine to what extent this assumption can be confirmed by experiment.

For this purpose, the effect of the EDTA concentration on Th(IV) sorption on TiO_2 (Aeroxide P25, Degussa, Germany) and a C-S-H phase (C:S=1.4) was measured in a series of preliminary batch sorption experiments.

TiO_2 was used as a reference material that is chemically stable under alkaline conditions allowing to investigate the surface adsorption behaviour of Th(IV) in the presence of EDTA under CPW conditions, whereas in the case of C-S-H phases, Th(IV) incorporation in the solid matrix is also possible due to the high recrystallisation rates of these materials (Tits & Wieland, 2024).

To get a first impression of the Th(IV) speciation in the experiments, initial speciation calculations were performed using the code 'Medusa' (https://www.kth.se/che/medusa/). The following sources were used for the thermodynamic stabilisation constants: (Thoenen et al., 2014): Th-hydroxy complexes, (Hummel et al., 2005): EDTA speciation, (Xia et al., 2003): Th-EDTA complexes. The thermodynamic stability constant for the quaternary $CaTh(OH)_4(EDTA)^{2-}$ complex was approximated by reducing the stability constant for the $CaPu(OH)_4(EDTA)^{2-}$ complex ($\log°\beta_{Pu}(1,4,1,1) = 8.9$ reported by DiBlasi et al. (2021) by 8 orders of magnitude (i.e., $\log°\beta_{Th}(1,4,1,1) = 0.9$. This reduction was made since a comparison of the stability constants of other Th(IV)-(OH)-EDTA complexes reported by Xia et al. (2003) with the respective Pu(IV)-(OH)-EDTA complexes used by DiBlasi et al. (2021) showed that the former are on average 8 orders of magnitude smaller.

The speciation plot in Fig. 4.1a shows that at pH = ~12.2, in the absence of Ca the stability of the Th(IV)-EDTA complexes is too small to exert an influence on the Th(IV) speciation. Hence, the Th(IV) is dominated by the $Th(OH)_4$ species in the whole EDTA speciation range. In the presence of 0.01 M Ca at pH = ~12.3, however, the quaternary $CaTh(OH)_4(EDTA)^{2-}$ complex dominates the Th(IV) speciation at EDTA concentrations above 10^{-4} M (Fig. 4.1c).

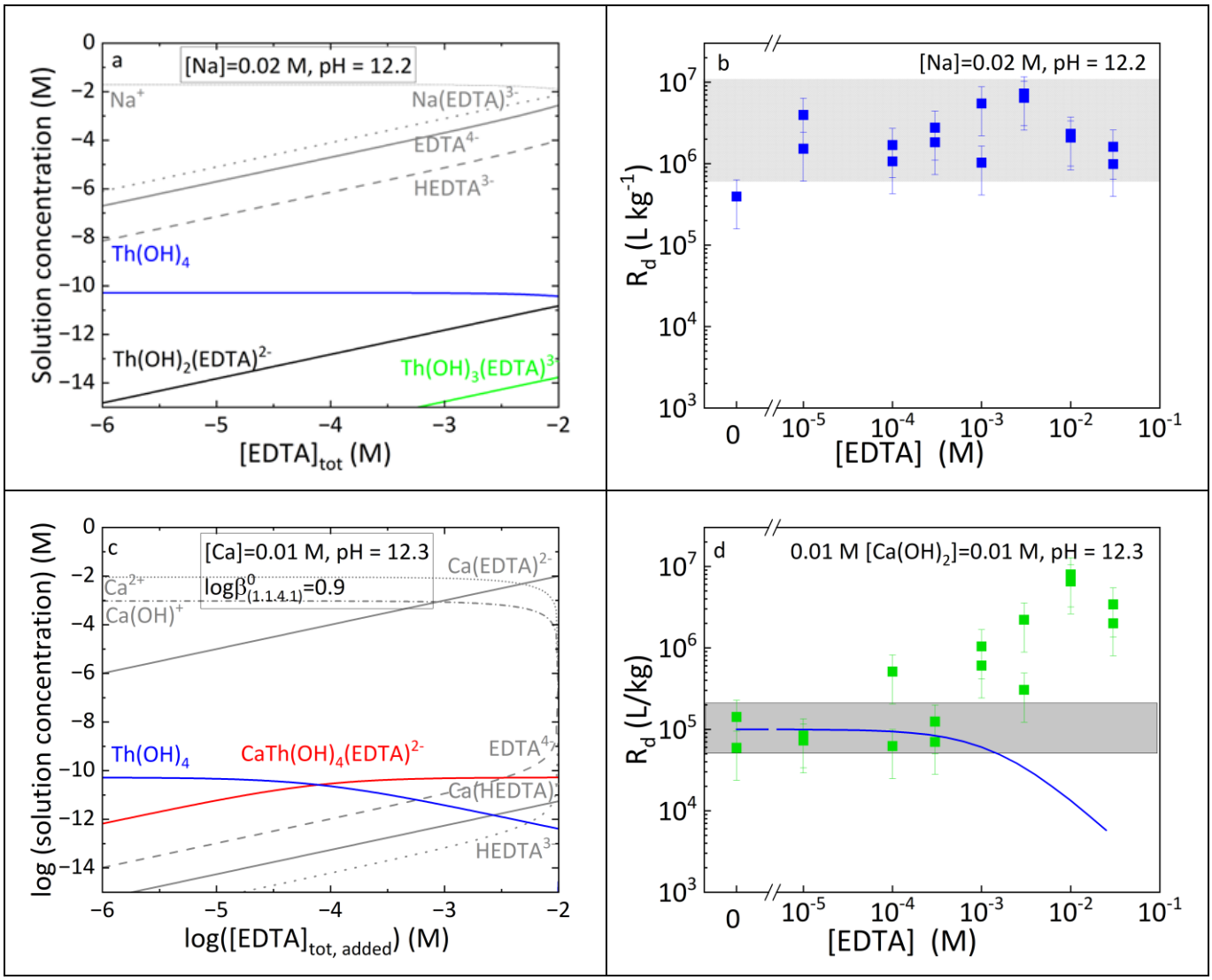

Fig. 4.1: Effect of the EDTA concentration added on the aqueous Th(IV) speciation (a, c) and on Th(IV) sorption onto TiO_2 in 0.02 M NaOH (a, b) and in 0.01 M $Ca(OH)_2$ (c, d). Solid lines are modelling curves, bullets are experimental data.

Figs. 4.1b and 4.1d show sorption R_d values of Th(IV) onto P25-TiO_2 at pH = ~12.3 as function of the equilibrium EDTA concentration in solution in the absence and in the presence of 10^{-2} M Ca. In absence of Ca (Fig. 4.1b), the measured R_d values are very high, varying between 10^6 L kg^{-1} and 10^7 L kg^{-1} in agreement with previous work on C-S-H phases and hardened cement paste (Tits & Wieland, 2018). Furthermore, it can be observed that the R_d values are constant independent of the EDTA concentration. In the presence of 10^{-2} M Ca and assuming that only the $Th(OH)_4$ species actually sorbs, a decrease of the R_d value would be expected at EDTA concentrations above 10^{-4} M as shown by the solid blue line in Fig. 4.1d. The experimental results, however, show lower R_d values at low EDTA concentrations compared to the experiment in the absence of Ca, and increasing R_d values with increasing EDTA concentrations. A potential qualitative explanation for this sorption behaviour relies on the surface characteristics of the P25-TiO_2. In the presence of 0.02 M NaOH, the surface hydroxyl groups are directly exposed to the solution allowing Th(IV) to form strong surface complexes. In the presence of 0.01 M $Ca(OH)_2$, however, Ca^{2+} ions can sorb onto the negative surface charge of P25-TiO_2 (resulting from deprotonation of the hydroxyl groups) turning the surface charge positive and making it more difficult for Th(IV) to form surface complexes with the surface hydroxyl groups and thus lowering the R_d values. At EDTA concentrations above 10^{-4} M, the negatively charged $CaTh(OH)_4(EDTA)^{2-}$ complex becomes stable and is attracted by the positively charged P25-TiO_2 surface on which it then can form strong surface complexes. This change in aqueous speciation explains the increase in R_d value at high EDTA concentrations.

The initial results from this study suggest that the reduction factors applied in the new PSI-Nagra sorption database to describe the effect of quaternary Ca-An(IV)-(OH)-EDTA complexes on An(IV) sorption were probably chosen very conservatively, and that the effect of these complexes on An(IV) sorption is much smaller than assumed. The results of the adsorption experiments with C-S-H phases are underway.

4.4 Synthesis and analysis of cementitious hydrate phases

To enable the accurate description and prediction of cement evolution in the short to long term (i.e. on timescales from a few minutes up to hundreds of thousands of years), it is essential to understand each of the potential constituent phases that can result from the interaction of cementitious materials initially with water as it hardens, and then later with groundwater and other chemical environments. It is only when this database is fully populated and validated, that we will be able to confidently and accurately predict the (geo)chemical evolution of cements throughout their entire life cycle. Cementitious hydrates tend to be complex hydrated minerals, with extensive substitution of different elements possible into different sites within their structures, and form solid solutions across wide ranges of compositions. Understanding this behaviour is essential to developing an accurate description of elemental substitutions and their effects on cement chemistry, both in the solid state and in the pore fluid that coexists with a hardened cement. Many of these important cementitious hydrate phases are incompletely understood – in part because of their complexity – and LES has for many years participated in world-leading research in synthesising and characterising the crystallographic phases that are relevant to cement systems. Calcium silicate hydrate (C-S-H) is the key binding phase in Portland cement, and its blends with supplementary cementitious materials. The synthesis of phase-pure and stoichiometrically controlled C-S-H is rather complex, and many approaches using either solid or dissolved precursors, or a mixture of both forms, are available in the literature (Walker et al., 2016). To support a line of research in understanding the mechanisms of doping and substitution of different transition metals into C-S-H, a new methodology involving dual-titration has been implemented (Bayram, in progress), and has been shown to give highly reproducible synthesis of pure C-S-H under stoichiometrically-controlled and pH-controlled conditions, Fig. 4.2.

4.5 Hydrotalcite-pyroaurite layered double hydroxide solid solution

Layered double hydroxides (LDHs) can be represented by the general chemical formula $[M^{II}_{1-x}M^{III}_x(OH)_2]^{z+}\cdot A^{n-}_{z/n}\cdot mH_2O$. Here, M^{II} and M^{III} represent divalent and trivalent metal cations, respectively, occupying octahedral positions within the positively charged main hydroxide layers; A^{n-} denotes the exchangeable interlayer anion that compensates for the positive charge of the hydroxide layers and, together with H_2O, forms the interlayer structure. LDHs are used in a wide range of applications, particularly in environmental and waste management processes. They are expected to be efficient scavengers for hazardous anions, e.g., CrO_4^{2-}, AsO_4^{3-}, I^-, SeO_3^{2-}, and TcO_4^-, and thus may play a critical role in their chemical immobilization during stabilization/solidification (S/S) (Rives, 2001).

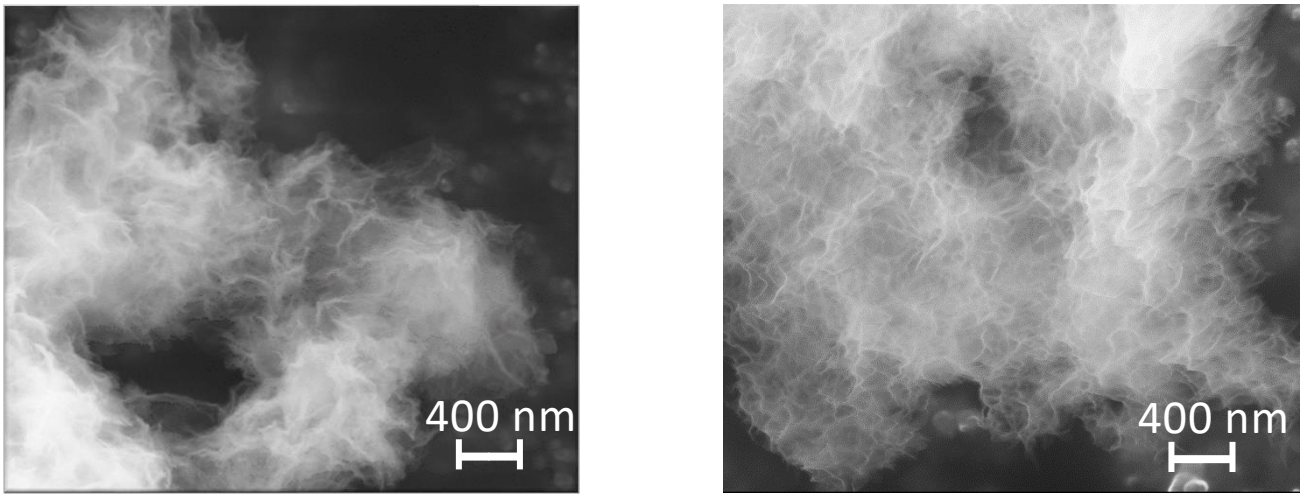

Fig. 4.2: TEM images of C-S-H synthesised using the new dual titration method, with $Ca((NO)_3)_2$ and Na_2SiO_3 solutions dosed into an initial solution of NaOH at molar ratios of (left) 1.0 and (right) 2.0. The molar dosing rate ratios are also reflected in the stoichiometry of the synthesised products. From (Bayram, in progress).

Hydrotalcite, a member of the LDH family, is also known as an "anionic clay", and is the archetype of a group of minerals which widely exist in nature with a general formula of $Mg_{4\text{-}8}Al_2CO_3(OH)_{12\text{-}20}\cdot 4(H_2O)$. It is also a common hydration product in cement binders rich in Al and Mg. In Portland cement, it typically forms in a semi-amorphous state, often resulting in various solid solutions. Hydrotalcite is also one of the primary precipitation products in alkali-activated materials, owing to the high Al and Mg content of precursors like blast furnace slag. In some emerging MgO-based cements, hydrotalcite can form alongside the major product M-S-H if the raw materials blend contains sufficient aluminium (Walling & Provis, 2016).

Iron is ubiquitous in modern low-carbon cements due to the use of Fe-rich raw materials in their production, which yields e.g., tetracalcium aluminoferrite (brownmillerite) in Portland cement, and olivine $(Mg,Fe)_2SiO_4$ in MgO-based cements, and the widespread use of various Fe-rich supplementary cementitious materials or precursors. Fe^{III} can incorporate into the host layer structure of hydrotalcite by substituting the octahedrally coordinated host metal Al^{III}, as they share the same valence states and have similar ionic radii to Al^{III} (~0.675 Å) and Fe^{III} (~0.785 Å) (Shannon, 1976). This allows for the formation of Mg^{II}–Al^{III}/Fe^{III} hydrotalcite solid solutions with varying levels of Fe^{3+} substitution, with pyroaurite $(Mg_6Fe_2(OH)_{16}CO_3\cdot nH_2O)$ as the Fe^{III}-endmember (Palmer et al., 2009; Rozov et al., 2010). Fig. 4.3 shows a schematic diagram of the structure of the solid solution phase. The structural incorporation of Fe^{III} significantly affects the charge density, the distribution of M^{III} sites, and the stacking sequence of host layers, thereby influencing the stability of LDH phases and their physicochemical properties.

A detailed, molecular-level understanding of the structure of this phase across the full solid-solution range is still lacking. Moreover, the current thermodynamic database, as seen in Cemdata (Lothenbach et al., 2019) and Rozov et al. (2010), is incomplete and requires additional primary data to confirm its reliability. Bridging this data gap by gathering deeper structural and more robust thermodynamic data is essential to deepen our understanding. This effort will also support more accurate thermodynamic modeling of material chemistry and cement binders.

We observed that as the Fe content increases, no second phase is formed, but the XRD peaks undergo a continuous shift (Fig. 4.4a), indicating the formation of a solid solution throughout the hydrotalcite–pyroaurite series. The diffraction peaks were indexed on a hexagonal unit cell with space group $R\bar{3}m$. Because the ionic radius of Fe^{3+} is larger than that of Al^{3+}, a_0=b_0 increases with Fe incorporation (Fig. 4.4b). The variation of the cell parameter a_0=b_0 aligns well with Vegard's law. The interlayer distance depends on the

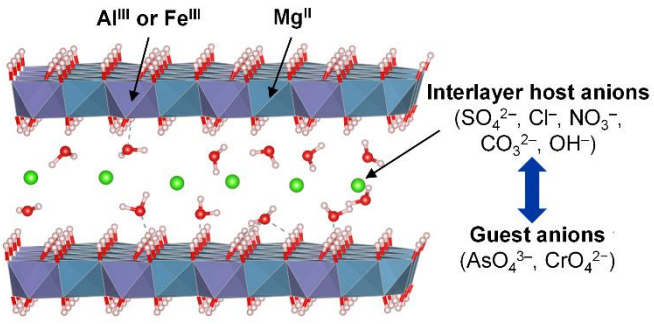

Fig. 4.3: Schematic diagram of molecular structure of the hydrotalcite-pyroaurite solid solution and possible structural replacement.

layer charge density, the nature of the interlayer anion (CO_3^{2-}), and the number of water molecules in the interlayer space. Since the $Mg^{2+}/(Al^{3+} + Fe^{3+})$ ratio is kept constant, the slight increase in c_0 with Fe replacement can reasonably be attributed to the replacement of Al^{3+} (R = 0.535 Å) by Fe^{3+}, which has a larger ionic radius (R = 0.645 Å).

Synchrotron-based X-ray absorption spectroscopy (XAS) was used to analyse the local structure of the hydrotalcite–pyroaurite solid solution (Fig. 4.5). It was observed that, with the substitution of Fe, both the Fe–O and Fe–Mg bond lengths in the crystal structure increase, which is consistent with the findings from XRD refinement.

The hydrotalcite-pyroaurite solid solutions were re-equilibrated in degassed Milli-Q water to measure their solubility. Three temperatures were set: 7°C, 20°C, and 65°C. The temperature dependence of the solubility products was determined using GEMS, based on the solubility measurements. This analysis applied the built-in three-term temperature extrapolation functions, with entropy (S^0) and heat capacity (C_p^0) adjusted to optimize the fit between calculated solubility products and experimental data. Subsequently, the experimentally measured K_{sp} data at room temperature were used to calculate the theoretical K_{sp} values of the solid solution using GEMS, thereby establishing a solid solution model. The results show that the newly developed model aligns more closely with the experimental data compared to the previous model (Rozov et al., 2010), Fig. 4.6.

4.6 Low carbon cements and concretes

The role of cements and concretes in the decarbonisation of global society (Provis et al., 2024) – as well as (and including) their role in nuclear waste disposal (Ma et al., 2024) – leads LES to participate in important and forward-looking research activities in this area. We particularly focus on innovative non-Portland cement chemistries, seeking materials that will serve as a high-quality and reliable basis for durable engineering structures. Binder systems of interest include alkali-activated/"geopolymer" cements (Kriven et al., 2024; Stefanini et al., 2024), magnesium silicate hydrates (Sreenivasan et al., 2024), magnesium phosphate cements (Dabarera et al., 2024), and innovative variants or blends with some (but reduced) Portland cement content (Baral et al., 2024; Vigor et al., 2024). Appropriate and accurate durability testing of these materials is essential in enabling their uptake in civil construction and other applications, as well as being particularly critical for use in the nuclear sector due to the much longer service lives (thousands of years or more) that are demanded from some cementitious materials used in the nuclear sector (Ma et al., 2024). However, even for the conventional service life range of 50-100 years that is commonly specified in the construction sector (Provis, 2024), it is essential that non-conventional materials are assessed fairly and appropriately, which is challenging when the established test methods are generally derived from – and assume the basic chemistry of – degradation processes that are applicable to conventional Portland cement. So, LES researchers work in collaboration with national and international partners to develop, and understand, the mechanisms that underpin cement and concrete durability, and the relationships between fundamental cement science and the engineering application of test results in designing and using sustainable cements and concretes for construction and waste conditioning applications (Bernal et al., 2024; Chaerun et al., 2024; Jin et al., 2024).

Working in collaboration with the University of Sheffield (UK) and Sumitomo Mitsui Construction Co. (Japan), we have published (Geddes et al., 2024) a description of the mechanisms that control long-term strength development (Fig. 4.7) and nano- and micro-

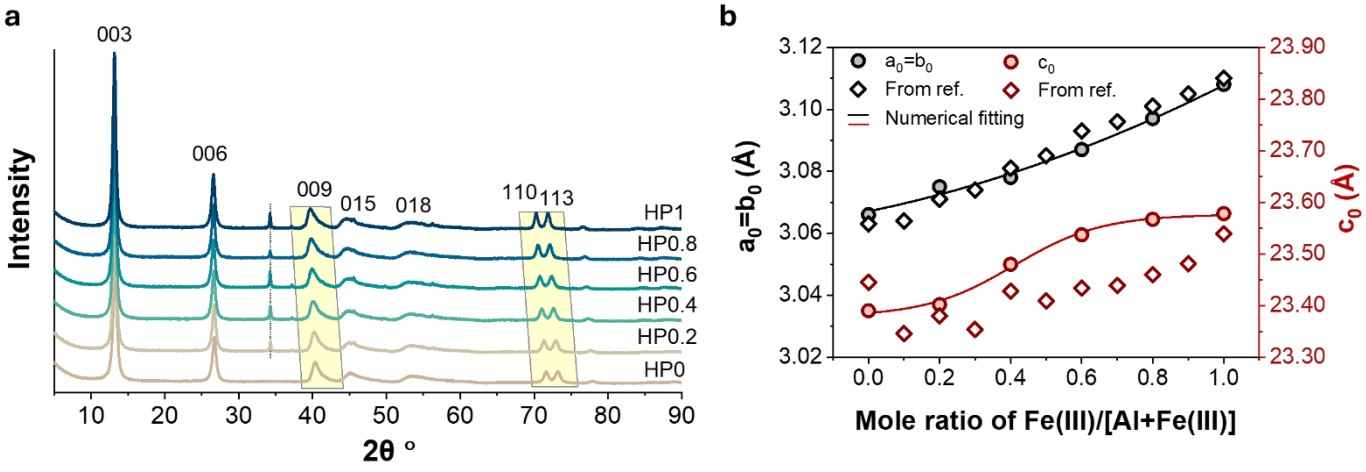

Fig. 4.4: XRD patterns and unit cell parameters in the hydrotalcite-pyroaurite solid solution system.

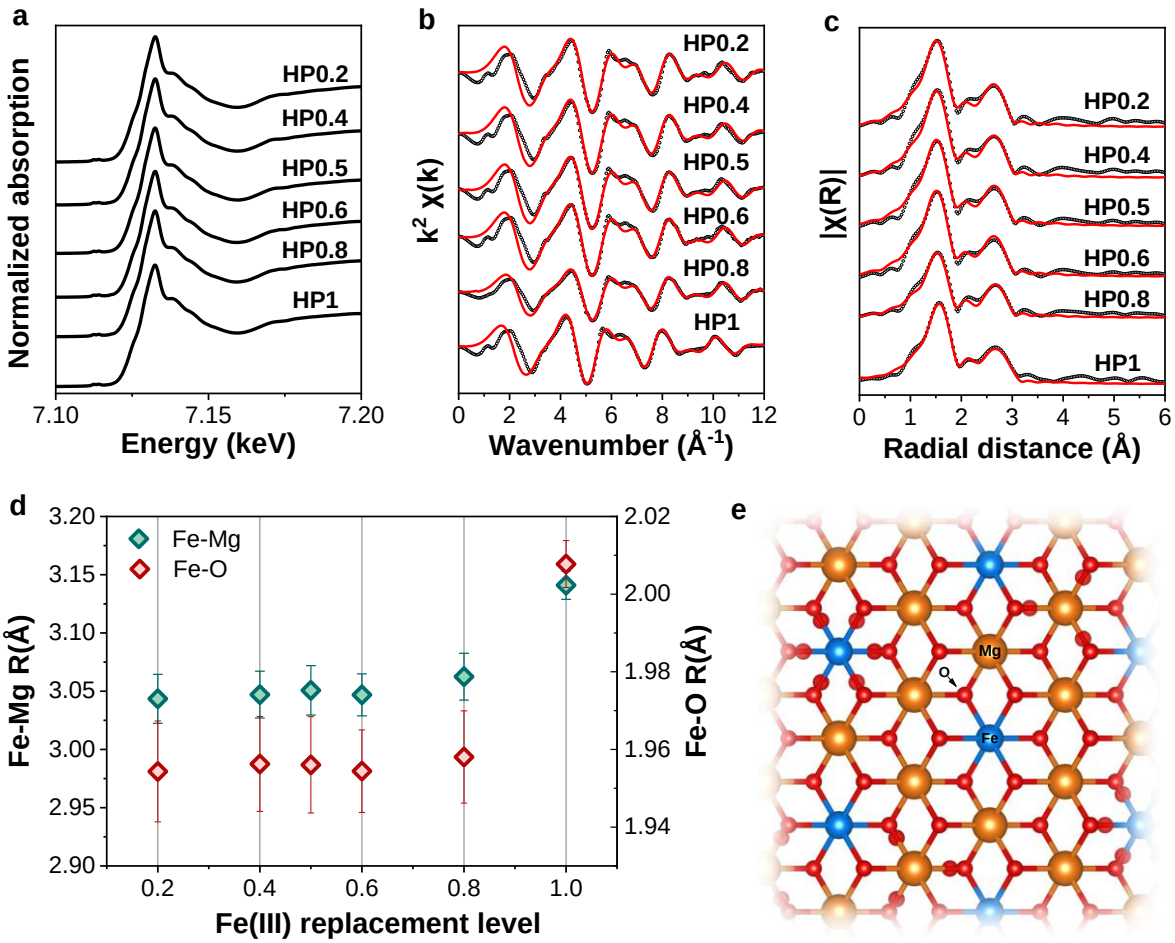

Fig. 4.5: Experimental Fe K-edge XAS spectra and fitting results of hydrotalcite-pyroaurite solid solution. (a) Normalized XANES spectra. (b) k^2-weighted EXAFS oscillations. (c) Fourier-transformed EXAFS signals. The black circles are experimental data, and the red solid curves are quantitative fitting results. (d) Local structure obtained from EXAFS refinement at Fe-K-edge. (e) Schematic diagram of the local structure. The yellow atoms are Mg, the blue atoms are Fe, and the red atoms are O.

structural evolution (Fig. 4.8) in some high-performance concretes that have been produced and formulated without Portland cement, and at exceptionally low water content (water/binder ratio 0.16). These concretes, which were developed and implemented by Sumitomo Mitsui Construction Co. (Shinozaki et al., 2021), gain their initial fluidity and setting from an innovative combination of chemical activation and pH-triggered release of superplasticisers (Walkley et al., 2022).

4.7 AI assisted discovery of green cement recipes "SCENE project"

Within the SCENE project (Swiss Center of Excellence for Net zero Emissions), research has been initiated in the direction of reducing the carbon emissions of cementitious materials. The specific study focuses on optimizing technical cycles and more specific on strategies to reduce carbon emissions from cement production, a sector responsible for approximately 8% of global CO_2 emissions. The aim of the project is to develop cementitious blends that lower environmental impact while maintaining material performance of cement products.

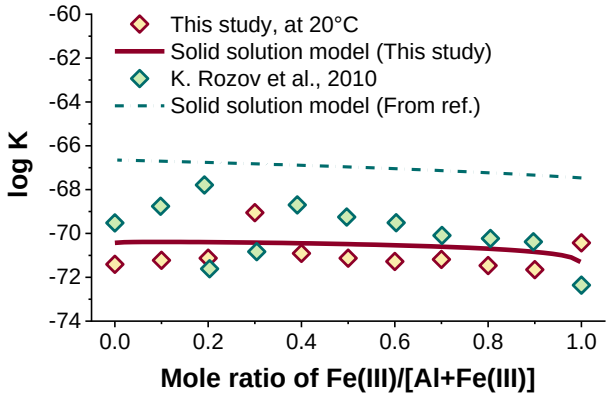

Fig. 4.6: Solubility products from experiment and solid solution model for hydrotalcite-pyroaurite solid solution compared to the data from literature as a function of Fe(III)/[Al+Fe(III)].

Traditionally, concrete and cement mix design has relied on trial-and-error lab testing and expert judgment, which are often costly and time-consuming. A novel approach is developed by combining thermodynamic and elasticity modeling, machine learning and multi-objective optimization by simultaneously considering the reduction of emissions and the maintenance of the material mechanical properties. The workflow consists of several steps, as illustrated in Fig. 4.9: I) A database is created for training the machine learning models, which relates the cement ingredients to the elastic properties of hardened cement, using the thermodynamic software GEMS; II) A neural network model is trained to accelerate calculations; III) discovery of optimum recipes using mathematical constrained multi-objective optimization techniques.

The underlying dataset for the parameter optimization is based on the results of thermodynamic modeling of cement paste hydration taking into account the initial recipe composition. These hydration products offer insights into paste-scale mechanical properties, such as elastic modulus, which in this case is estimated using a self-consistent homogenization scheme. This dataset is used to train an Artificial Neural Network (ANN) model to predict the elastic modulus directly from cement recipes composition, accelerating model evaluations by several orders of magnitude. The optimal recipes are determined through multi-objective constrained optimization to minimize CO_2 emissions while maximizing bulk modulus by using the non-dominated sorting genetic algorithm. The model leverages a Pareto front to effectively balance these objectives.

The optimization yields a series of optimal cement recipes on a Pareto front, showcasing optimal tradeoffs between bulk modulus (ranging from 21 to 28 GPa) and CO_2 emissions (0.48 to 0.57 kg CO_2 per kg of cement paste) for the considered constraints. This methodology demonstrates significant potential to reduce CO_2 emissions while maintaining or even enhancing the mechanical properties of cementitious materials, supporting sustainability goals in construction.

4.8 SNSF-Sinergia project: PRocesses at the INterface of iron and Cement (Prince)

The direct costs related to corrosion of infrastructure in the European Union, for example, are estimated at 250 billion EUR annually. Within the SNSF-Sinergia project PRINCE (https://data.snf.ch/grants/grant/10000099) a consortium of researchers from LES/PSI, EMPA, University of Berne and ETHZ seeks to make a breakthrough in the fundamental understanding of the processes that occur at the interface between steel and a porous medium, in particular in a cementitious environment. The project comprises 7 PhD students and 2 postdoctoral fellows working jointly on fundamental aspects of steel-concrete interface namely 1) the kinetics of electrochemical iron dissolution, which is coupled to 2) transport of dissolved ferrous and ferric ions through the liquid phase held within a porous medium, and the simultaneously occurring 3) chemical reactions (complexation, oxidation,…) and 4) interactions with solid phases (e.g. sorption in calcium silicate hydrates (C-S-H)) as well as 5) nucleation and precipitation of solids. The comprehensive and collaborative approach followed by the project partners involves scientific methods from physics, chemistry, electrochemistry, corrosion science, and civil engineering, in particular, molecular simulations, spectroscopic analyses, thermodynamic modelling, reactive transport modelling, and porous media characterization. A particular advantage of the proposed approach is that it not only holistically considers the processes of different type (chemical, electrochemical, physical) that occur at different length scales, but also considers the interfaces and interrelations between these.

This 4-year multidisciplinary project started in summer 2024 will boost the scientific progress needed to make technological breakthroughs and to address key socio-economic and environmental challenges, as well as to extend the service life of reinforced concrete structures.

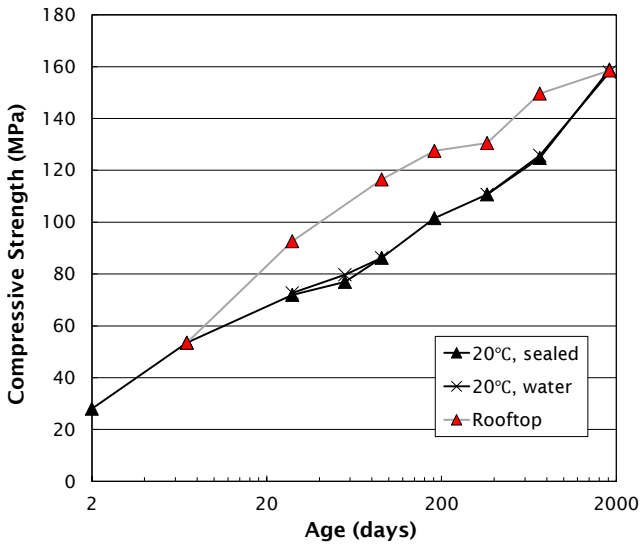

Fig. 4.7: Strength development of zero-cement concretes during very extended durations of sealed or underwater curing, or exposure on a rooftop in Tokyo. The concretes are produced from a blend of silica fume, fly ash, and blast furnace slag, with a ferronickel slag fine aggregate and conventional coarse aggregate, water/binder ratio 0.16, and using a commercial expansive additive as a chemical activator.

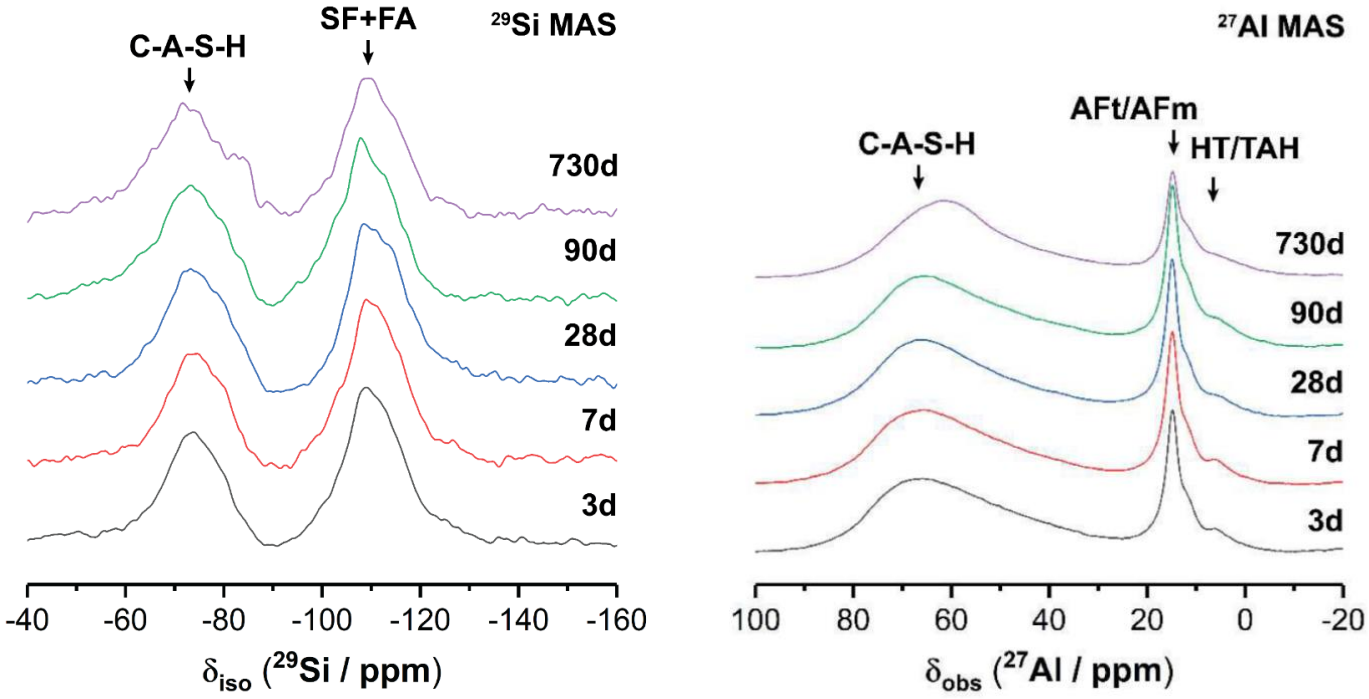

Fig. 4.8: Magic angle spinning nuclear magnetic resonance (MAS NMR) spectra of paste samples corresponding to the mix designs shown in Fig. 4.6, showing the progressive and continuous development of C-A-S-H as the main binding phase in these materials, even in the absence of any Portland cement, and the stability of the phase assemblage formed. SF and FA stands for Silica Fume (SF) and Fly Ash (FA).

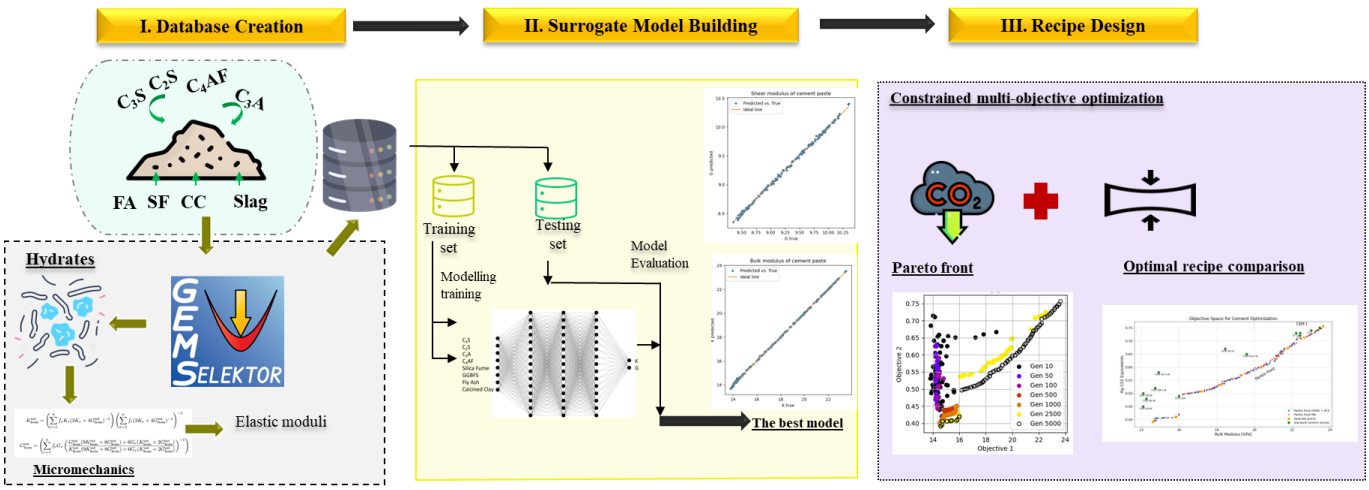

Fig. 4.9: The design workflow of green cement recipe discovery is illustrated (Figures are from Boiger et al., 2025, icons from flaticon.com).

4.9 References

Baral, A., Pesce, C., Yorkshire, A. S., Zhakiyeva, Z., Snellings, R., Hanein, T., Provis, J. L., & Peys, A. (2024)
Characterisation of iron-rich cementitious materials. *Cement and Concrete Research*, *177*, 107419.
https://doi.org/https://doi.org/10.1016/j.cemconres.2023.107419

Bayram, S. E. (in progress)
PhD thesis PSI, Villigen / EPFL, Lausanne.

Bernal, S. A., Dhandapani, Y., Elakneswaran, Y., Gluth, G. J. G., Gruyaert, E., Juenger, M. C. G., Lothenbach, B., Olonade, K. A., Sakoparnig, M., Shi, Z., Thiel, C., Van den Heede, P., Vanoutrive, H., von Greve-Dierfeld, S., De Belie, N., & Provis, J. L. (2024)
Report of RILEM TC 281-CCC: A critical review of the standardised testing methods to determine carbonation resistance of concrete. *Materials and Structures*, *57*(8), 173.
https://doi.org/https://doi.org/10.1617/s11527-024-02424-9

Boiger, R., Xi, B., Miron, G.-D., Bonvin, M., Provis, J.L., Churakov, S.V., & Prasianakis N.I. (2025)
Machine Learning-Accelerated Discovery of Green Cement Recipes. *Materials and Structures*, accepted.

Chaerun, R. I., Ishimura, M., Prihutami, P., Niu, X., Ohya, Y., Kuroda, K., Toda, K., Kikuchi, R., Otake, T., Provis, J. L., Elakneswaran, Y., & Sato, T. (2024)
Immobilisation of iodide in alkali-activated materials. *Chemosphere*, *369*, 143871.
https://doi.org/10.1016/j.chemosphere.2024.143871

Cvetković, B. Z., Salazar, G., Kunz, D., Szidat, S., & Wieland, E. (2018a)
Analysis of ^{14}C-bearing compounds released by the corrosion of irradiated steel using accelerator mass spectrometry. *Analyst*, *143*(13), 3059-3067.
https://doi.org/https://doi.org/10.1039/C8AN00237A

Cvetković, B. Z., Salazar, G., Kunz, D., Tits, J., Szidat, S., & Wieland, E. (2018b)
Quantification of dissolved organic ^{14}C-containing compounds by accelerator mass spectrometry in a corrosion experiment with irradiated steel. *Radiocarbon*, *60*(6), 1711-1727.
https://doi.org/https://doi.org/10.1017/RDC.2018.90

Dabarera, A., Fernández, R., & Provis, J. L. (2024)
A systematic review of engineering properties of magnesium potassium phosphate cement as a repair material. *Frontiers in Materials*, *11*, 1451079.
https://doi.org/https://doi.org/10.3389/fmats.2024.1451079

DiBlasi, N. A., Tasi, A. G., Gaona, X., Fellhauer, D., Dardenne, K., Rothe, J., Reed, D. T., Hixon, A. E., & Altmaier, M. (2021)
Impact of Ca(II) on the aqueous speciation, redox behavior, and environmental mobility of Pu(IV) in the presence of EDTA. *Science of The Total Environment*, *783*, 146993.
https://doi.org/https://doi.org/10.1016/j.scitotenv.2021.146993

DiBlasi, N. A., Tasi, A. G., Trumm, M., Schnurr, A., Gaona, X., Fellhauer, D., Dardenne, K., Rothe, J., Reed, D. T., Hixon, A. E., & Altmaier, M. (2022)
Pu(III) and Cm(III) in the presence of EDTA: aqueous speciation, redox behavior, and the impact of Ca(II). *RSC Advances*, *12*(15), 9478-9493.
https://doi.org/https://doi.org/10.1039/D1RA09010K

Geddes, D. A., Walkley, B., Matsuda, T., & Provis, J. L. (2024)
Multi-year cementitious hydrate product formation in non-Portland high performance concretes. *CEMENT*, *18*, 100111.
https://doi.org/https://doi.org/10.1016/j.cement.2024.100111

Guillemot, T., Salazar, G., Cvetković, B. Z., Kunz, D., Szidat, S., & Wieland, E. (2020)
Determination of ultra-low concentrations of gaseous ^{14}C-bearing hydrocarbons produced during corrosion of irradiated steel using accelerator mass spectrometry. *Analyst*, *145*(24), 7870-7883.
https://doi.org/10.1039/D0AN01517B

Hummel, W., Anderegg, G., Puigdomènech, I., Rao, L., & Tochiyama, O. (Eds.) (2005)
Chemical Thermodynamics of Compounds and Complexes of U, Np, Pu, Am, Tc, Se, Ni and Zr with Selected Organic Ligands. Chemical Thermodynamics, vol.9. Elsevier.

Hummel, W., Kulik, D. A., & Miron, G. D. (2022)
Solubility of Radionuclides and Influence of EDTA for Use in the Development of the Cement Sorption Database. *Nagra Arbeitsbericht NAB 22-38.*

Jin, H., Ghazizadeh, S., & Provis, J. L. (2024)
Thermodynamic modelling of alkali-silica reactions in blended cements. *Cement and Concrete Research*, *181*, 107543.
https://doi.org/https://doi.org/10.1016/j.cemconres.2024.107543

Kriven, W. M., Leonelli, C., Provis, J. L., Boccaccini, A. R., Attwell, C., Ducman, V. S., Ferone, C., Rossignol, S., Luukkonen, T., van Deventer, J. S. J., Emiliano, J. V., & Lombardi, J. E. (2024)
Why geopolymers and alkali-activated materials are key components of a sustainable world: A perspective contribution. *Journal of the American Ceramic Society*, *107*, 5159-5177.
https://doi.org/https://doi.org/10.1111/jace.19828

Lothenbach, B., Kulik, D. A., Matschei, T., Balonis, M., Baquerizo, L., Dilnesa, B., Miron, G. D., & Myers, R. J. (2019)
Cemdata18: A chemical thermodynamic database for hydrated Portland cements and alkali-activated materials. *Cement and Concrete Research*, *115*, 472-506.
https://doi.org/https://doi.org/10.1016/j.cemconres.2018.04.018

Ma, B., Provis, J. L., Wang, D., & Kosakowski, G. (2024)
The essential role of cement-based materials in a radioactive waste repository. *npj Materials Sustainability*, *2*(1), 21.
https://doi.org/https://doi.org/10.1038/s44296-024-00025-9

Nagra. (2023)
Chemical criteria for waste group classification: A model approach. *Nagra Arbeitsbericht NAB 23-28.*

Palmer, S. J., Frost, R. L., & Nguyen, T. (2009) Hydrotalcites and their role in coordination of anions in Bayer liquors: Anion binding in layered double hydroxides. *Coordination Chemistry Reviews*, *253*(1), 250-267.
https://doi.org/https://doi.org/10.1016/j.ccr.2008.01.012

Provis, J. L. (2024)
Material durability, material failure, and material investment—the complexity of concrete. *Communications Engineering*, *3*(1), 23.
https://doi.org/https://doi.org/10.1038/s44172-024-00172-w

Provis, J. L., Bernal, S. A., & Zhang, Z. (2024)
The decarbonization of construction — How can alkali-activated materials contribute? *Engineering*, *37*(6), 18-21.
https://doi.org/https://doi.org/10.1016/j.eng.2023.09.014

Rives, V. (2001)
Layered Double Hydroxides: Present and Future. Nova Science Publishers, New York.

Rozov, K., Berner, U., Taviot-Gueho, C., Leroux, F., Renaudin, G., Kulik, D., & Diamond, L. W. (2010) Synthesis and characterization of the LDH hydrotalcite–pyroaurite solid-solution series. *Cement and Concrete Research*, *40*(8), 1248-1254.
https://doi.org/https://doi.org/10.1016/j.cemconres.2009.08.031

Shannon, R. (1976)
Revised effective ionic radii and systematic studies of interatomic distances in halides and chalcogenides. *Acta Crystallographica Section A*, *32*(5), 751-767.
https://doi.org/10.1107/S0567739476001551

Shinozaki, H., Sasaki, W., Sanga, T., & Matsuda, T. (2021)
Trial of PC bridge in pursuit of sustainability. *Concrete Journal (JCI)*, *59*(6), 511-518.
https://doi.org/https://doi.org/10.3151/coj.59.6_511

Sreenivasan, H., Bernard, E., Santos, H. S., Nguyen, H., Moukannaa, S., Adediran, A., Provis, J. L., & Kinnunen, P. (2024)
A critical review of magnesium silicate hydrate (M-S-H) phases for binder applications. *Cement and Concrete Research*, *178*, 107462.
https://doi.org/https://doi.org/10.1016/j.cemconres.2024.107462

Stefanini, L., Ansari, D., Walkley, B., & Provis, J. L. (2024)
Characterisation of calcined waste clays from kaolinite extraction in alkali-activated GGBFS blends. *Materials Today Communications*, *38*, 107777.
https://doi.org/https://doi.org/10.1016/j.mtcomm.2023.107777

Thoenen, T., Hummel, W., Berner, U., & Curti, E. (2014)
The PSI/Nagra Chemical Thermodynamic Database 12/07. *PSI Bericht Nr. 14-04.*

Tits, J., Kunz, D., Lechleitner, F., Szidat, S., & Guillemot, T. (2024)
3rd annual report of the IGD-TP Project: "LOng-term Monitoring of C-14 compounds released during corrosion of IRradiated steel" (LOMIR).

Tits, J., & Wieland, E. (2018)
Actinide Sorption by Cementitious Materials. *Nagra Arbeitsbericht 18-04.*

Tits, J., & Wieland, E. (2024)
Radionuclide Retention in the Cementitious Near Field of a Repository for L/ILW: Development of the Cement Sorption Data Base for Use in the License Application. *Nagra Technical Report NTB 23-07.*

Vigor, J. E., Prentice, D. P., Xiao, X., Bernal, S. A., & Provis, J. L. (2024)
The pore structure and water absorption in Portland/slag blended hardened cement paste determined by synchrotron X-ray microtomography and neutron radiography. *RSC Advances*, *14*(7), 4389-4405.
https://doi.org/10.1039/D3RA06489A

Walker, C. S., Sutou, S., Oda, C., Mihara, M., & Honda, A. (2016)
Calcium silicate hydrate (C-S-H) gel solubility data and a discrete solid phase model at 25 °C based on two binary non-ideal solid solutions. *Cement and Concrete Research*, *79*, 1-30.
https://doi.org/http://dx.doi.org/10.1016/j.cemconres.2015.07.006

Walkley, B., Geddes, D. A., Matsuda, T., & Provis, J. L. (2022)
Reversible adsorption of polycarboxylates on silica fume in high pH, high ionic strength environments for control of concrete fluidity. *Langmuir*, *38*(5), 1662-1671.
https://doi.org/https://doi.org/10.1021/acs.langmuir.1c02419

Walling, S. A., & Provis, J. L. (2016)
Magnesia based cements – a journey of 150 years, and cements for the future? *Chemical Reviews*, *116*(7), 4170-4204.
https://doi.org/https://doi.org/10.1021/acs.chemrev.5b00463

Xia, Y., Felmy, A. R., Rao, L., Wang, Z., & Hess, N. J. (2003)
Thermodynamic model for the solubility of ThO_2(am) in the aqueous Na^+-H^+-OH^--NO_3^--H_2O-EDTA system. *Radiochimica Acta*, *91*(12), 751-760.
https://doi.org/https://doi.org/10.1524/ract.91.12.751.23416

5 THERMODYNAMIC MODELS AND DATABASES

Authors: Miron G.D., Glaus M.A, Marques Fernandes M., Marinich O., Churakov S.V.

5.1 Introduction

Accurate thermodynamic data and models are a prerequisite for predictive geochemical modelling of the environmental and industrial systems. LES has a long history of developing state of the art thermodynamic datasets and models based on in-house and literature experimental data. The databases and models have been the basis for the safety assessment of deep repository options and the design of engineered barriers.

An update and extension of the sorption and diffusion databases for Opalinus Clay, confining geological units, and bentonite were developed for safety assessments repository in 3 siting regions of Northern Switzerland using a unified model for sorption and diffusion, together with the newest version of the PSI/NAGRA thermodynamic database.

The ongoing SOREDA project aims to develop a sorption database for radionuclides, essential for the safety case of a deep geological repository. This database will cover a wide list of dose-relevant radionuclides as well as variety of minerals found in clay-rich host rocks and buffer materials, including clay minerals, quartz, carbonates, and iron-bearing minerals.

Thanks to the support of the Open Research Data Program of the ETH Board, a workflow for curating and importing thermodynamic datasets in a standardized format, ensuring they are accessible and traceable to their original bibliographic sources, has been implemented (THRACE project).

Funded by BGE (Bundesgesellschaft für Endlagerung) as a contribution to the THEREDA database, a Pitzer model for Al-Si speciation was developed to extend its applicability to model cement materials in saline systems.

5.2 Sorption Databases for Opalinus Clay, Confining Geological Units, and Bentonite

The safety assessment for the general licence application requires site-specific state-of-the-art sorption databases (SDBs) tailored to relevant radionuclides and the specific geological barriers, including the Opalinus Clay and bentonite buffer in the near and far field.

For several decades an extensive experimental research program of LES has been focused on developing thermodynamic sorption models for key clay minerals, such as montmorillonite and illite. These efforts support Nagra's site selection process within the Sectoral Plan for Deep Geological Repositories. Consequently, new site-specific SDBs for host rocks and the bentonite buffer were calculated, and the methodology is comprehensively described in a Nagra Technical Report (Miron et al., 2024).

The modeling utilized a robust thermodynamic framework based on the in-house ClaySor model, specifically designed for illite and montmorillonite. ClaySor employs the 2-site protolysis non-electrostatic surface complexation and cation exchange (2SPNE SC/CE) model (Baeyens & Bradbury 1997; Bradbury & Baeyens 1997, 2009a, 2009b) within the GEM-Selektor geochemical software (Kulik et al., 2013). Model parameters were revised (Marinich et al., 2024) to align with the updated PSI/Nagra chemical thermodynamic database (TDB 2020; Hummel & Thoenen, 2023). The approach was validated for key radionuclides through blind predictions of experimentally measured sorption isotherms using rock samples from drill cores taken from the three siting regions and corresponding synthetic porewaters (NTB 23-01).

Distribution coefficients (Rd values) for radionuclides of interest were computed by incorporating the clay mineral composition (illite, smectite, and illite/smectite mixed layers) and site-specific porewater chemistry. This was achieved in a single, consistent, fully coupled thermodynamic equilibrium calculation that included models for sorption on illite and montmorillonite, aqueous speciation, and solubility-limiting solid phases. For radionuclides with established sorption models, R_d values were derived for site-specific conditions, with 95% confidence intervals reflecting parameter uncertainties (Fig. 5.1).

SDBs for site-specific in situ conditions defined by pore water composition variants (reference and high-pCO_2) were produced in the form of lookup tables for varying content of 2:1 clay minerals (illite, smectite, and illite/smectite mixed layers). These tables allow for the generation of high-resolution continuous profiles of sorption properties along any borehole or stratigraphic columns with known mineralogical compositions (Fig. 5.2), for extracting data to be used in radionuclide transport models, upscaling, and for statistical approaches to provide reference, upper and lower bounding values of stratigraphic units identified in models of the geological underground.

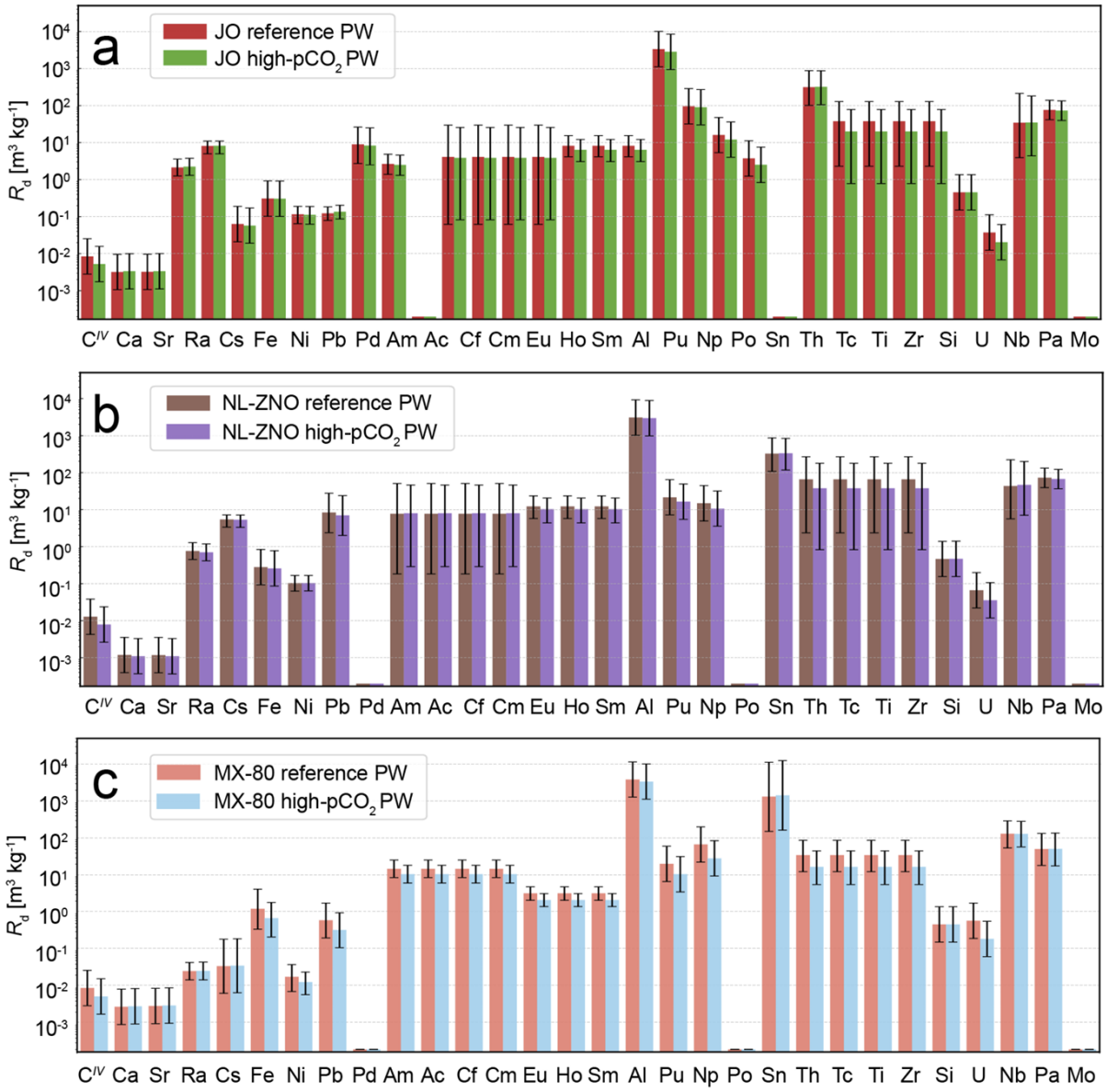

Fig. 5.1: Comparison of the calculated R_d values for argillaceous rocks with 100 wt.% 2:1 clay mineral content, for reference and high-pCO_2 porewaters (PW): (a) Jura Ost (JO), (b) Nordlich Lägern-Zürich Nord Ost (NL-ZNO) and (c) MX-80 bentonite. Plot taken from Miron et al. (2024).

5.3 Diffusion Databases for Opalinus Clay, Confining Geological Units and Bentonite

In safety assessment, diffusive properties of clay rock and bentonite need to be known for a wide range of porewater compositions, and concentrations of radionuclides are needed for dose calculations. To provide an integrated view of diffusive transport of radionuclides in dense clay-rich rocks, including the retardation induced by sorption processes at the clay surface, the use of a coherent chain of models and modelling tools is necessary for: a) a traceable description of the results, and b) minimisation of intrinsic uncertainties and errors. The effective diffusion coefficients (D_e) of charged radionuclide species in charged clay-rich rocks depend on several physical, geometrical and chemical factors (cf. Fig. 5.3).

A practicable approach for the implementation of the model scheme shown in Fig. 5.3 for clay-rich rocks has been developed by Van Loon et al. (2023) and Glaus et al. (2024b) using an electrostatic approach to incorporate chemical factors for diffusion of ions in porous media with intrinsic surface charge. In these works, diffusion data for tritiated water (HTO), $^{36}Cl^-$ and $^{22}Na^+$ tracers from more than a hundred representative rock samples from the Opalinus Clay and the confining geological units were used to set up and calibrate an approach for predictive modelling of

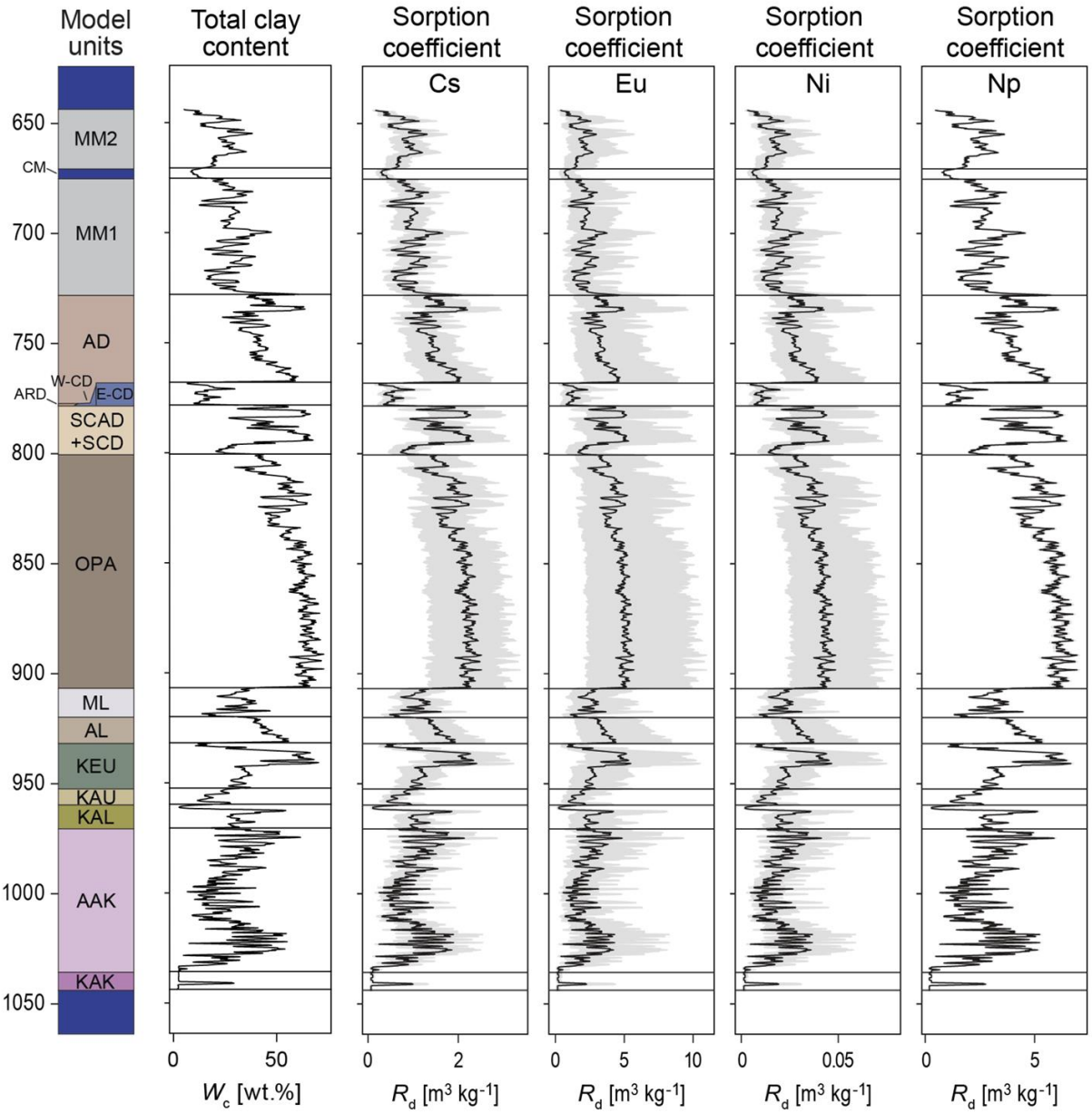

Fig. 5.2: Illustration of downhole R_d profiles for Cs, Eu, Ni and Np generated from the lookup tables, across different model geological stratigraphic units (e.g., OPA – Opalinus Clay unit) in the Nordlich Lägern region and reference pore water. Plot taken from Miron et al. (2024).

diffusive tracer transport as a function of the total clay content in the rock and the pore water composition as the main independent variables.

The diffusion data for all dose-relevant elements (Glaus et al. 2024a) are predicted using a generic implementation of electrostatic effects of the diffusion of charged species in charged porous media. Such effects are described using the so-called «Mean-Potential Donnan Layer» (MPDL) approach to quantify the equilibrium distribution of charged species between the bulk porewater and the Donnan phase (a defined volume of charged solution near the charged rock surfaces). The empirical geometrical relationships and the MPDL approach are implemented in the so-called ClaySorDif model (as an extension of the previously developed ClaySor sorption model) using a Python interface to GEMS codes. The model calibration relies on an extensive series of diffusion measurements on rock samples obtained from Nagra's deep drilling campaign in Northern Switzerland.

The results are provided in the form of look-up tables in which the diffusion-relevant parameter values are compiled for given conditions of pore water composition as a function of the total content of clay in rock (W_c). The D_e and values for the diffusion-accessible porosity (ε_{acc}) are inherently linked to the speciation of a given radioelement. Low D_e and ε_{acc} values result for elements that are predominantly present as anionic species, which is the case e.g. for Np or Th. The highest values for D_e are found for elements

predominantly present as cationic species, such as Cs^+, alkaline earth metal cations (e.g. Sr^{2+}, Ra^{2+}) or the trivalent actinides (e.g. Am^{3+}). Halogenides (e.g. I^-) generally exhibit rather low D_e and ε_{acc} values. A graphical representation of the predictions of D_e values for a typical W_c value of 56 wt.% (taken as a representative value for the Opalinus Clay and clay-rich rocks) is shown in Fig. 5.4. As can be seen from the comparison of the two types of porewater, the impact of the carbonate content and the pH on the diffusion parameters is comparatively moderate. For some elements, no impact can be documented at all. The reason is that these elements are predicted to be present as uncharged elemental species, thus showing no effects of surface diffusion or anion exclusion. The obtained data and the methodology are summarised in a dedicated Nagra Technical Report (Glaus et al., 2024a) providing a consistent description of diffusion and sorption based on the same thermodynamic input data for speciation, solubility of radionuclides, and reactive transport simulations of repository nearfield.

The compilation of look-up tables for D_e and ε_{acc} values as a function of the total clay content in rock and the reference porewaters allows for statistical analysis of a huge amount of data sets, with the aim to derive representative average values along with their statistical variances for dedicated model lithostratigraphic units used in performance assessment.

Compared with previous methods applied to derive diffusion databases for the safety analysis (Van Loon, 2014), the new approach is applicable for a broader range of conditions with regard to the mineralogical composition of the rocks and the variations of porewater chemistry. Furthermore, the model parameterization is based on a much broader set of experimental data which include the diffusion of tritiated water, $^{36}Cl^-$ and $^{22}Na^+$ tracers in more than 100 rock samples gained from the deep drilling campaign of Nagra (Van Loon et al., 2023). The comparison between the diffusion data from previous safety analyses (Van Loon, 2014) and the present data compilation shows good agreement (i.e. within the specified parameter uncertainties) for clay-rich lithologies (e.g., Opalinus clay as shown in Fig. 5.5). At the same time, notable discrepancies are reported for compacted clay minerals. These, however, can be readily explained by the different assumptions made for the assessment of "geometrical properties" properties of the clay pore network. The newly developed model covers a broader range of geochemical conditions, based on a larger experimental dataset, and thus allows us to dismiss a number of conservative assumptions imposed in earlier studies, thus reducing the overall uncertainties.

5.4 Updates of Sorption Models for Illite and Montmorillonite, and Application of the 2SPNE SC/CE Model to Kaolinite

5.4.1 Refinement of Protolysis Constants of Illite and Montmorillonite

A careful review of potentiometric titration data available in literature revealed strong correlations between sorption model parameters and protolysis constants, which are used together in sorption modelling. To improve the sorption model and to evaluate the uncertainties of the model parameter, the protolysis constants we re-fitted to the existing potentiometric titration data using the GEMSFITS package (Miron et al., 2015). The estimated parameter uncertainties are provided in Tab. 5.1. The site capacities were left unchanged, remaining consistent with the values specified in the 2SPNE SC/CE model (Bradbury & Baeyens, 1997).

As shown in Tab. 5.1, the previously estimated values of the protolysis constants fall within the 95% confidence interval of the refitted constants. The uncertainties in the $\log_{10}K$ values are smaller for illite than for montmorillonite due to the larger number of observations for illite. The updated protolysis constants were used to refit the surface complexation constants, which were adjusted in response to the changes in protolysis constants. In some cases, this resulted in reduced uncertainty in the surface complexation constants.

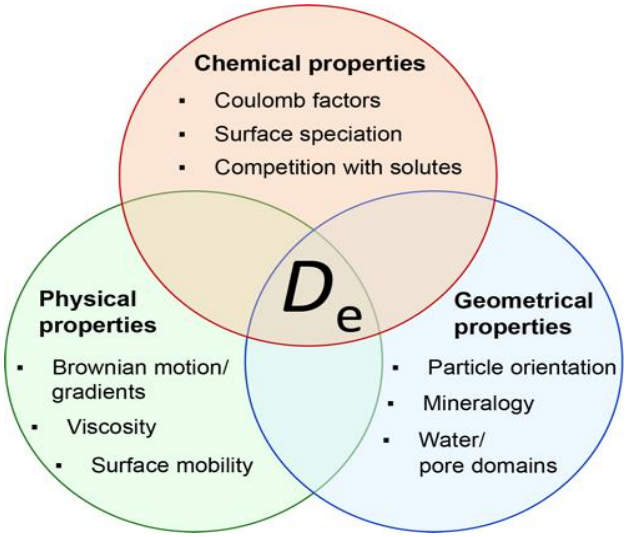

Fig. 5.3: Schematic representation of the typically most important geometrical, physical and chemical factors influencing the diffusive transport of ions species in porous media with intrinsic surface charge.

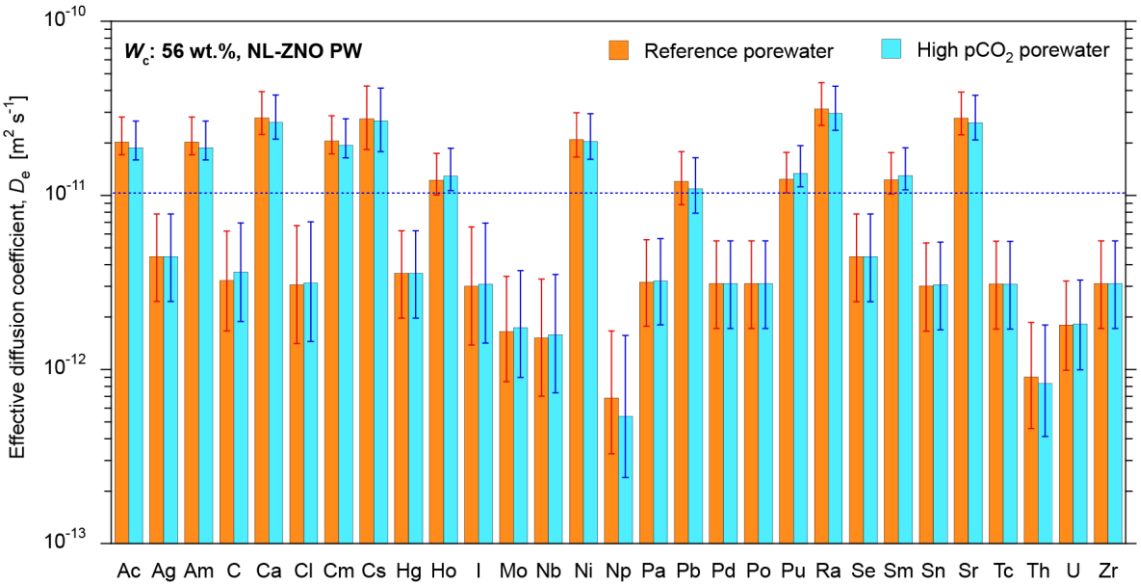

Fig. 5.4: Comparison of the prediction of D_e values for argillaceous rocks with a W_c of 56 wt.% for the Nördlich Lägern-Zürich Nord-Ost reference porewater (pH = 7.07, I = 0.33 mol kg^{-1}), and its high-pCO_2 variant (pH = 6.87, I = 0.34 mol kg^{-1}). Plot taken from Glaus et al. (2024a). The dashed line indicates the prediction for the uncharged HTO tracer to give an approximate idea of the effects of surface diffusion or anion exclusion.

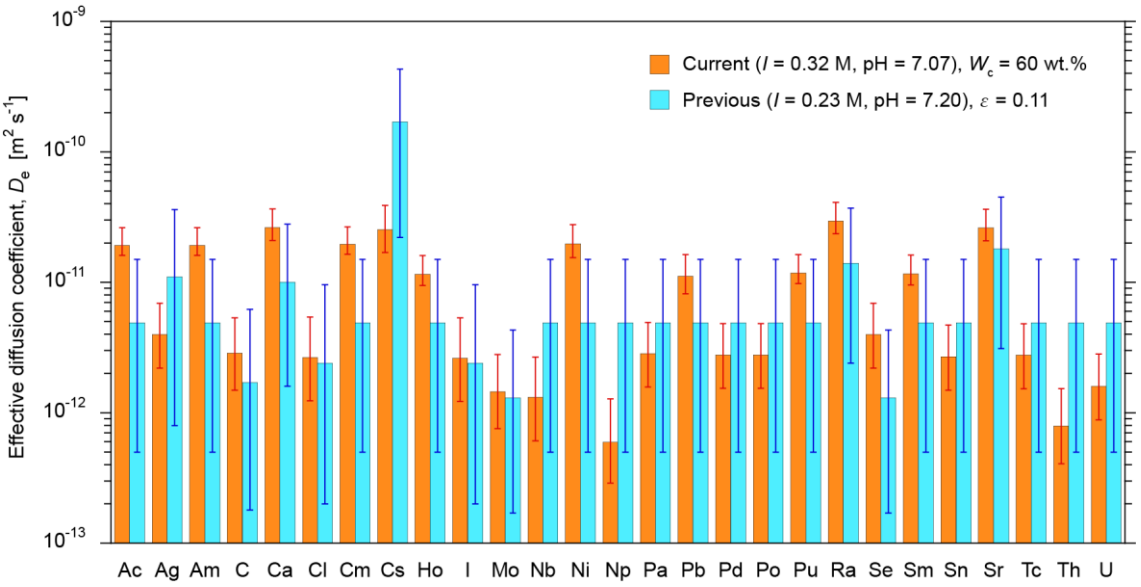

Fig. 5.5: Comparison of the prediction of D_e values for Opalinus Clay according to the previous procedures in Van Loon (2014) based on a porosity of 11%, with the current predictions (ClaySorDif), for the conditions of the NL-ZNO reference porewater and a W_c of 60 wt.%. Plot taken from Glaus et al. (2024a). The differences in porewater composition are given in the legend.

Tab. 5.1: Updated protolysis constants ($log_{10}K$) of illite and montmorillonite, in comparison to the values previously determined (shown in brackets) by Bradbury & Baeyens, 2009b and Baeyens & Bradbury, 1997 for the 2SPNE SC/CE model.

Protolysis reactions	illite		montmorillonite	
	$\equiv S^{S/W1}OH$	$\equiv S^{W2}OH$	$\equiv S^{S/W1}OH$	$\equiv S^{W2}OH$
$\equiv SOH + H^+ \Leftrightarrow \equiv SOH_2^+$	(4.0) 3.91±0.61	(8.5) 8.85±1.01	(4.5) 3.75±1.42	(6.0) 5.93±0.86
$\equiv SOH \Leftrightarrow \equiv SO^- + H^+$	(-6.2) -5.88±0.79	(-10.5) -10.43±0.68	(-7.9) -8.68±1.06	(-10.5) -10.55±0.99

5.4.2 Updates to sorption models for illite and montmorillonite

Since the sorption constants are coupled to the acid-base behaviour of the sorption sites, the sorption models for Cs(I), Ra(II), Ni(II), Np(IV), Pu(IV), Sn(IV), Th(IV), and U(IV/VI) were made consistent with the newly refined protolysis constants of illite and montmorillonite. In most cases, selected external datasets were used to supplement PSI/LES experimental data. Sorption models for Sr(II) on illite and montmorillonite were newly parameterized. For illite, the preliminary model including cation exchange reactions on three planar site types, according to the Generalized Caesium Sorption Model, along with a reaction on edge weak type 2 sites was proposed. However, this model did not adequately fit experimental data across varying ionic strengths, suggesting that the effect of competing ions (such as Ca^{2+}, Mg^{2+}, and Al^{3+}, which arise from illite dissolution) should be investigated and accounted for in future modelling. For montmorillonite, a model with one cation exchange reaction on planar sites and one reaction on edge weak type two sites provided an excellent fit to the experimental data.

Based on recent updates to the ClaySor sorption thermodynamic database, a consistent trend was observed in the ratio of surface complexation reaction constants between strong and weak sites for all investigated elements. The average difference in their logK ($\Delta \log K$) was approximately 2.8±0.4. This value was used to reparameterize the U(VI) model on montmorillonite to prevent a phenomenon observed in earlier studies, when trace sorption occurred on weak sites according to the modelling results (Marques Fernandes et al., 2012). The adjusted model provided a good fit to the U(VI) experimental data on montmorillonite. This approach was also successfully applied to Ni(II) and U(VI) sorption data on illite. Constraining the difference in constants for strong and weak sites reduced uncertainties and improved model consistency, especially for elements with limited datasets. This approach enables predictions of weak site constants even in the absence of sorption isotherms. However, spectroscopic validation of the empirically determined $\Delta \log K$ would support the development of physically justified sorption models.

5.4.3 Sorption models for kaolinite

Selected potentiometric titration datasets for kaolinite, including unpublished data in house data, were fitted using the 2SPNE SC/CE model.

The main differences between the kaolinite model and the 2:1 type clay models include the absence of strong sites, the distinct ratio of weak type 1 to weak type 2 site capacities, the exclusion of protonation reactions for weak type 2 sites, and a significantly lower cation exchange capacity (planar sites). Efforts to differentiate strong sites from sorption isotherms on kaolinite revealed that the capacity values of strong sites were similar to those of weak type 1 sites, suggesting that separation of these sites was not necessary. A ratio of 2:3 for weak type 1 to weak type 2 site capacities provided a better fit to the experimental titration and sorption data compared to the 1:1 ratio used for illite and montmorillonite. The protonation reaction for weak type 2 sites was excluded, justified by the asymmetry in titration curves relative to the net consumed amount of H^+/OH^- ions (see Fig. 5.6).

The model was applied to selected sorption datasets for Cs(I), Ra(II), and U(VI), yielding good fits (see Fig. 5.7).

5.5 Thrace: traceable thermodynamic dataset for chemical modeling

Models used to predict the chemical evolution of natural systems, biosynthesis, and industrial processes require datasets containing essential thermodynamic properties and parameters. As new and updated data are generated frequently, many datasets exist across different modeling tools in varied formats, making them challenging to use and compare. This project aimed to enhance the ThermoHub database (https://thermohub.org/thermohub/thermohub/) to ensure the traceability and completeness of thermodynamic data by developing a streamlined workflow for curating, uploading, and continuously updating datasets.

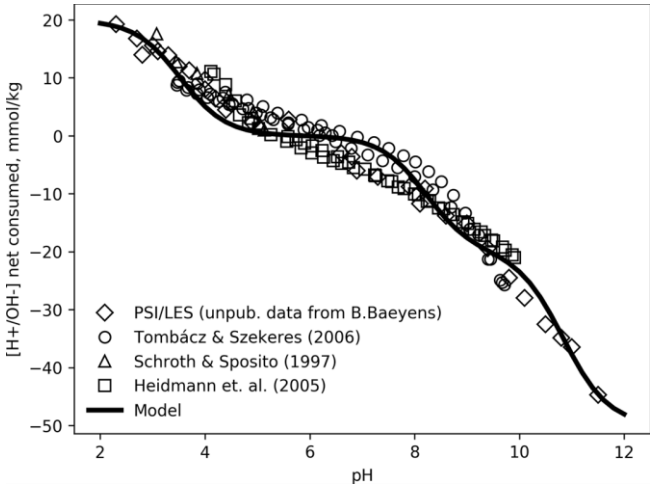

Fig. 5.6: Kaolinite sorption model based on potentiometric titration data from (Tombácz & Szekeres, 2006), (Schroth & Sposito, 1997), (Heidmann et al., 2005), and unpublished experimental data provided by Bart Baeyens (PSI/LES).

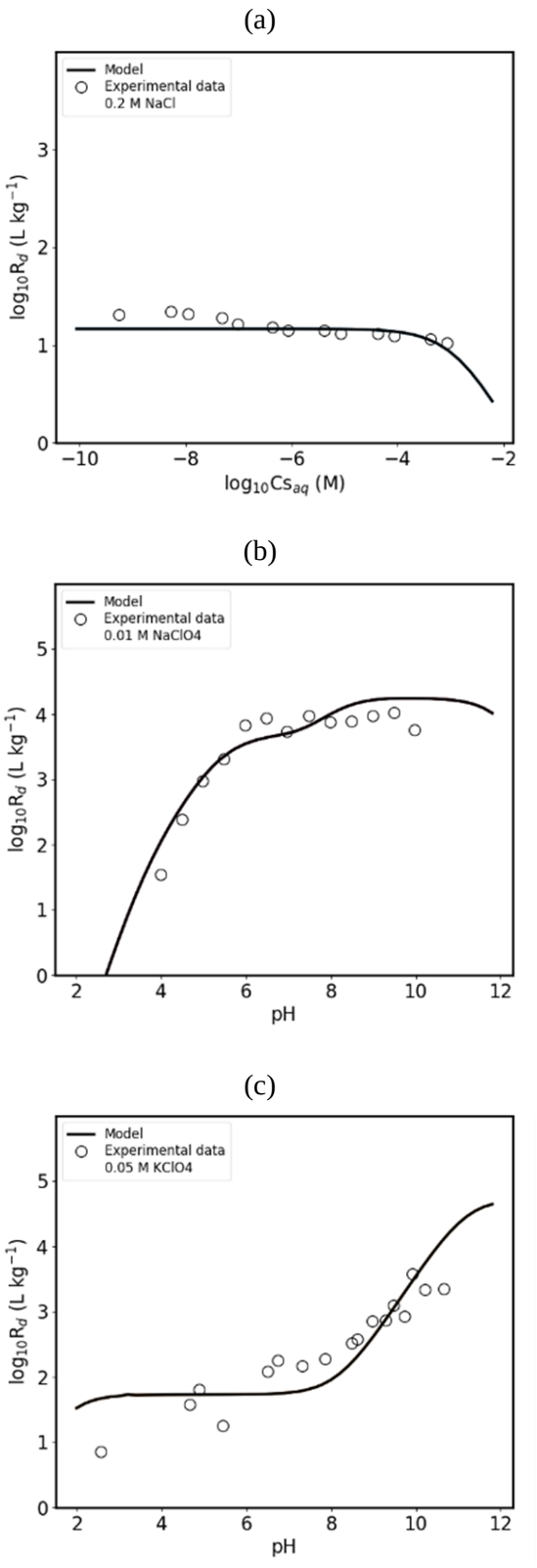

Fig. 5.7: Example sorption data fitted with kaolinite model: (a) Cs(I) sorption isotherm by (Missana et al., 2014); (b) Ra(II) sorption edge by (Reinoso-Maset & Ly, 2016); (c) U(VI) sorption edge by (Křepelová et al., 2006).

The project improved existing open-source tools in ThermoEcos for data processing, adapted import scripts for various data formats, and modified schemas to make data types machine-readable. A semi-automated workflow was established to incorporate data from major chemical modeling databases and link them to corresponding bibliographic sources, leveraging ThermoHub's graph structures. This workflow allows datasets to be updated seamlessly and can be adapted for other data sources. The imported data can support modeling codes like GEMS (https://gems.web.psi.ch/) and Reaktoro (https://reaktoro.org/), broadening their applicability across diverse chemical systems and a wide range of conditions.

ThermoHub's open format for thermodynamic data storage is structured in JSON (JavaScript Object Notation), with formal specifications and constraints defined in JSON schemas to ensure data interoperability and reusability. These schemas were expanded to accommodate fields typical of bibliographic formats like BibTeX and RIS. Considerable effort went into creating import scripts tailored to each dataset and data type (e.g., elements, substances, reactions, data sources). These scripts map specific fields, keys, and columns from diverse input formats to ThermoHub's data records, making it easy to reimport files of a given format without further editing, unless the format changes. These import/export templates are then easily adaptable for other datasets.

Withing the project eight widely used thermodynamic databases were curated and imported: CEMDATA (cement chemistry), CODATA (fundamental values), HERACLES (materials science), NASA (combustion), PSINA2020 (geological repositories and radionuclide chemistry), SUPCRT (hydrothermal geochemistry), MINES23 (ore metal geochemistry), and THERMOCHIMIE (geological repositories and radionuclide chemistry). The data curation process emphasized linking original published sources to each dataset, converting them into bibliographic JSON files to ensure traceability. During the import process, these records are automatically linked to bibliographic sources using graph-based relationships of the ThermoHub database (Fig. 5.8).

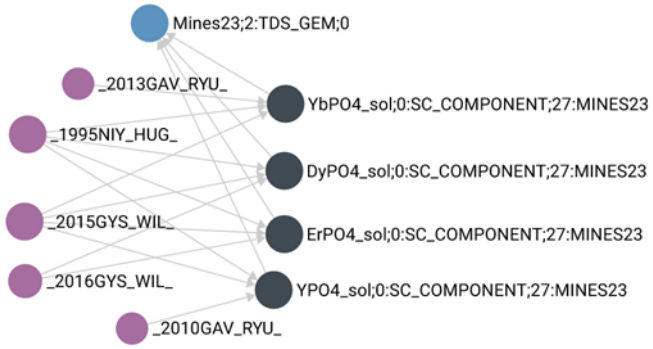

Fig. 5.8: Example of a graph database subset view of records (circles) and links (arrows) in (db.thermohub.net). Blue circle Mines23 ThermoDataSet, grey circles solid components (rare earths phosphate records containing thermodynamic properties), and pink circles DataSources (bibliographic records).

A primary goal in the project was to capture the curator's workflow, including data preparation and script configuration, in a repeatable format. This process, previously dependent on a graphical user interface, required extensive user familiarity and setup knowledge. To simplify, document the workflow, and make it reusable, a Jupyter notebook, that contained the needed code with documentation was implemented. The import workflow includes input files with data and bibliographic references, scripts that map external format fields to ThermoHub's schema, and a Jupyter notebook to document and run the import process. With this setup, datasets can be updated or newly imported with ease. The curated data are accessible in ThermoHub, with schemas supporting reusability and interoperability, and graph structures enabling traceability to original sources.

5.6 Pitzer model for Al and Si for saline systems

The thermodynamic data and Pitzer interaction parameters (IPs) for Si and Al components from the THEREDA (https://www.thereda.de/) database were re-evaluated to broaden its application to modeling cementitious systems in highly saline environments (Miron, 2024). This work involved revisiting the reference thermodynamic data for aqueous Si and Al aqueous species, as well as solids such as quartz, gibbsite, and boehmite, and generating a new set of consistent polythermal Pitzer IPs for Si and Al species within the oceanic salt system Al–Si–Ca–Mg–Na–K–Cl–SO_4–CO_3–H_2O. Experimental data spanning various compositions and temperatures were used for the optimization of interaction parameters and their temperature coefficients. Where data were unavailable, estimation methods were used, employing analogous species or correlations with parameters from the SIT (specific ion interaction theory) aqueous activity model.

For Si in acidic to neutral pH conditions, IPs for $Si(OH)_4(aq)$ were determined based on amorphous silica solubility in binary electrolyte solutions and were sufficient to independently describe data in ternary systems (Fig. 5.9 a, b). The stability and IPs of the silicic acid hydrolysed species were derived based on potentiometric method complemented by osmotic coefficient measurements in NaCl, NaOH and $NaClO_4$ solutions (Fig. 5.9 c, d). At elevated Si concentrations, polymeric species impact aqueous Si speciation; here, the silica tetramer ($Si_4O_8(OH)_4^{4-}$) and its binary IPs were selected to approximate amorphous Si solubility in NaCl solutions.

For the aluminium-bearing systems, the standard thermodynamic properties of Al hydroxide phases and hydrolyzed species were re-evaluated based on gibbsite solubility measurements from the literature. Pitzer IPs and their temperature coefficients were derived from measurements in acidic to alkaline pH solutions of various electrolytes (Fig. 5.10). No temperature coefficients were needed for interactions within the Al–Cl–H_2O system, which proved consistent in ternary and quaternary systems. Aluminium-sulfate complexation was implicitly accounted for via IPs. Interactions between hydrolyzed aluminium species and calcium or magnesium at high pH cannot be derived due to the precipitation of solids and the low concurrent concentrations of these species in such systems.

The revised Pitzer model for Si and Al aqueous speciation, together with data for cement hydrate phases from CEMDATA18 (Lothenbach et al., 2018), and the updated dataset, has been incorporated into THEREDA (https://www.thereda.de/) for practical application.

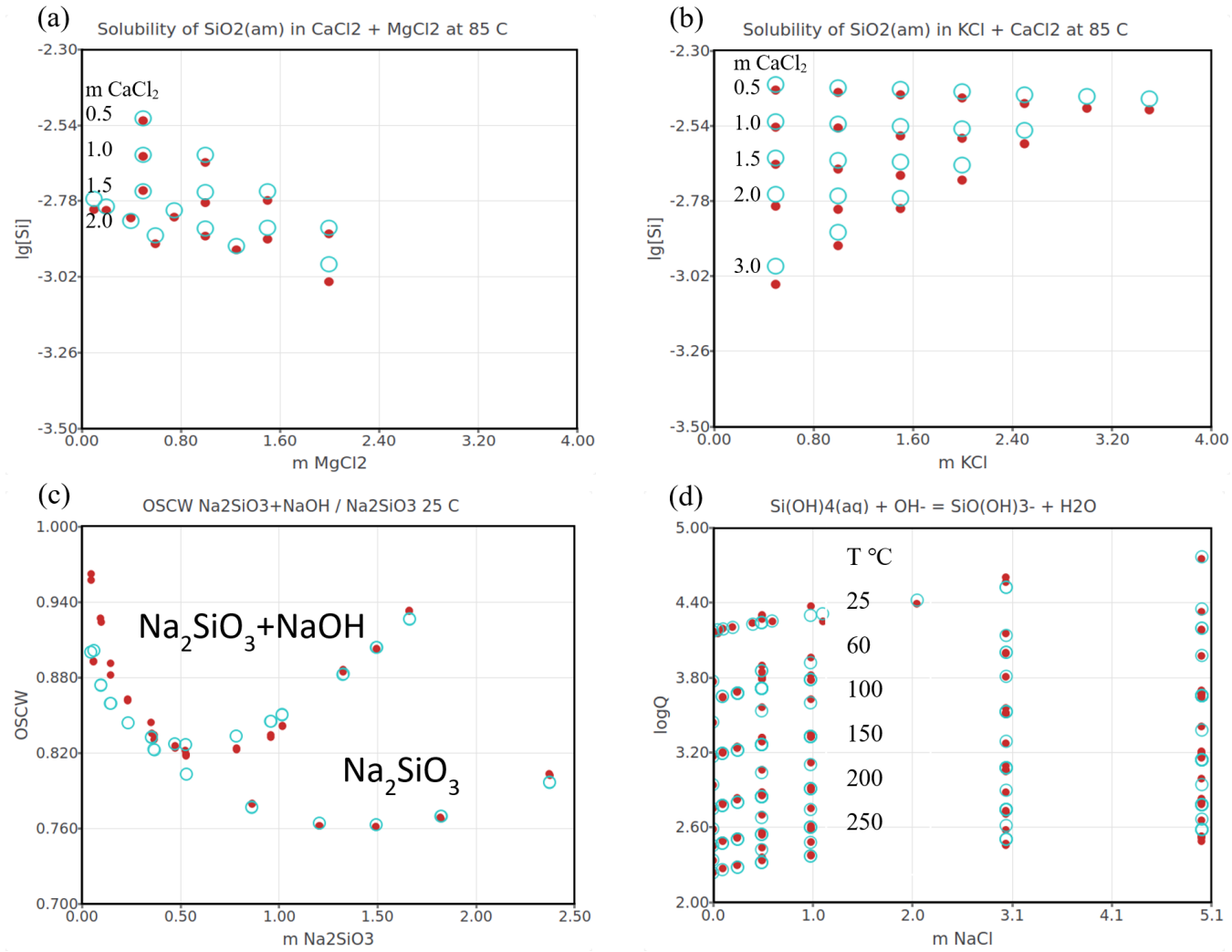

Fig. 5.9: Example comparisons between measured (full circles) and calculated (empty circles) data: (a), (b) $SiO_{2(am)}$ solubility in ternary electrolyte solutions at 85 °C. Datasets of Meyer and Willms (2008); (c) osmotic coefficients (Park & Englezos, 1998); (d) first hydrolysis of silicic acid from potentiometric measurements (Busey & Mesmer, 1977).

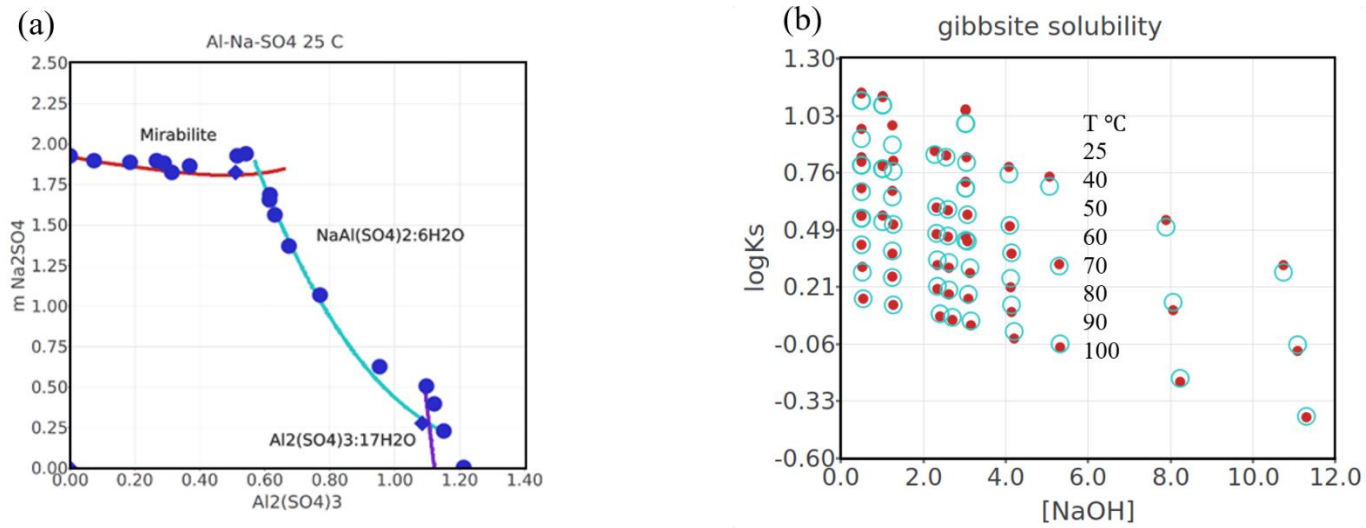

Fig. 5.10: Example comparisons between measured (full circles) and calculated (empty circles/lines) data: (a) system Na_2SO_4–$Al_2(SO_4)_3$ circles (Dobbins & Addleston, 1931), diamonds (Druzhinin et al., 1961); (b) gibbsite solubility at different T in NaOH solutions (Wesolowski, 1992) and (Russell et al., 1955).

5.7 References

Baeyens, B., & Bradbury, M. H. (1997)
A mechanistic description of Ni and Zn sorption on Na-montmorillonite. Part I: Titration and sorption measurements. *Journal of Contaminant Hydrology, 27*(3–4), 199–222.
https://doi.org/10.1016/s0169-7722(97)00008-9

Bradbury, M. H., & Baeyens, B. (1997)
A mechanistic description of Ni and Zn sorption on Na-montmorillonite. Part II: Modelling. *Journal of Contaminant Hydrology, 27*(3–4), 223–248.
https://doi.org/10.1016/s0169-7722(97)00007-7

Bradbury, M. H., & Baeyens, B. (2009a)
Sorption modelling on illite. Part I: Titration measurements and the sorption of Ni, Co, Eu and Sn. *Geochimica et Cosmochimica Acta, 73*(4), 990–1003.
https://doi.org/10.1016/j.gca.2008.11.017

Bradbury, M. H., & Baeyens, B. (2009b)
Sorption modelling on illite. Part II: Actinide sorption and linear free energy relationships. *Geochimica et Cosmochimica Acta, 73*(4), 1004–1013.
https://doi.org/10.1016/j.gca.2008.11.016

Busey, R. H., & Mesmer, R. E. (1977)
Ionization equilibriums of silicic acid and polysilicate formation in aqueous sodium chloride solutions to 300°C. *Inorganic Chemistry, 16*(10), 2444–2450.
https://doi.org/10.1021/ic50176a004

Dobbins, J. T., & Addleston, J. A. (1931)
A study of the soda–alum system. *Journal of Physical Chemistry, 39*(5), 637–642.
https://doi.org/10.1021/j150365a007

Druzhinin, I. G., Imanakunov, B., & Kuznetsov, V. G. (1961)
Solubility in the aqueous aluminum, sodium, nickel, sulphate quaternary system. *Zhur. Neorg. Khim, 6*, 1304–1308.

Glaus, M. A., Kulik, D. A., Miron, G. D., Van Loon, L. R., Wüst, R. A. J., Becker, J., & Li, X. (2024a)
Diffusion databases for Opalinus Clay, confining geological units, and bentonite: Methods, concepts, and upscaling of data. *Nagra Technical Report NTB 23-08*.

Glaus, M. A., Van Loon, L. R., & Wüst, R. A. J. (2024b)
Diffusion of HTO, ^{36}Cl and ^{22}Na in the Mesozoic rocks of northern Switzerland: II. Data interpretation in terms of an electrical double layer model. *Applied Geochemistry, 162*, 105842.

Heidmann, I., Christl, I., Leu, C., & Kretzschmar, R. (2005)
Competitive sorption of protons and metal cations onto kaolinite: Experiments and modeling. *Journal of Colloid and Interface Science, 282*(2), 270–282.
https://doi.org/10.1016/j.jcis.2004.08.019

Kulik, D. A., Wagner, T., Dmytrieva, S. V., Kosakowski, G., Hingerl, F. F., Chudnenko, K. V., & Berner, U. R. (2013)
GEM-Selektor geochemical modeling package: Revised algorithm and GEMS3K numerical kernel for coupled simulation codes. *Computational Geosciences, 17*(1), 1–24.
https://doi.org/10.1007/s10596-012-9310-6

Křepelová, A., Sachs, S., & Bernhard, G. (2006) Uranium(VI) sorption onto kaolinite in the presence and absence of humic acid. *Radiochimica Acta, 94*(12), 825–833.
https://doi.org/10.1524/ract.2006.94.12.825

Lothenbach, B., Kulik, D. A., Matschei, T., Balonis, M., Baquerizo, L., Dilnesa, B., Miron, G. D., & Myers, R. J. (2018)
Cemdata18: A chemical thermodynamic database for hydrated Portland cements and alkali-activated materials. *Cement and Concrete Research, 115*, 472–506.
https://doi.org/10.1016/j.cemconres.2018.04.018

Marinich, O., Marques Fernandes, M., Miron, G. D., & Kulik, D. A. (2024)
ClaySor 2023: Update of 2SPNE SC/CE sorption model for illite and montmorillonite in GEMS implementation. *Nagra Technical Report NTB 23-05*.

Marques Fernandes, M., Baeyens, B., Dähn, R., Scheinost, A. C., & Bradbury, M. H. (2012)
U(VI) sorption on montmorillonite in the absence and presence of carbonate: A macroscopic and microscopic study. *Geochimica et Cosmochimica Acta, 93*, 262–277.
https://doi.org/10.1016/j.gca.2012.04.017

Marques Fernandes, M., Marinich, O., Miron, G. D., & Baeyens, B. (2024)
Sorption of Cs, Ni, Eu, Th, and U on drill core samples of Opalinus Clay and confining geological units from deep boreholes in the potential siting regions Nördlich Lägern, Zürich Nordost, and Jura Ost: Measurements and predictive sorption modelling. *Nagra Technical Report NTB 23-01*.

Meyer, T., & Willms, T. (2008)
Geochemische Modellierung des Langzeitverhaltens von silikatischen und alumosilikatischen Materialien im Temperaturbereich bis 90 °C. *GRS–A–3493*.

Miron, G. D. (2024)
Si–Al Pitzer dataset: Consistent set of Pitzer activity model interaction parameters of Al and Si species, for modelling cements in saline systems with THEREDA. *ChemRxiv*.
https://doi.org/10.26434/CHEMRXIV-2024-M02F1-V2

Miron, G. D., Kulik, D. A., Dmytrieva, S. V., & Wagner, T. (2015)
GEMSFITS: Code package for optimization of geochemical model parameters and inverse modeling. *Applied Geochemistry*, *55*, 28–45.
https://doi.org/10.1016/j.apgeochem.2014.10.013

Missana, T., García-Gutiérrez, M., Benedicto, A., Ayora, C., & De-Pourcq, K. (2014)
Modelling of Cs sorption in natural mixed-clays and the effects of ion competition. *Applied Geochemistry*, *49*, 95–102.
https://doi.org/10.1016/j.apgeochem.2014.06.011

Park, H., & Englezos, P. (1998)
Osmotic coefficient data for Na_2SiO_3 and Na_2SiO_3–NaOH by an isopiestic method and modeling using Pitzer's model. *Fluid Phase Equilibria*, *153*(1), 87–104.
https://doi.org/10.1016/S0378-3812(98)00400-2

Reinoso-Maset, E., & Ly, J. (2016)
Study of uranium(VI) and radium(II) sorption at trace level on kaolinite using a multisite ion exchange model. *Journal of Environmental Radioactivity*, *157*, 136–148.
https://doi.org/10.1016/j.jenvrad.2016.03.014

Russell, A. S., Edwards, J. D., & Taylor, C. S. (1955)
Solubility and density of hydrated aluminas in NaOH solutions. *JOM*, *7*(10), 1123–1128.
https://doi.org/10.1007/bf03377627

Schroth, B. K., & Sposito, G. (1997)
Surface charge properties of kaolinite. *Clays and Clay Minerals*, *45*, 85–91.
https://doi.org/10.1557/PROC-432-87

Tombácz, E., & Szekeres, M. (2006)
Surface charge heterogeneity of kaolinite in aqueous suspension in comparison with montmorillonite. *Applied Clay Science*, *34*(1–4), 105–124.
https://doi.org/10.1016/j.clay.2006.05.009

Van Loon, L. R. (2014)
Effective diffusion coefficients and porosity values for argillaceous rocks and bentonite: Measured and estimated values for the provisional safety analyses for SGT-E2. *Nagra Technical Report NTB 12-03*.

Van Loon, L. R., Bunic, P., Frick, S., Glaus, M. A., & Wüst, R. A. J. (2023)
Diffusion of HTO, ^{36}Cl and ^{22}Na in the Mesozoic rocks of northern Switzerland. I: Effective diffusion coefficients and capacity factors across the heterogeneous sediment sequence. *Applied Geochemistry*, *159*, 105843.
https://doi.org/10.1016/j.apgeochem.2023.105843

Wesolowski, D. J. (1992)
Aluminum speciation and equilibria in aqueous solution: I. The solubility of gibbsite in the system Na-K-Cl-OH-$Al(OH)_4$ from 0 to 100°C. *Geochimica et Cosmochimica Acta*, *56*(3), 1065–1091.
https://doi.org/10.1016/0016-7037(92)90047-M

6 LANDFILLS GEOCHEMISTRY AND SECONDARY RAW MATERIALS

Churakov S.V., Eggenberger U., Weibel G., Wolffers M., Boiger R., Ingold P. (PhD Student), Gfeller, F., Bosoppi, I., Schumacher W.

6.1 Introduction

The Competence Center for Secondary Raw Materials (German: Fachstelle Sekundärrohstoffe (FSSR)) at the Institute of Geological Sciences (University of Bern) conducts applied research in the field of environmental geochemistry and secondary raw materials. The core competencies of the FSSR include the topics of recycling management and disposal quality of conventional non-radioactive waste. The sustainable implementation of recycling technologies is waste type-specific and requires detailed knowledge of the chemical and phase composition of the materials, their long-term leaching behaviour, and the processes controlling material degradation. To close material cycles and preserve primary raw material, new approaches and technologies are needed to enhance the reuse of secondary raw materials on a larger scale and in new application areas.

In the context of the project “Ersatzrohstoffe in der Kreislaufwirtschaft” at the Wyss Academy for Nature, an inventory of material qualities of various mineral wastes in Switzerland has been carried out. Over 220 material samples of different material categories were sampled and are being analyzed for their chemical and mineralogical composition.

The Swiss waste disposal ordinance defines an aftercare period of 50 years for the monitoring of landfill sites for bottom ash. A large body of field characterisation and monitoring data has been collected and used to develop hydro-geochemical model of landfill site evolution. The model takes into account chemical equilibrium between domains with distinct hydrodynamic transport properties, and semi-quantitatively explains the chemical and hydraulic behaviour of landfill discharge systems.

Column leaching tests are used to evaluate the hydraulic properties of materials disposed in landfills, their reactivity and metal concentration in the leachate. These tests are time-consuming and need to run over several weeks to months to give a glimpse into processes taking place over several decades in the natural environment. To obtain an estimate for long term bottom ash leaching behavior, a machine learning approach has been applied to the data delivered by the early-stage measurements. For selected elements, this study could successfully demonstrate the potential of machine learning to streamline environmental monitoring of long-term landfill management.

6.2 Recycling potential of mineral wastes as secondary raw material in the cement industry

The main contribution to the carbon footprint of building materials such as concrete is caused by the decarbonization of limestone in clinker production. The substitution of limestone, with *geogenic* CO_2, thus offers a great CO_2 savings potential: For each ton of calcium oxide substituted by *CO_2-free* or *CO_2-neutral raw materials*, 785 kg of CO_2 can be saved. Thus, the partial replacement of primary resources with secondary raw materials in clinker production represents a major environmental benefit due to an improved CO_2 balance.

In total, around 4 million tonnes of cement are produced in Switzerland every year. Almost 5 million tonnes of raw material are required for clinker production. In addition, around 1 million tonnes of additives (gypsum, limestone) are used in cement production. As of 2021, the share of secondary raw materials used for clinker production accounted for 10% (cemsuisse, 2021). This share has increased by approx. 1/3 in the last 5 years. A further increase in the use of secondary raw materials is to be expected due to environmental benefits. A major share of secondary raw materials used today for clinker production are contaminated soils from the remediation of contaminated sites. These soils are often enriched with organic pollutants, which are thermally decomposed in the process of clinker production. The recycling of these soils in the cement plant is therefore environmentally beneficial over a deposition in landfills. In order to further increase the share of secondary raw materials, promising secondary raw materials with suitable chemical composition and processing parameters must be found. Materials that are rich in one of the four main chemical components of clinker (CaO, SiO_2, Fe_2O_3, Al_2O_3) are generally suitable for raw material replacement. The physical properties of the material are also important for material handling and process control. Ideally, these should be similar to the natural raw materials limestone and marl that are processed today. Grain size and moisture play a particularly important role here. Limiting factors for the use of large quantities of excavated material as a raw material substitute include the availability of sufficient storage capacity.

6.3 Recycling potential of mineral wastes as supplementary cementitious materials (SCMs) in the cement industry

Another way to minimize the CO_2 footprint in the cement industry is to reduce the proportion of clinker in cement by increasing the use of supplementary cementitious materials (SCMs). In Switzerland, the SCMs used are mainly limestone (cemsuisse, 2022). In order to increase the share of SCMs in cements, efforts are being made worldwide to assess suitable materials for the use as SCMs. In addition to ground limestone, the use of calcined clays is also being highly discussed. Calcined clays have the potential to replace approx. 30-40% of clinker in cements (Snellings, 2016). When heating clay-rich materials, the clay minerals lose their water of crystallization at temperatures of approx. 400-900°C and therefore undergo structural transformations that lead to the disruption of the long-range order in the crystal structure. These disordered structures show latent hydraulic or pozzolanic properties in the cement (Hanein et al., 2022). The focus of the utilization of calcined clays has so far been primarily on kaolinite-rich raw materials. For illite-dominated clay materials, as we find in Switzerland, there is still the need for further research on the suitability of their use as raw material for calcined clays.

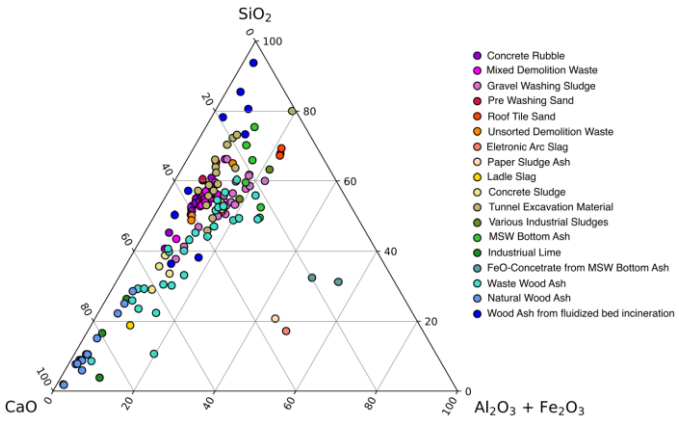

Fig. 6.1: Chemical composition of the different mineral wastes in Switzerland plotted in the ternary system CaO-SiO_2-Al_2O_3+Fe_2O_3.

6.4 Material characterization of various mineral wastes in Switzerland

Figure 6.1 shows the chemical composition of different mineral wastes in Switzerland plotted in the ternary system CaO-SiO_2-Al_2O_3+Fe_2O_3. The materials paper ash, natural wood grate and cyclone ash, sea chalk, and limestone are particularly promising secondary Ca sources. Materials such as the fine fractions of concrete and mixed demolition granulate, gravel washing sludge and tunnel excavation material show a similar chemical composition to marl. Due to the elevated Si:Ca ratio, the maximal amount of secondary raw material that can be used is limited.

The FeO concentrates from slag processing and steelworks slags could be interesting as corrective materials. Due to their high clay mineral content, gravel washing sludges have a high potential for use as calcined clays in cement. Therefore, activation experiments are being prepared to investigate the change in mineralogical composition as a function of heating and the potential to be used as SCMs. The characterization of the material qualities of mineral wastes forms an important data basis for the assessment of the recycling potential. The recording of the material qualities of mineral wastes is still ongoing over the next years. As a result of quality optimization processes, new materials are constantly being produced. Additional parameters of the existing materials are also being collected on an ongoing basis in order to be able to assess their recycling potential for various applications in more detail.

6.5 Leachate formation in bottom ash landfills

Since the year 2000, Switzerland has committed itself to the full thermal treatment of municipal waste from industry and households. All over Switzerland, 30 incineration plants process approximately 4 million tonnes of waste annually, resulting in around 670,000 tonnes of MSW bottom ash (FOEN, 2021). Thermal recycling reduces waste volume and minimizes the pollution hazards by destroying and/or immobilizing substances (Swiss Confederation, 2023b). Physical treatment processes (magnetic separation, induction separation processes, etc.) enable the reduction of the residual metal content and recovery of valuable metals. The bottom ash is then temporarily stored in open landfill sites, usually for several weeks, and then placed in the landfill in layers of around 50 cm and compacted with the aid of a roller. Due to the open-air landfilling approach rainwater infiltrates the highly reactive bottom ash and produce contaminated leachate. This is collected in a controlled manner and discharged into the sewerage system in accordance with the guidelines of the Swiss Water Protection Act (Swiss Confederation, 2023a). After completion of the bottom ash deposition in the landfill, a legally clearly defined surface cover is applied (Swiss Confederation, 2023b).

Tracer experiments provide insights into the landfill structure, the infiltration of water and its flow in bottom ash landfills (Fig. 6.2.). Due to the layer by layer deposition strategy, the landfilled material builds a stratified structure composed of fine-grained compacted layer (5-15 cm), created by rolling, and a coarse-grained, skeletally supported layer (20-35 cm), which is essentially produced by backfilling. The tracer solution allows the division of the landfill body into

four different hydrological zones. The applied solution shows homogeneous infiltration in the uppermost 5-10 cm of the landfill, forming the infiltration. Ponding effects and horizontal water flow are observed at the landfill surface if the tracer supply exceeds the maximal infiltration rate in the bottom ash material. With increasing infiltration depth, the flow patterns become heterogeneous, forming preferential flow paths with a predominantly vertical flow direction under saturated conditions. The compacted layers within the bottom ash landfill body reduce water flow, causing water accumulation and the formation of horizontal flow patterns, until a new vertical flow path is found. The preferential flow path is surrounded by a non-colorized zone with increased water content, which represents the landfill zone affected by the incoming water. With further distance to the preferential flow path, the water content decreases to initial (i.e., pre-experimental) conditions, representing the unaffected zone. These observations reflect the major influence of the structural properties of the bottom ash landfill system on fluid flow within the landfill body. The dye tracer enables visualization that most of the deposited material is not in contact with the incoming precipitation, resulting in localised fluid flow and thus, continuous leaching processes being limited to these preferential flow paths.

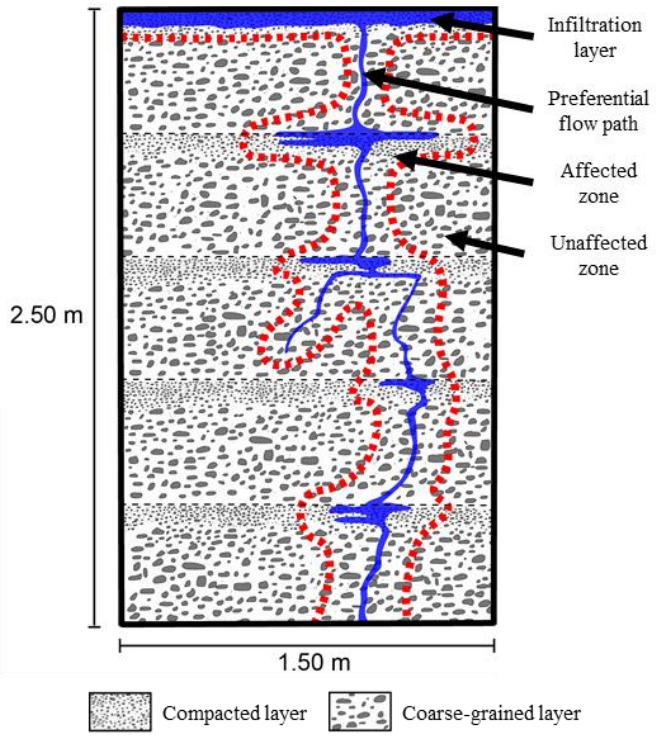

Fig. 6.2: Conceptual visualization of the bottom ash landfill structure and observed flow zones observed during the applied tracer experiment. Adapted from Ingold et al. (2024).

Leachate sampling during heavy precipitation events revealed the immediate reaction of the leachate system on the incoming rainwater, causing a rapid increase in flux and a significant change in composition (Fig. 6.3). As leachate discharge increases, the electrical conductivity (EC) decreases, with lowest values at highest flux values. This decrease in EC is reflected in the main element concentrations (e.g., Ca, S), which decrease significantly during the event. In contrast, numerous trace elements (e.g., Cu, Zn) show an increase in concentration, with maximum values delayed with respect to the maximum flux values.

Hydrological modelling of fluid flow through bottom ash material confirmed the formation of the different flow zones visualized with the dye tracer (Fig. 6.2) and highlighted the importance of the preferential flow paths as the primary transport system during heavy rain events. Also, the rapid transport of water within the preferential flow path resulted in flushing of the matrix zone surrounding the flow patterns, forming an affected rim zone. After the peak flux, backflow of water from the matrix zone into the preferential flow path is observed, with flux rates significantly higher compared to matrix flux rates at the lower boundary. These observations highlight the importance of the preferential flow path as a secondary transport system for matrix water. However, fluid flow through the modeled bottom ash body was too slow to explain the leachate responses observed at the bottom ash landfill (Fig. 6.4).

Based on the observations at the landfill site, the leachate responses during the precipitation events, and the results from the hydrological modelling, edge zone flow, occurring at the boundary between the deposited bottom ash and the surrounding drainage layer or within the gravel-containing drainage layer, is identified as representing the transport system responsible for the observed leachate responses, which resulted an improved hydrogeochemical concept of a bottom ash landfill system (Fig. 6.5):

- During dry periods, fluid flow from the matrix zone is responsible for the observed landfill leachate. The fluid drains very slowly due to the unsaturated conditions present in the landfill body (illustrated as curved arrows in Figure 6.5(a)), resulting in a long residence time of several years.

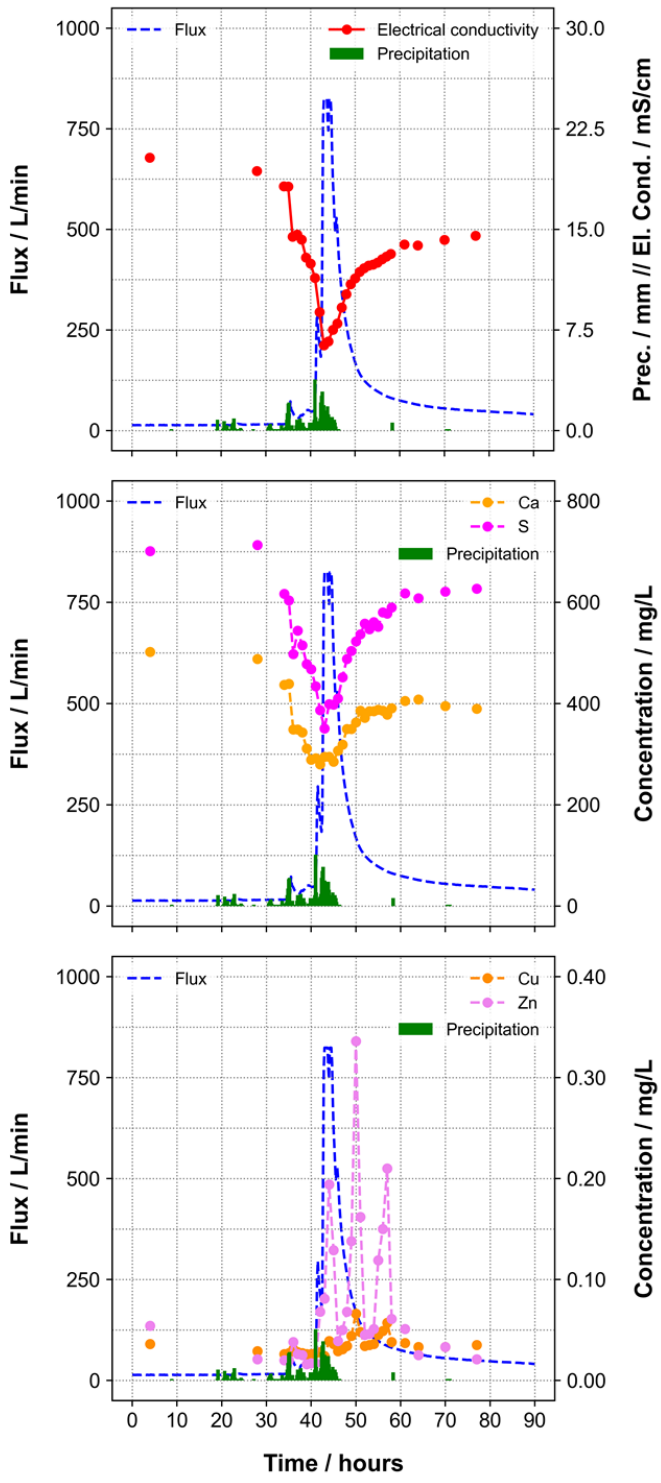

Fig. 6.3: Flux (blue dashed line), electrical conductivity (red dotted line), precipitation (green columns), Ca (yellow dotted line), S (pink dotted line), Cu (orange dotted line), and Zn concentrations (light pink dotted line) in a bottom ash landfill leachate during a heavy precipitation event as a function of time. Adapted from Ingold et al. (2024).

- With incoming precipitation, surface ponding results in water accumulation and the localised formation of preferential flow paths. Compacted layers within the landfill body retain water volumes and further accumulate the incoming rainwater (indicated as red arrows in Figure 6.5(b)). If located near edge zones, fluids accumulated by surface ponding or at compacted layers within the landfill body infiltrate into the drainage layer, resulting in rapid transport and the observed leachate response, causing immediate increase in flux and dilution of main elements. Furthermore, the matrix zone surrounding the preferential flow path is being flushed by the fast-flowing fluid (indicated with green arrows in Figure 6.5(c)).
- As precipitation stops, the preferential flow paths successively deactivate, resulting in backflow of highly interacted pore fluid from the matrix zone into the flow paths. Near the edge zone, these fluids infiltrate into the drainage layer and are then transported into the leachate system, forming the enhanced trace element concentrations observed with a delay compared to the maximum flux rate (Figure 6.5(d,e)).

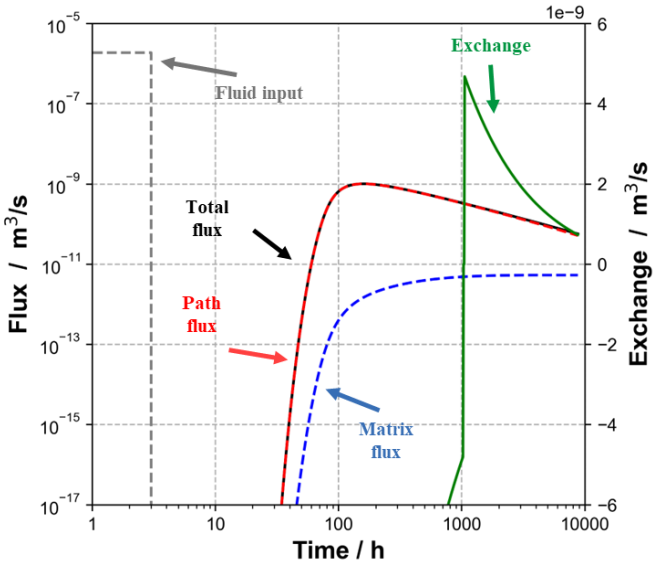

Fig. 6.4: Modelled flux at the lower boundary, with total flux (black line), preferential flow path flux (dashed red line), matrix flux (dashed blue line), and exchange flux (green line) between the matrix zone and the preferential flow path, with positive values indicating flow into the flow path system.

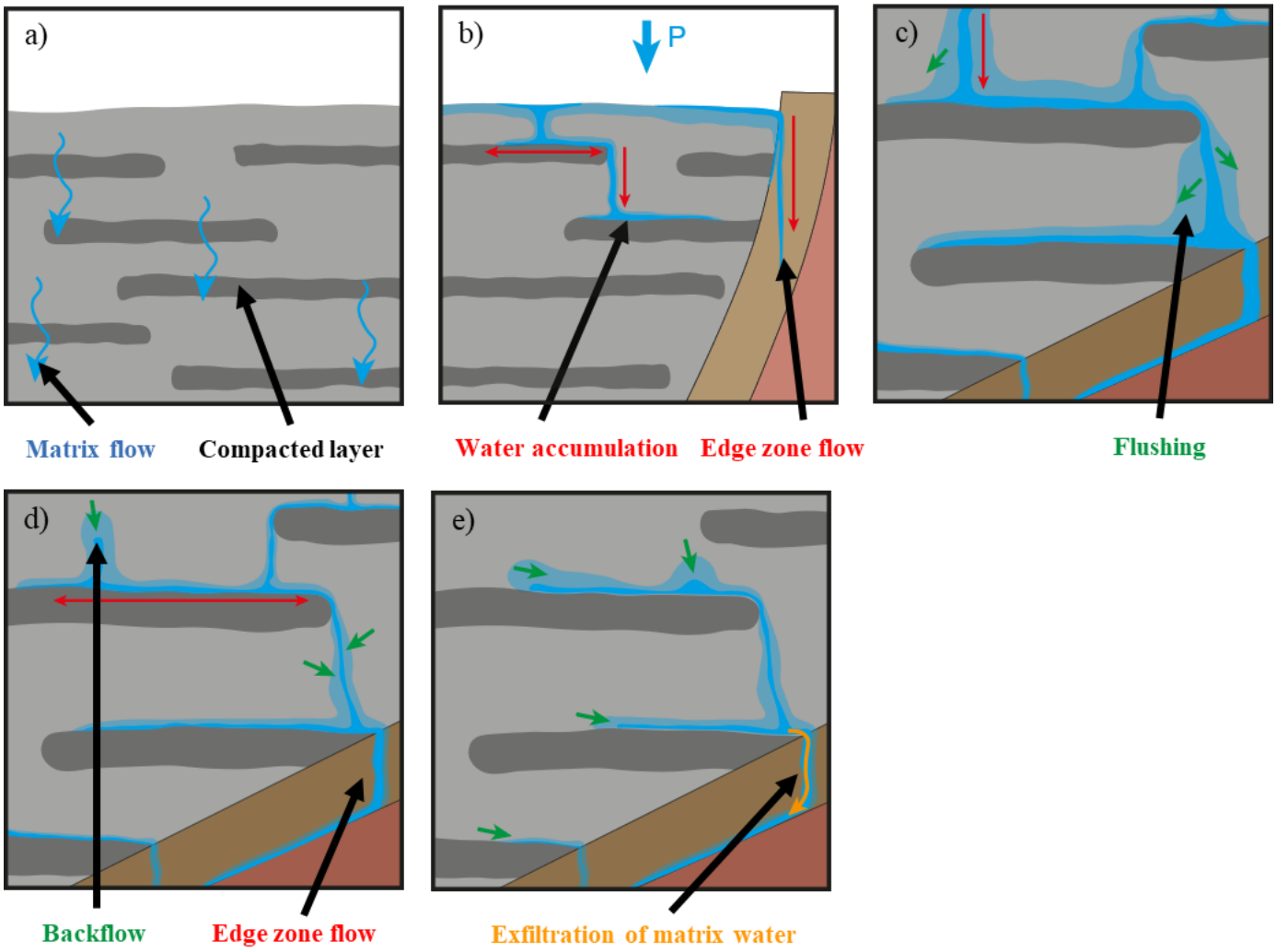

Fig. 6.5: Conceptual illustration of fluid transport through the bottom ash landfill, including a) matrix flow during dry periods (blue curved lines), b) and c) formation of preferential flow paths within the landfill body and the edge zones (red vertical arrows) and accumulation of water at compacted layers (red horizontal arrows) and flushing of the matrix zone surrounding the preferential flow paths (green arrows), and d) and e), backflow of matrix water into the preferential flow paths (green arrows) and its exfiltration into the edge zone (orange arrow).

6.6 Machine learning based model for contaminant leaching assessment

Potential leaching of contaminants out of landfill deposits is of environmental concern. Typically, column leaching tests are used to evaluate the hydraulic properties of disposed materials, their reactivity and metal concentration in the leachate. These tests are time-consuming and need to run over several weeks to months to give a glimpse into processes taking place over several decades in the natural environment. In such tests, the liquid-to-solid (LS) ratio – representing the amount of water added to the bottom ash in the column – can be treated as a proxy for reaction time in the landfill. To obtain an estimate for long term bottom ash leaching behavior, a machine learning approach has been applied to the data delivered by the early-stage measurements. This approach has the potential to reduce testing durations from weeks to just a few days.

This study considered a dataset comprising 23 column leaching tests conducted on different ash types (wet, dry, mixed and magnetic) across 7 LS ratios, ranging from 0.1 to 10. From a broad list of measured elements, the modeling was focused on 15 key elements with the largest potential for environmental impact (e.g., arsenic, cadmium, zinc). A comprehensive data preprocessing pipeline was implemented to address missing measurement points, scale features, and engineer input features to enhance model performance.

Various machine learning algorithms (ridge regression, lasso regression, random forests, neural networks, Gaussian processes) were tested. These models were trained using experimental data at all available LS ratios. The surrogate models were designed to take the LS 0.1, 0.2, 0.5 data as input, and to predict the elements at a later stage of the experiment characterized by LS ratios of 1, 2, 5 and 10. An

extensive hyperparameter optimization process was conducted to determine the best model parameters, input features, and input scaling methods. Final model training involved cross-validation, where data from one column leaching test was excluded as a test set and the remaining 22 experiments were used for training. This process was repeated 23 times to calculate average errors of the model predictions. The entire workflow is visualized in Fig. 6.6.

The obtained results indicated that the models performed well for certain elements. For instance, manganese predictions achieved a mean absolute percentage error of just 12 %, as shown in Figure (Fig. 6.7). However, for several elements, the error was considerable. Additionally, a sensitivity analysis using SHapley Additive exPlanations (SHAP) revealed that the LS ratio and initial elemental concentration levels were the most critical features for predicting contaminant leaching, as depicted in Fig. 6.7 for cobalt.

For selected elements, this study could successfully demonstrate the potential of machine learning to streamline environmental monitoring of long-term landfill management. By significantly reducing the time and cost of long-term leaching assessments while maintaining accuracy, this approach could offer substantial practical benefits. To generalize the study and improve the model predictions, more measurement data points would be necessary.

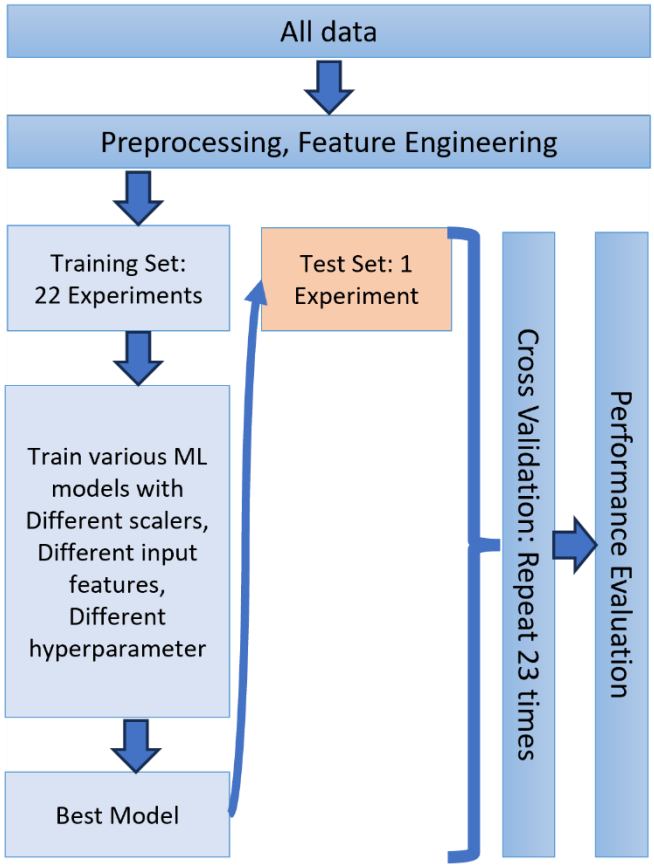

Fig. 6.6: Machine Learning based workflow for predicting contaminant leaching behavior of incineration bottom ashes.

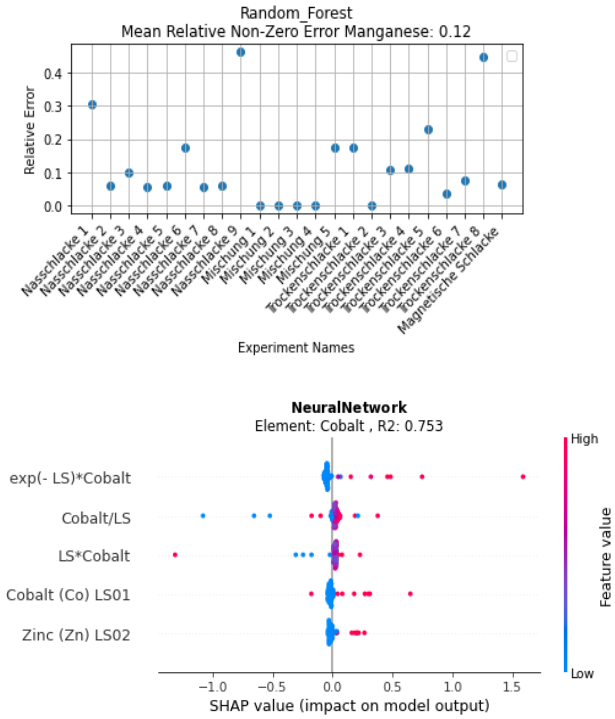

Fig. 6.7: Top: Relative error for manganese for each experiment. Bottom: typical SHAP plot indicating feature importance.

6.7 References

Cemsuisse (2022)
Jahresbericht cemsuisse 2022, pp. 19.

Cemsuisse (2021)
Roadmap 2050 - Klimaneutraler Zement als Ziel, Verband der Schweizerischen Cementindustrie, pp 13.

Federal Office for the Environment FOEN (2021) Einheitliche Heizwert- und Energiekennzahlen-berechnung der Schweizer KVA nach europäischem Standardverfahren.

Hanein, T., Thienel, K., Zunino, F., Marsh, A. T. M., Maier, M., Wang, B., Canut, M., Juenger, M. C. G., Haha, M. B., Avet, F., Parashar, A., Al-Jaberi, L. A., Almenares-Reyes, R. S., Alujas-Diaz, A., Scrivener, K. L., Bernal, S. A., Provis, J. L., Sui, T., Bishnoi, S., & Martirena-Hernández, F. (2022)
Clay Calcination Technology: State-of-the-Art Review by the RILEM TC 282-CCL. *Materials and Structures*, *55*(1), 3.
https://doi.org/10.1617/s11527-021-01807-6

Snellings, R. (2016)
Assessing, understanding and unlocking supplementary cementitious materials. *RILEM Technical Letters*, *1*, 50–55.
https://doi.org/10.21809/rilemtechlett.2016.12

Swiss Confederation (2023a)
Gewässerschutzverordnung (GSchV).

Swiss Confederation (2023b)
Verordnung über die Vermeidung und die Entsorgung von Abfällen (VVEA).

7 FUNDAMENTAL ASPECTS OF MINERAL REACTIVITY AND STRUCTURAL TRANSFORMATIONS

Churakov S.V., Cametti G., Katheras A.

7.1 Introduction

PSI/LES and the Institute for Geological Science at the University of Bern (UBERN/IfG) collaborate in the fields of mineralogy, crystallography and environmental geochemistry. The research field of the Mineralogy Group at the University of Bern covers fundamental aspects of mineral surface reactivity, crystal structure characterization, and temperature driven phase transitions in condensed matter. The dedicated laboratories operated by the group are equipped with powder and single-crystal diffractometers for structural studies of minerals, and an atomic force microscopy laboratory used for in-situ characterization of mineral surface reactivity. The experimental studies are widely supported by theoretical modeling activities. In particular, we develop and apply numerical methods for investigation of reaction mechanisms and theoretical predictions of the thermodynamic properties of minerals. One such research activity is focused on the characterization of mineral structure transformations in natural and synthetic microporous minerals (e.g., zeolites) as result of dehydration and cation exchange processes. These structural studies are conducted by combining single crystal X-ray diffraction experiments, spectroscopic measurements, and atomistic simulations.

Zeolites are a class of porous crystalline materials, which are exploited in a widespread range of technological and industrial applications. In the last decades, particular attention was paid to their gas-sorption and separation capacity, with a special focus on CO_2 removal. Zeolites are particularly competitive because of their tuneable structure, faster adsorption kinetics, high selectivity for CO_2, and extended thermal stability. In collaboration with colleagues from University of Urbino Carlo Bo, Italy, the structural transformation and reactivity of temperature-activated CHA zeolites has been investigated. The structural characterization reveals that despite their low Si content, CHA zeolites do not lose crystallinity up to 350 °C and can be a good candidate for selective gas-sorption (see section 7.2).

In the framework of an interactional project on kinetics of radionuclide immobilization funded by the German Federal Ministry of Education and Research, the uptake of radionuclides by magnetite nanoparticles has been investigated. To reveal favorable conditions for the uptake of Tc and U, the structure, stability, and redox state of magnetite nanoparticles were investigated by atomistic simulation employing density functional theory. For the first time the pH-Eh stability and redox state of the full scale nanometer sized octahedral crystals of magnetite were characterized in the presence of explicit solvent. The simulations reveal particular importance and reactivity of the edge and corner sites dominating the nanoparticle morphology, in comparison to the typical speciation of the idealized macroscopic octahedral facets of magnetite (see section 7.3).

Xonotlite is an industrially important calcium silicate mineral, which is considered as a possible alternative to more common calcium silicate hydrates. The solubility of xonotlite remains poorly constrained experimentally. In a collaborative PhD project with EMPA, the thermodynamic properties of xonotlite were investigated by combining wet chemistry studies and ab initio thermodynamic modeling. Based on ab initio simulation the structure of the most stable polymorphs was revealed, and used for Rietveld refinement of the synthesized samples. The study explains the origin of discrepancies between the solubility data reported for natural and synthetic xonotlite. The thermodynamic data obtained provide reliable predictions of xonotlite performance in construction materials, and for reactive transport modelling of cement evolution at elevated temperatures (see section 7.4).

Ruddlesden-Popper (RP) phases are composed of two-dimensional perovskite-like motifs of intercalated interleaved mono and di-valent cations. Similar to perovskites, RP-phases are known for their peculiar properties including magnetoresistance, photoluminescence, catalytic activity, and superconductivity. Thus, RP phases are widely used as electronic and magnetic functional materials. A new mineral karlleuite, approved by International Mineralogical Association, was discovered in the xenolith sample at the Bellerberg volcano lava field, Eastern Eifel region, Germany. Its structural characterization was conducted by a group of scientists from the University of Silesia, Poland, University of Innsbruck, Austria, and the University of Bern (see section 7.5).

7.2 The flexibility of CHA framework-type zeolites: implications for gas separation processes

Zeolites with the CHA framework type are among the most exploited porous-materials in the field of gas separation and sorption processes (Fu and Davis, 2022). Gas admission in the porous framework is dictated by a complicated interplay of several factors, i.e. the extraframework (EF) cation content, the Si/Al ratio of the aluminosilicate framework, and most importantly the temperature applied for catalyst activation. Given that all zeolitic materials are subjected to a thermal treatment prior to their use in gas separation/sorption processes, knowledge about the temperature-induced transformations is of great interest (Boer et al., 2023). Despite several studies focused on temperature-activated CHA zeolites, at present the contradictory data are reported for the dehydrated form of Na-CHA (Mortier et al., 1977; Pham et al., 2014). For this reason, the behavior of Na-CHA as a function of temperature was characterized in a series of *in situ* X-ray diffraction experiments at 20-350°C and under variable humidity conditions (RH = 0, RH = 50%). The main objectives were: i) to shed light on the high-temperature modifications of Na-CHA; ii) to clarify the role of the Si/Al ratio and EF cation type in determining the response to the heating stimuli; iii) to determine how flexible is the CHA framework under the applied conditions. To test the effect of EF cation type, new data were collected on Cu-exchanged CHA. This zeolite has been extensively investigated in the literature (Fickel & Lobo, 2010; Andersen et al., 2014; Borfecchia et al., 2015), and was therefore used as a reference for our study. It could be shown that at 75°C, Na-CHA undergoes a severe contraction of the unit-cell volume (-12%) accompanied by a symmetry lowering (*R*-3*m* to *I*2/*m*) (Fig. 7.1a). The transformation is reversible, if the dehydrated Na-CHA is exposed to ambient conditions. In contrast, Cu-CHA experiences a significantly different dehydration path, which involves minor changes in the CHA framework, and a net positive thermal expansion after dehydration (Fig. 7.1b).

Different mechanisms were hypothesized to describe the gas sorption and separation capacity of CHA zeolites. These mechanisms are a result of the interplay of several parameters, i.e. extraframework cation-type, Si/Al ratio, and temperature (Shang et al., 2012).

Low Si/Al ratio zeolites have a higher number of charge-balancing cations, which work as active sites for adsorption of gas molecules. However, the higher Al content can lower their hydrothermal stability. For small-pore zeolites, like chabazite, it is generally accepted that the size exclusion effect is the dominant mechanism controlling the sorption process. For these zeolites, the eight-member ring (8MR) window is the only one providing access to the internal pores. Shang and co-workers (Shang et al., 2012) suggested a specific mechanism for gas separation of CO_2, CH_4 and N_2 in chabazite with Si/Al ≤ 3. This mechanism, called the "molecular trapdoor mechanism", refers to the displacement of large EF cations (e.g. K^+, Cs^+), located at the 8MR, by CO_2 molecules. The latter can strongly interact with the cations because of its high quadrupole moment. Molecules with low quadrupole moment, like N_2 and CH_4, are not able to displace the cation from the 8MR, because of the weaker interactions, and therefore they are blocked out from the pores. According to this process, the presence of a large cation is necessary to block the larger molecules (e.g. N_2 and CH_4). Similarly, lower temperatures are favored, because above 300 K the occupancy of the site at the 8MR decreases. Based on the measurement results, the dehydrated structure of Na-CHA (Si/Al ≤ 3) seems to be very promising for selective sorption of small molecules like CO_2. Considering the kinetic diameter of CO_2 (3.3 Å), the only accessible window is the 8MR_M4, the size of which (3.27 × 4.23 Å at 200°C) is too small for both N_2 and CH_4 (kinetic diameters of 3.64 and 3.80 Å, respectively). Based on our findings, we could conclude that the Si/Al ratio plays a key role in the HT transformations of Na-CHA. With a given Si/Al content, the CHA framework shows distinct behavior depending on the EF cations type (e.g. Na-CHA vs Cu-CHA). Despite their low Si content, both zeolites do not lose crystallinity up to 350°C, and can be good candidates for selective gas-sorption.

7.3 Crystal structure and thermodynamics of magnetite nanoparticles in solvents

Magnetite (Fe_3O_4) is a mixed Fe(II,III) oxide formed as the main corrosion product of steel in deep geological repositories. Following previous studies on dominant surface terminations that are stable under relevant environmental conditions, magnetite nanoparticles (MNPs) were investigated by large-scale ab initio simulation. Atomistic models were based on the

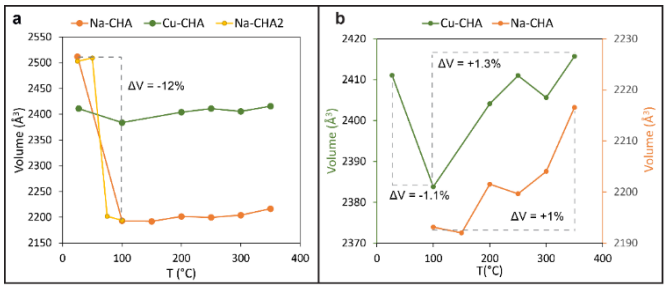

Fig. 7.1: Unit-cell volume trend of Na- and Cu-CHA as a function of temperature (a, b). Panel (b) compares the trend observed for the two zeolites between 100 and 350°C.

octahedrally terminated magnetite (111) surface forming octahedrally shaped 2 nm sized MNPs (Fig. 7.2, left).

The nanoparticle surfaces were protonated for charge balancing, and various symmetric and symmetry-broken H-distributions were analyzed. Systems with octahedral Fe charges ranging from (idealized) 2.5+ to 3+ were simulated. By comparing the respective energies, a preference for edge- and vertex-protonation could be deduced at these under-coordinated oxygen surface sites. In lower oxidized systems, this in turn leads to a distinct charge distribution of the surface-Fe cations. Towards the edges and vertices with more H, a charge resembling the idealized mixed Fe oxidation state is reached, while at the center of the nanoparticle facets with less protonation, a higher charge and Fe^{3+} can be assumed (Fig. 7.3).

The analysis of the system-specific surface energies showed that under repository relevant conditions, an elevated Fe oxidation state is preferred. This is in line with the previous analysis of the infinite magnetite surface. The oxidation state of the surface-located Fe ions would influence the interaction with solvent and potential contaminants including a potential reduction to a less mobile form. To investigate the interaction with a solvent, classical molecular dynamics (MD) simulations were performed, surrounding the MNP with water. The strong interaction was confirmed by the entrapment of water molecules by the structural inherent cavities formed by octahedrally coordinated Fe at the surface (Fig. 7.2, right). In a setup with NaCl, localization of Na cations at the vertices was observed reflecting the experimentally observed competitive behavior of NaCl in the retention of contaminants such as Se (Urbánová et al., 2024). Moreover, the Fe-octahedra at the vertices were found to be deformed in presence of the Na ions. In combination with the preference for Fe cations with higher oxidation state, these results are in line with the potential dissolution of the MNP and a transformation to maghemite, an Fe(III) oxide with a defective magnetite crystal structure.

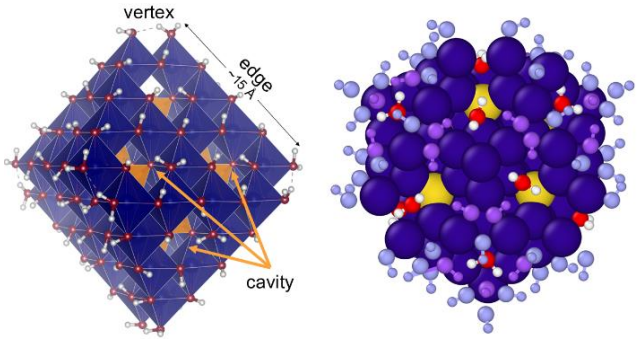

Fig. 7.2: Schematic representation of a protonated magnetite nanoparticle (MNP) (left). Octahedrally coordinated Fe ions (blue) at the surface form cavities with underlying tetrahedrally coordinated Fe (orange). These cavities readily entrap water molecules, as was observed in MD simulations (right, main part of MNP blue, surface-OH groups violet, edge-OH groups light blue). O is depicted in red, H in white.

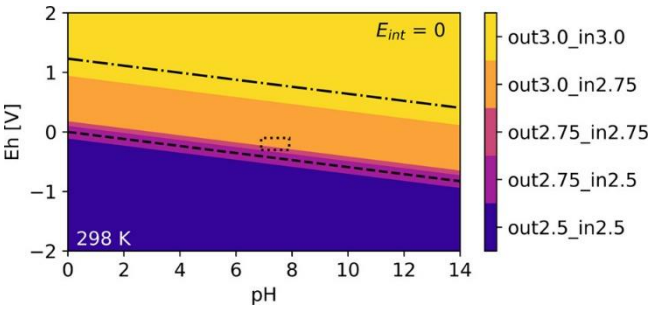

Fig. 7.3: Surface stability of Eh and pH diagram for hydrated MNP at 298 K obtained by ab initio simulations at a DFT level of theory. The dotted box indicates the expected in situ conditions in a geological repository for high level nuclear waste in argillaceous rocks. The dashed and dash-dotted lines indicate the lower and the upper water stability range. The 'out' and 'in' subscripts refer to the expected oxidation states of the octahedrally coordinated Fe at the surface or at the center of the MNP, respectively.

7.4 Thermodynamic stability of xonotlite

Xonotlite is an industrially important calcium silicate mineral, which is considered as possible alternative to more common calcium silicate hydrates, due to its stability at higher temperature and ability to form durable phases essential for development of high-strength-high thermal resistant low-porosity materials.

The solubility of xonotlite remains poorly constrained experimentally, such that the data reported in literature differ by as much as 10 log units. In a collaborative PhD project with EMPA, the thermodynamic properties of xonotlite were investigated, combining wet chemistry experiments and ab initio thermodynamic modelling (Mingione et al., 2024).

Based on ab initio simulation, the structure of the most stable xonotlite polymorphs was revealed, and used for the Rietveld refinement of the synthesized samples. Calculations predict that the monoclinic *Ma2b2c* and triclinic *M2a2b2c* xonotlite polymorphs are expected to be more stable than the *Ma2bc* and *M2a2bc* polymorphs. Rietveld refinement of the XRD data also indicates the presence of different polymorphs and a prevalence of the monoclinic modification, in agreement with theoretical calculations. Xonotlite formation is thus controlled not only by thermodynamic but also by kinetic processes,

explaining why different polymorphs might form, including the less stable forms. The derived solubility data are comparable to those reported in the literature at 25 °C for synthesized xonotlite, which is substantially lower than the data reported for natural xonotlite. The higher solubility of natural samples can be attributed to the presence of other amorphous or crystalline C-S-H phases. Thus, xonotlite was found to coexist with tobermorite at temperatures below 7 °C. The newly derived thermodynamic dataset for xonotlite provides reliable prediction of xonotlite performance in construction materials, and in reactive transport modeling of cement evolution at elevated temperatures.

7.5 Karlleuite Ca_2MnO_4 the first mineral with the Ruddlesden-Popper type structure

Ruddlesden-Popper (RP) phases are usually represented by perovskite-like layered oxides with the general formula $A_{n+1}BnX_{3n+1}$, or $AX(ABX_3)n$ (n = 1, 2, 3, …, ∞), where A is typically an alkali, alkaline-earth or rare-earth metal ion, B is a transition or post-transition metal ion, and X is usually oxygen, which can be partially replaced by other non-metallic elements such as N, S, and Cl (Sharma & Singh, 1998; Nirala et al., 2020). The RP phases are known to exhibit a range of versatile and functional physical and optical properties such as magnetoresistance, photoluminescence, catalytic activity, superconductivity, as well as wide applications as electronic and magnetic functional materials (Bassat et al., 2004; Ding et al., 2021). Karlleuite is a new mineral, which has been found in the xenolith sample within the basaltic lava from the Caspar quarry locality, Bellerberg volcano lava field, Eastern Eifel region, Germany. It is also the first layered perovskite mineral with an n = 1 Ruddlesden-Popper type structure. The new mineral (IMA2023-102), proposed name and symbol (Kll) have been approved by the Commission on New Minerals, Nomenclature and Classification (CNMNC) of the International Mineralogical Association (IMA). The physical, structural and optical properties were determined by a combination of different experimental techniques. The empirical formula of karlleuite calculated on the basis of 4 O atoms per formula unit is $(Ca_{1.97}Ce^{3+}_{0.06})_{2.03}(Mn^{4+}_{0.39}Ti_{0.36}Fe^{3+}_{0.19}Al_{0.09})_{1.03}O_4$, which leads to the simplified formula $(Ca, Ce^{3+})_2(Mn^{4+},Ti, Fe^{3+},Al)O_4$. The crystal structure of karlleuite displays a modular nature and consists of $CaBO_3$ perovskite layers with B = (Mn, Ti, Fe, Al), packed between CaO rock-salt layers arranged along the c-axis (Fig. 7.4). The Ca atoms, located at the boundary between the perovskite and rock salt layers, are coordinated by nine oxygen atoms. A careful analysis of the diffraction pattern excluded the presence of superlattice reflections related to the tilting of the octahedra in consecutive perovskite layers. In conclusion, the space group of karlleuite could be unambiguously determined in space group $I4/mmm$.

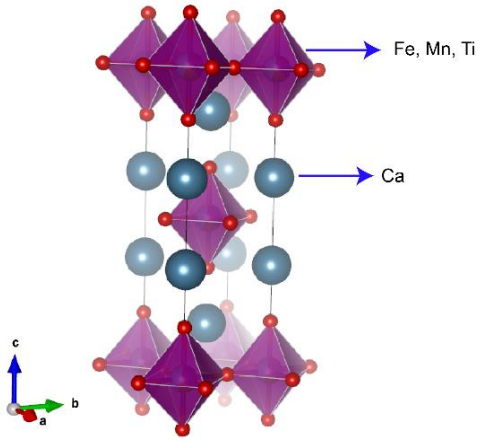

Fig. 7.4: The Ruddlesden-Popper crystal structure of the mineral karlleuite.

7.6 References

Andersen, C. W., Borfecchia, E., Bremholm, M., Jørgensen, M. R. V., Vennestrøm, P. N. R., Lamberti, C., Lundegaard, L. F., & Iversen, B. B. (2017)
Redox-driven migration of copper ions in the Cu-CHA zeolite as shown by the in situ PXRD/XANES technique. *Angewandte Chemie International Edition*, *56*(35), 10367–10372.
https://doi.org/10.1002/anie.201703808

Bassat, J. M., Odier, P., Villesuzanne, A., Marin, C., & Pouchard, M. (2004)
Anisotropic ionic transport properties in $La_2NiO_{4+\delta}$ single crystals. *Solid State Ionics*, *167*(3–4), 341–347.
https://doi.org/10.1016/j.ssi.2003.12.012

Boer, D. G., Langerak, J., & Pescarmona, P. P. (2023)
Zeolites as selective adsorbents for CO_2 separation. *ACS Applied Energy Materials*, *6*(5), 2634–2656.
https://doi.org/10.1021/acsaem.2c03605

Borfecchia, E., Lomachenko, K. A., Giordanino, F., Falsig, H., Beato, P., Soldatov, A. V., Bordiga, S., & Lamberti, C. (2015)
Revisiting the nature of Cu sites in the activated Cu-SSZ-13 catalyst for SCR reaction. *Chemical Science*, *6*(1), 548–563.
https://doi.org/10.1039/c4sc02907k

Ding, P., Li, W., Zhao, H., Wu, C., Zhao, L., Dong, B., & Wang, S. (2021)
Review on Ruddlesden–Popper perovskites as cathode for solid oxide fuel cells. *Journal of Physics Materials*, *4*(2), 022002.
https://doi.org/10.1088/2515-7639/abe392

Fickel, D. W., & Lobo, R. F. (2010)
Copper coordination in Cu-SSZ-13 and Cu-SSZ-16 investigated by variable temperature XRD. *The Journal of Physical Chemistry C*, *114*(3), 1633–1640.
https://doi.org/10.1021/jp9105025

Fu, D., & Davis, M. E. (2022)
Carbon dioxide capture with zeotype materials. *Chemical Society Reviews*, *51*(22), 9340–9370.
https://doi.org/10.1039/d2cs00508e

Katheras, A. S., Karalis, K., Krack, M., Scheinost, A. C., & Churakov, S. V. (2024)
Computational study on the octahedral surfaces of magnetite nanoparticles and their solvent interaction. *Environmental Science & Technology*, *58*(47), 21068–21076.
https://doi.org/10.1021/acs.est.4c06531

Mingione, S., Jansen, D., Winnefeld, F., Churakov, S. V., & Lothenbach, B. (2024)
Effect of temperature on the solubility of xonotlite. *Cement and Concrete Research*, *188*, 107732.
https://doi.org/10.1016/j.cemconres.2024.107732

Mortier W. J., Pluth J. J., Smith J. V. (1977)
Positions of cations and molecules in zeolites with the chabazite framework III. Dehydrated Na-exchanged chabazite. *Materials Research Bulletin 12*, 241-250.

Nirala, G., Yadav, D., & Upadhyay, S. (2020)
Ruddlesden-Popper phase A_2BO_4 oxides: recent studies on structure, electrical, dielectric, and optical properties. *Journal of Advanced Ceramics*, *9*(2), 129–148.
https://doi.org/10.1007/s40145-020-0365-x

Pham, T. D., Hudson, M. R., Brown, C. M., & Lobo, R. F. (2014)
Molecular basis for the high CO_2 adsorption capacity of chabazite zeolites. *ChemSusChem*, *7*(11), 3031–3038.
https://doi.org/10.1002/cssc.201402555

Shang, J., Li, G., Singh, R., Gu, Q., Nairn, K. M., Bastow, T. J., Medhekar, N., Doherty, C. M., Hill, A. J., Liu, J. Z., & Webley, P. A. (2012)
Discriminative separation of gases by a "molecular trapdoor" mechanism in chabazite zeolites. *Journal of the American Chemical Society*, *134*(46), 19246–19253.
https://doi.org/10.1021/ja309274y

Sharma, I. B., & Singh, D. (1998)
Solid state chemistry of Ruddlesden-Popper type complex oxides. *Bulletin of Materials Science*, *21*(5), 363–374.
https://doi.org/10.1007/bf02744920

Urbánová, L., Bujdoš, M., Matulová, M., Miglierini, M. B., Vyhnáleková, S., Orovčík, Ľ., Machata, P., Mičušík, M., Dobročka, E., Kollár, J., Matúš, P., & Urík, M. (2024)
Investigating the sorption behavior of selenite on commercial partially oxidized magnetite nanopowder under aerobic conditions: Characterization and mechanisms. *Separation and Purification Technology*, *348*, 127688.
https://doi.org/10.1016/j.seppur.2024.127688

8 PUBLICATIONS

8.1 Peer reviewed research articles

Abdullayev[1,2], E., Paterson[1], J. R., Kuszynski[1], E. P., Hamidi[3], M. D., Nahar[4], P., Greenwell[3,5], H. C., Neumann, A., & Sharple[1], G. J. (2024)
Evaluation of the antibacterial properties of commonly used clays from deposits in Central and Southern Asia. *Clays and Clay Minerals*, *72*, e9.
https://doi.org/10.1017/cmn.2024.7

[1] Department of Biosciences, Durham University, UK
[2] Department of Life Sciences, Khazar University, Azerbaijan
[3] Department of Earth Sciences, Durham University, UK
[4] Department of Global Health and Infection, Brighton and Sussex Medical School, Sussex University, UK
[5] Department of Chemistry, Durham University, UK

Ait-Mouheb[1], N., Yang[1], Y. K., Deissmann[1], G., Klinkenberg[1], M., Poonoosamy[1], J., Vinograd[1], V., Van Loon, L. R. & Bosbach[1], D. (2024)
Retention of ^{226}Ra in the sandy Opalinus Clay facies from the Mont Terri rock laboratory, Switzerland. *Applied Geochemistry*, *170*, 106048.
https://doi.org/10.1016/j.apgeochem.2024.106048

[1] Institute of Energy and Climate Research – Nuclear Waste Management (IEK-6), Forschungszentrum Jülich GmbH, 52428, Jülich, Germany

Albà[1,2], A., Adelmann[1], A., Münster[1,2], L., Rochman[3], D., & Boiger, R. (2024)
Fast uncertainty quantification of spent nuclear fuel with neural networks. *Annals of Nuclear Energy*, *196*, 110204.
https://doi.org/10.1016/j.anucene.2023.110204

[1] PSI Center for Scientific Computing, Theory and Data, 5232 Villigen PSI, Switzerland
[2] ETH Zürich, Rämistrasse 101, Zürich, 8092, Switzerland
[3] PSI Center for Nuclear Engineering and Sciences, 5232 Villigen PSI, Switzerland

Aschwanden[1], L., Waber[2], H.N., Eichinger[3], F., & Gimmi, T. (2024)
Isotope diffusive exchange experiments for deriving porewater isotope composition in low-permeability rocks – Improvements in experimental procedure and data processing. *Applied Geochemistry*, *160*, 105844.
https://doi.org/10.1016/j.apgeochem.2023.105844

[1] RWI, Institute of Geological Sciences, University of Bern, Switzerland
[2] WaterGeoChem Consulting, Bern, Switzerland
[3] Hydroisotop GmbH, Schweitenkirchen, Germany

Baral[1], A., Pesce[1], C., Yorkshire[1], A. S., Zhakiyeva[1,2], Z., Snellings[3], R., Hanein[1], T., Provis, J. L., & Peys[4], A. (2024)
Characterisation of iron-rich cementitious materials. *Cement and Concrete Research*, *177*, 107419.
https://doi.org/10.1016/j.cemconres.2023.107419

[1] University of Sheffield, Sheffield, United Kingdom
[2] Nazarbayev University, Astana, Kazakhstan
[3] KU Leuven, Leuven, Belgium
[4] VITO, Mol, Belgium

Bernal[1], S. A., Dhandapani[1], Y., Elakneswaran[2], Y., Gluth[3], G. J. G., Gruyaert[4], E., Juenger[5], M. C. G., Lothenbach[6], B., Olonade[7], K. A., Sakoparnig[8], M., Shi[9], Z., Thiel[10], C., Van den Heede[11], P., Vanoutrive[4], H., von Greve-Dierfeld[12], S., De Belie[11], N., & Provis, J. L. (2024)
Report of RILEM TC 281-CCC: A critical review of the standardised testing methods to determine carbonation resistance of concrete. *Materials and Structures*, *57*(8), 173.
https://doi.org/10.1617/s11527-024-02424-9

[1] University of Leeds, Leeds, UK
[2] Hokkaido University, Sapporo, Japan
[3] Bundesanstalt für Materialforschung und -prüfung (BAM), Berlin, Germany
[4] KU Leuven - Ghent, Ghent, Belgium
[5] University of Texas at Austin, Austin TX, USA
[6] Swiss Federal Laboratories for Materials Science and Technology (Empa), Dübendorf, Switzerland
[7] University of Lagos, Lagos, Nigeria
[8] Graz University of Technology, Graz, Austria
[9] Hunan University, Changsha, Hunan, China
[10] OTH Regensburg University of Applied Sciences, Regensburg, Germany
[11] Ghent University, Ghent, Belgium
[12] TFB Technology and Research for Concrete Structures, Wildegg, Switzerland

Bettoni[1], S., Orlandi[1], G. L., Salomone[1], F., Boiger, R., Ischebeck[1], R., Xue[1], R., & Mostacci[2], A. (2024) Machine learning based longitudinal virtual diagnostics at SwissFEL. *The Review of Scientific* I*nstruments*, *95*(1), 015110.
https://doi.org/10.1063/5.0179712

[1] PSI Center for Accelerator Science and Engineering, 5232 Villigen PSI, Switzerland
[2] Sapienza University of Rome, 00161 Rome, Italy

Boiger, R., Churakov, S. V., Llagaria[1], I. B., Kosakowski, G., Wüst[2,3], R., & Prasianakis, N. I. (2024)
Direct mineral content prediction from drill core images via transfer learning. *Swiss Journal of Geosciences*, *117*(1), 8.
https://doi.org/10.1186/s00015-024-00458-3
[1] ETH Zürich, Rämistrasse 101, Zürich, 8092, Switzerland
[2] Nagra, Switzerland
[3] Earth and Environmental Science, James Cook University, Townsville, 4811, Australia

Chaerun[1,2], R. I., Ishimura[1], M., Prihutami[1], P., Niu[1], X., Ohya[1], Y., Kuroda[3], K., Toda[4], K., Kikuchi[1], R., Otake[1], T., Provis, J. L., Elakneswaran[1], Y., & Sato[1], T. (2024)
Immobilisation of iodide in alkali-activated materials. *Chemosphere*, *369*, 143871.
https://doi.org/10.1016/j.chemosphere.2024.143871
[1] Hokkaido University, Sapporo, Japan
[2] Japan Atomic Energy Agency (JAEA), Ibaraki, Japan
[3] Central Research Institute of Electric Power Industry, Chiba, Japan
[4] University of Tokyo, Tokyo, Japan

Chen[1], L., Zhu[2], Z., Zhang[3], Y., Wang[4], L., Ma, B., Zheng[1], Y., Poon[5], C. S., Yan[4], J., & Tsang[3,4], D. C. W. (2024)
Carbonation-enhanced interfacial transition zone in biochar-cement mortar. *Construction and Building Materials*, *451*, 138606.
https://doi.org/10.1016/j.conbuildmat.2024.138606
[1] Dongguan University of Technology, Dongguan, China
[2] University of California, Berkeley, USA
[3] Hong Kong University of Science and Technology, Clear Water Bay, Hong Kong
[4] Zhejiang University, Hangzhou, China
[5] Hong Kong Polytechnic University, Hong Kong

Chen[1], Y., Miranda de Lima[2], L., Li[3], Z., Ma, B., Lothenbach[4], B., Yin[1], S., Yu[1], Q., & Ye[2], G. (2024) Synthesis, solubility and thermodynamic properties of N-A-S-H gels with various target Si/Al ratios. *Cement and Concrete Research*, *180*, 107484.
https://doi.org/10.1016/j.cemconres.2024.107484
[1] South China University of Technology, Guangzhou, China
[2] Delft University of Technology, Delft, Netherlands
[3] Harbin Institute of Technology, Shenzhen, China
[4] Empa, Dubendorf, Switzerland

Claret[1], F., Prasianakis, N. I., Baksay[2], A., Lukin[3], D., Pepin[4], G., Ahusborde[5], E., Amaziane[5], B., Bátor[6], G., Becker[7], D., Bednár[6], A., Béreš[8], M., Bérešová[8], S., Böthi[2], Z., Brendler[9], V., Brenner[10], K., Březina[11], J., Chave[10], F., Churakov, S. V., Hokr[11], M., Horák[8], D., Jacques[12], D., Jankovský[13], F., Kazymyrenko[14], C., Koudelka[15], T., Kovács[6], T., Krejčí[16], T., Kruis[16], J., Laloy[12], E., Landa[11], J., Ligurský[8], T., Lipping[17], T., López-Vázquez[18], C., Masson[10], R., Meeussen[19], J. C. L., Mollaali[20], M., Mon[21], A., Montenegro[21], L., Pisani[21], B., Poonoosamy[22], J., Pospiech[9], S. I., Saâdi[23], Z., Samper[21], J., Samper-Pilar[21], A.-C., Scaringi[15], G., Sysala[8], S., Yoshioka[2], K., Yang[2], Y., Zuna[13], M., & Kolditz[21], O. (2024)
EURAD state-of-the-art report: development and improvement of numerical methods and tools for modeling coupled processes in the field of nuclear waste disposal. *Frontiers in Nuclear Engineering*, *3*.
https://doi.org/10.3389/fnuen.2024.1437714
[1] BRGM, Orléans, France
[2] TS Enercon, Budapest, Hungary
[3] SURAO, Praha, Czechia
[4] Andra, Chatenay Malabry, France
[5] Universite de Pau et des Pays de l'Adour, E2S UPPA, CNRS, LMAP, Pau, France
[6] Social Organization for Radioecological Cleanliness, Veszprem, Hungary
[7] GRS gGmbH, Braunschweig, Germany
[8] Institute of Geonics, Czech Academy of Sciences, Ostrava, Czechia
[9] Helmholtz Zentrum Dresden-Rossendorf, Dresden, Germany
[10] CNRS, Inria, LJAD, University Côte d'Azur, Nice, France
[11] Technical University of Liberec, Liberec, Czechia
[12] Belgian Nuclear Research Centre, Mol, Belgium
[13] Waste Disposal Processes and Safety Department, Radioactive Waste and Decommissioning Division, ÚJV Řež, a.s., Husinec, Czechia
[14] EDF R&D, IMSIA - UMR CNRS 9219, Institut des Sciences de la mécanique et Applications industrielles, Palaiseau, France
[15] Institute of Hydrogeology, Engineering Geology and Applied Geophysics, Faculty of Science, Charles University, Prague, Czechia
[16] Faculty of Engineering, Czech Technical University in Prague, Prague, Czechia
[17] Faculty of Information Technology and Communication Sciences, Tampere University, Pori, Finland
[18] LatinGEO Lab IGM+ORT, Universidad ORT Uruguay, Montevideo, Uruguay
[19] Nuclear Research and Consultancy Group, Petten, Netherlands
[20] Helmholtz Centre for Environmental Research UFZ, Leipzig, Germany
[21] Civil Engineering School, Interdisciplinary Center for Biology and Chemistry (CICA), Universidade de A Coruña, Campus de Elviña, A Coruña, Spain
[22] Institute of Energy and Climate Research, Nuclear Waste Management (IEK-6), Forschungszentrum Juelich, Germany
[23] Institut de Radioprotection et de Sûreté Nucléaire (IRSN), PSE-ENV/SPDR/UEMIS, Fontenay-aux-Roses, France

Churakov, S. V., Claret[1], F., Idiart[2], A., Jacques[3], D., Govaerts[3], J., Kolditz[4], O., Prasianakis, N. I., & Samper[5] J. (2024)
Position paper on high fidelity simulations for coupled processes, multi-physics and chemistry in geological disposal of nuclear waste. *Environmental Earth Sciences*, *83*(17), 521.
https://doi.org/10.1007/s12665-024-11832-7
[1] BRGM, Orléans, France
[2] Amphos 21, Barcelona, Spain
[3] Belgium Nuclear Research Centre (SCK CEN), Mol, Belgium
[4] Helmholtz Centre for Environmental Research - UFZ, Leipzig, Germany
[5] CICA (Interdisciplinary Center for Chemistry and Biology) & amp; Civil Engineering School and Department, University of A Coruña, Coruña, Spain

Collin[1], M., Prentice[1], D. P., Geddes[2], D., Provis, J. L., Ellison[3], K., Balonis[1], M., Simonetti[1], D., & Sant[1], G. N. (2024)
Thermochemical data and phase equilibria of halide (Cl^-, Br^-, I^-) containing AFm and hydrotalcite compounds. *Journal of the American Ceramic Society*, *107*(5), 3562-3576.
https://doi.org/10.1111/jace.19665
[1] University of California Los Angeles, Los Angeles CA, USA
[2] University of Sheffield, Sheffield, UK
[3] Electric Power Research Institute, Charlotte NC, USA

Dabarera[1], A., Fernández[2], R. & Provis, J. L. (2024) A systematic review of engineering properties of magnesium potassium phosphate cement as a repair material. *Frontiers in Materials*, *11*, 1451079.
https://doi.org/10.3389/fmats.2024.1451079
[1] University of Hertfordshire, Hatfield, UK
[2] Autonomous University of Madrid, Madrid, Spain

Damiani, L. H., Kosakowski, G., Vinsot[1], A., & Churakov, S. V. (2024)
Hydrogen gas transfer between a borehole and claystone: Experiment and geochemical model. *Environmental Geotechnics*, *11*(3), 180–193.
https://doi.org/10.1680/jenge.21.00061
[1] Andra, France

Geddes[1], D. A., Walkley[1], B., Matsuda[2], T., & Provis, J. L. (2024)
Multi-year cementitious hydrate product formation in non-Portland high performance concretes. *CEMENT*, *18*, 100111.
https://doi.org/10.1016/j.cement.2024.100111
[1] University of Sheffield, Sheffield, UK
[2] Sumitomo Mitsui Construction Co. Ltd., Nagareyama-shi, Chiba, Japan

Gimmi, T., Aschwanden[1], L., Waber[2], H. N., Gaucher[1], E. C., Ma[1], J., & Traber[3], D. (2024)
Profiles of $\delta^{18}O$ and $\delta^{2}H$ in porewater of a Mesozoic rock sequence: Regional variability and relation to large-scale transport regimes. *Applied Geochemistry*, *160*, 105846.
https://doi.org/10.1016/j.apgeochem.2023.105846
[1] RWI, Institute of Geological Sciences, University of Bern, Switzerland
[2] WaterGeoChem Consulting, Bern, Switzerland
[3] Nagra, Switzerland

Glaus, M. A., Van Loon, L. R., & Wüst[1], R. A. J. (2024)
Diffusion of HTO, ^{36}Cl and ^{22}Na in the Mesozoic rocks of northern Switzerland: II. Data interpretation in terms of an electrical double layer model. *Applied Geochemistry*, *162*, 105842.
https://doi.org/10.1016/j.apgeochem.2023.105842
[1] Nagra, Switzerland

Goethals[1], J., De Windt[2], L., Miron, G.D., Wittebroodt[3], C., & Abdelouas[1], A. (2024)
Anoxic corrosion of carbon steel in high pH cementitious media and high temperature conditions: New insights on the formation of (Fe, Al) Si-hydrogarnet corrosion product. *Corrosion Science*, *237*, 112318.
https://doi.org/10.1016/j.corsci.2024.112318
[1] Laboratoire Subatech, UMR 6457, 4 Rue Alfred Kastler, La Chantrerie CS 20722, Nantes CEDEX 3 44307, France
[2] Mines Paris, PSL University, Centre for Geosciences and Geoengineering, 35 Rue St-Honoré, Fontainebleau 77300, France
[3] Institut de Radioprotection et de Sûreté Nucléaire (IRSN)/LETIS, 31 Avenue de la Division Leclercq, BP 17, Fontenay-aux-Roses Cedex 92262, France

Hauser[1], J., Miron, G. D., Kyas[2], S., Leal[2], A. M. M., & Gunning[3], J. (2024)
Towards a model-Based interpretation of measurements of mineralogical and chemical Compositions. *Mathematical Geosciences*, *56*(6), 1285–1302.
https://doi.org/10.1007/s11004-023-10121-6
[1] Mineral Resources, CSIRO, Clunies Ross Street, Acton, ACT, 2601, Australia
[2] Geothermal Energy and Geofluids Group, Department of Earth Sciences, ETH Zurich, Sonneggstrasse 5, 8092, Zurich, Switzerland
[3] Energy, CSIRO, Clayton, VIC, 3168, Australia

Hu, G., Prasianakis, N. I., Churakov, S. V., & Pfingsten, W. (2024)
Performance analysis of data-driven and physics-informed machine learning methods for thermal-hydraulic processes in Full-scale Emplacement experiment. *Applied Thermal Engineering*, *245*, 122836.
https://doi.org/10.1016/j.applthermaleng.2024.122836

Ingold P., Weibel, G., Wanner, C., Gimmi, T., & Churakov, S. V. (2024)
Hydrological and geochemical properties of bottom ash landfills. *Environmental Earth Sciences, 83, 180.* https://doi.org/10.1007/s12665-024-11471-y

Jäger[1], T., Mokos, A., Prasianakis, N. I., & Leyer[1], S. (2024)
Validating the Transition Criteria from the Cassie-Baxter to the Wenzel State for Periodically Pillared Surfaces with Lattice Boltzmann Simulations. *ACS Omega*, *9*(9), 10592 – 10601.
https://doi.org/10.1021/acsomega.3c08862
[1] Department of Engineering, Faculty of Science, Technology and Medicine, University of Luxembourg, Luxembourg, L-1359, Luxembourg

Jenni[1], A., Gimmi, T., & Mäder[2], U. (2024)
Coupling of porosity and diffusive transport in highly reactive systems: Open issues of reactive transport modelling. *Applied Geochemistry*, *170*, 106076.
https://doi.org/10.1016/j.apgeochem.2024.106076
[1] RWI, Institute of Geological Sciences, University of Bern, Switzerland
[2] Rock-Water Consulting, Boll, Switzerland

Jin[1], H., Ghazizadeh[2], S., & Provis, J. L. (2024)
Thermodynamic modelling of alkali-silica reactions in blended cements. *Cement and Concrete Research*, *181*, 107543.
https://doi.org/10.1016/j.cemconres.2024.107543
[1] University of Sheffield, Sheffield, UK
[2] Mott MacDonald, London, UK

Katheras, A. S., Karalis, K., Krack, M., Scheinost[1,2], A. C., & Churakov, S. V. (2024)
Computational study on the octahedral surfaces of magnetite nanoparticles and their Solvent Interaction. *Environmental Science & Technology*, *58*(47), 21068–21076.
https://doi.org/10.1021/acs.est.4c06531
[1] The Rossendorf Beamline at the European Synchrotron Radiation Facility (ESRF), France
[2] Institute of Resource Ecology, Helmholtz Zentrum Dresden Rossendorf, Germany

Khatoonabadi, M., Prasianakis, N. I., & Mantzaras, J. (2024)
A pore-level 3D lattice Boltzmann simulation of mass transport and reaction in catalytic particles used for methane synthesis. *International Journal of Heat and Mass Transfer*, *221*, 125025.
https://doi.org/10.1016/j.ijheatmasstransfer.2023.125025

Kriven[1], W. M., Leonelli[2], C., Provis, J. L., Boccaccini[3], A. R., Attwell[4], C., Ducman[5], V. S., Ferone[6], C., Rossignol[7], S., Luukkonen[8], T., van Deventer[9], J. S. J., Emiliano[10], J. V., & Lombardi[10], J. E. (2024)
Why geopolymers and alkali-activated materials are key components of a sustainable world: A perspective contribution. *Journal of the American Ceramic Society*, *107*, 5159-5177.
https://doi.org/10.1111/jace.19828
[1] University of Illinois at Urbana-Champaign, Urbana IL, USA
[2] University of Modena and Reggio Emilia, Modena, Italy
[3] University of Erlangen-Nuremberg, Erlangen, Germany
[4] ARC Innovations, Benoni, South Africa
[5] Slovenian National Building and Civil Engineering Institute (ZAG), Ljubljana, Slovenia
[6] University of Naples "Parthenope", Naples, Italy
[7] Limoges University, Limoges, France
[8] Oulu University, Oulu, Finland
[9] Zeobond Group, Somerton, Victoria, Australia
[10] National University of Singapore, Singapore

Lothenbach[1], B., Nedyalkova, L., Wieland, E., Mäder, U., Rojo, H., & Tits, J. (2024)
Sorption of Se(VI) and Se(IV) on AFm phases. *Applied Geochemistry*, *175*, 106177.
https://doi.org/10.1016/j.apgeochem.2024.106177
[1] Swiss Federal Laboratories for Materials Science and Technology (Empa), Dübendorf, Switzerland

Ma, B., Provis, J. L., Wang, D., & Kosakowski, G. (2024)
The essential role of cement-based materials in a radioactive waste repository. *npj Materials Sustainability*, *2*(1), 21.
https://doi.org/10.1038/s44296-024-00025-9

Marques Fernandes, M., Mazurek[1], M., Wersin[1], P., Wüst[2,3], R., & Baeyens, B. (2024)
Cation-exchange properties of the Mesozoic sedimentary sequence of Northern Switzerland and modelling of the Opalinus Clay porewater. *Applied Geochemistry*, *162*, 105852.
https://doi.org/10.1016/j.apgeochem.2023.105852
[1] Rock-Water Interaction (RWI), Institute of Geological Sciences, University of Bern, Switzerland
[2] National Cooperative for the Disposal of Radioactive Waste (Nagra), Switzerland
[3] Earth and Environmental Science, James Cook University, Australia

Marsh[1], A. T. M., Brown[2], A. P., Freeman[1], H. M., Neumann, A., Walkley[3], B., Pendlowski[4], H., & Bernal[1], S. A. (2024)
Mineralogical characteristics and processing effects: influences on the structure and pozzolanic reactivity of mechano-chemically activated meta-kaolinites, *Journal of Materials Chemistry A, 12*, 24260–24277.
https://doi.org/10.1039/D4TA02545H
[1] School of Civil Engineering, University of Leeds, UK
[2] School of Chemical and Process Engineering, University of Leeds, UK
[3] Department of Chemical and Biological Engineering, University of Sheffield, UK
[4] The James Hutton Institute, UK

Mingione, S., Jansen[1], D., Winnefeld[2], F., Churakov, S. V., & Lothenbach[2], B. (2024)
Effect of temperature on the solubility of xonotlite. *Cement and Concrete Research*, *188*, 107732.
https://doi.org/10.1016/j.cemconres.2024.107732
[1] Friedrich-Alexander-University of Erlangen-Nürnberg, GeoZentrum Nordbayern, Mineralogy, Germany
[2] Swiss Federal Laboratories for Materials Science and Technology (Empa), Dübendorf, Switzerland

Mitchell[1], R. L., Holwell[1], A., Torelli[2], G., Provis, J., Selvaranjan[2], K., Geddes[2], D., Yorkshire[2], A., & Kearney[2], S. (2024)
Cements and concretes materials characterisation using machine-learning-based reconstruction and 3D quantitative mineralogy via X-ray microscopy. *Journal of Microscopy*, *294*, 137-145.
https://doi.org/10.1111/jmi.13278
[1] Carl Zeiss Microscopy, Cambridge, UK
[2] University of Sheffield, Sheffield, UK

Mokos, A., Patel, R., Karalis, K., Churakov, S. V., & Prasianakis, N. I. (2024c)
Surface controlled mechanism of water boiling for nuclear reactor fuel assembly. *International Journal of Heat and Mass Transfer*, *230*, 125747.
https://doi.org/10.1016/j.ijheatmasstransfer.2024.125747

Mokos, A., Sato, Y., Niceno, B., Churakov, S. V., & Prasianakis, N. I. (2024b)
Nucleate boiling within a fuel assembly affected by CRUD. *EPJ Web of Conferences*, *302*, 03003.
https://doi.org/10.1051/epjconf/202430203003

Pan[1,3], R., Gysi[1,2], A., Miron, G.D., Zhu[3], C. (2024)
Optimized thermodynamic properties of REE aqueous species (REE^{3+} and $REEOH^{2+}$) and experimental database for modeling the solubility of REE phosphate minerals (monazite, xenotime, and rhabdophane) from 25 to 300 °C. *Chemical Geology*, *643*, 121817.
https://doi.org/10.1016/j.chemgeo.2023.121817
[1] New Mexico Bureau of Geology and Mineral Resources, New Mexico Institute of Mining and Technology, Socorro, USA
[2] Department of Earth and Environmental Science, New Mexico Institute of Mining and Technology, Socorro, USA
[3] Department of Earth and Atmospheric Sciences, Indiana University, Bloomington, USA

Pang[1], L., Wang, D., & Wang[1], Q. (2024)
Utilizing spodumene slag as a supplementary cementitious material: A quantitative study. *Journal of Building Engineering*, *98*, 111384.
https://doi.org/10.1016/j.jobe.2024.111384
[1] Tsinghua University, Beijing, China

Peng, H., Fei[1], L., He[2], X., Carmeliet[1], J., Churakov, S. V., & Prasianakis, N. I. (2024)
Three-dimensional modelling of cavitation bubble collapse using non-orthogonal multiple-relaxation-time lattice Boltzmann method. *Ocean Engineering*, *294*, 116720.
https://doi.org/10.1016/j.oceaneng.2024.116720
[1] Chair of Building Physics, Department of Mechanical and Process Engineering, ETH Zürich, Switzerland
[2] State Key Laboratory of Hydraulics and Mountain River Engineering, Sichuan University, Chengdu, China

Perrot[1], A., Jacquet[1], Y., Caron[2], J. F., Mesnil[2], R., Ducoulombier[3], N., De Bono[3], V., Sanjayan[4], J., Ramakrishnan[4], S., Kloft[5], H., Gosslar[5], J., Muthukrishnan[6], S., Mechtcherine[6], V., Wangler[7], T., Provis, J. L., Dörfler[8], K., Krakovska[8], E., Roussel[9], N., & Keita[9], E. (2024)
Snapshot on 3D printing with alternative binders and materials: Earth, geopolymers, gypsum and low carbon concrete. *Cement and Concrete Research*, *185*, 107651.
https://doi.org/10.1016/j.cemconres.2024.107651
[1] Université Bretagne-Sud, Lorient, France
[2] École des Ponts ParisTech, Marne-La-Vallée, France
[3] XTree, Rungis, France
[4] Swinburne University of Technology, Hawthorn, Victoria, Australia
[5] Technische Universität Braunschweig, Braunschweig, Germany
[6] TU Dresden, Dresden, Germany
[7] ETH Zürich, Zürich, Switzerland
[8] Technical University of Munich, Munich, Germany
[9] Université Gustave Eiffel, École des Ponts, CNRS, Champs-sur-Marne, France

Pothanamkandathil[1], V., Neumann, A., Thompson[2], A., & Gorski[1], C. A. (2024)
Redox properties of structural Fe in clay minerals: 4. Reinterpreting redox profiles by accounting for electron transfer and structural rearrangement kinetics. *Environmental Science & Technology*, *58*, 19702-19713.
https://doi.org/10.1021/acs.est.4c07835
[1] Department of Civil and Environmental Engineering, The Pennsylvania State University, USA
[2] Department of Crop and Soil Sciences, The University of Georgia, USA

Prasianakis, N. I. (2024)
AI-enhanced X-ray diffraction analysis: towards real-time mineral phase identification and quantification. *IU Crystallography Journal*, *11*, 647 – 648.
https://doi.org/10.1107/S2052252524008157

Provis, J. L. (2024)
Material durability, material failure, and material investment—the complexity of concrete. *Communications Engineering*, *3*(1), 23.
https://doi.org/10.1038/s44172-024-00172-w

Provis, J. L., Bernal[1], S. A., & Zhang[2], Z. (2024) The decarbonization of construction — How can alkali-activated materials contribute? *Engineering*, *37*(6), 18-21.
https://doi.org/10.1016/j.eng.2023.09.014
[1] University of Leeds, Leeds, UK
[2] Tongji University, Shanghai, China

Qian[1], Y. T., Scheinost[2,3], A. C., Grangeon[4], S., Hoving[5], A., Churakov[1], S. V., & Marques Fernandes, M. (2024)
Influence of structural Fe content in clay minerals on selenite redox reactions: Kinetics and structural transformations. *Geochimica et Cosmochimica Acta*, *377*, 19-33.
https://doi.org/10.1016/j.gca.2024.05.012
[1] Institute of Geological Sciences, University of Bern, Switzerland
[2] The Rossendorf Beamline at the European Synchrotron Radiation Facility (ESRF), France
[3] Institute of Resource Ecology, Helmholtz Zentrum Dresden Rossendorf, Germany
[4] BRGM – French Geological Survey, France
[5] TNO Geological Survey of the Netherlands, The Netherlands

Robins[1], K., O'Donnell[1], G., Neumann, A., Schmidt[2], W., Hart[2], A., & Graham[1], D. W. (2024)
Antimicrobial resistance in rural rivers: Comparative study of the Coquet (Northumberland) and Eden (Cumbria) River catchments. *Science of the Total Environment*, 172348.
https://doi.org/10.1016/j.scitotenv.2024.172348
[1] School of Engineering, Newcastle University, UK
[2] Chief Scientists Group, Environment Agency, UK

Sreenivasan, H., Bernard, E., Santos, H. S., Nguyen, H., Moukannaa, S., Adediran, A., Provis, J. L., & Kinnunen, P. (2024)
A critical review of magnesium silicate hydrate (M-S-H) phases for binder applications. *Cement and Concrete Research*, *178*, 107462.
https://doi.org/https://doi.org/10.1016/j.cemconres.2024.107462

Stefanini[1,2], L., Ansari[3], D., Walkley[1], B., & Provis, J. L. (2024)
Characterisation of calcined waste clays from kaolinite extraction in alkali-activated GGBFS blends. *Materials Today Communications*, *38*, 107777.
https://doi.org/10.1016/j.mtcomm.2023.107777
[1] University of Sheffield, Sheffield, UK
[2] VTT Technical Research Centre of Finland, Espoo, Finland
[3] Imerys, Par, Cornwall, UK

Stefanini[1,2], L., Walkley[1], B., & Provis, J. L. (2024) Basic oxygen furnace (BOF) slag as an additive in sodium carbonate-activated slag cements. *Materials and Structures*, *57*(7), 153.
https://doi.org/10.1617/s11527-024-02425-8
[1] University of Sheffield, Sheffield, UK
[2] VTT Technical Research Centre of Finland, Espoo, Finland

Tits, J., Curti, E., Laube, A., Wieland, E., & Provis, J. L. (2024)
Sorption of ^{32}Si and ^{45}Ca by isotopic exchange during recrystallisation of cement phases. *Applied Geochemistry*, *173*, 106117.
https://doi.org/10.1016/j.apgeochem.2024.106117

Van Laer[1], L., Aertsens[1], M., Maes[1], N., Van Loon, L. R., Glaus, M. A. & Wüst[2,3], R. A. J. (2024)
Diffusion of HTO, ^{36}Cl and ^{22}Na in the Mesozoic rocks of northern Switzerland: II. Data interpretation in terms of an electrical double layer model. *Applied Geochemistry*, *162*, 105840.
https://doi.org/10.1016/j.apgeochem.2023.105840
[1] SCK-CEN, Belgian Nuclear Research Centre, Boeretang 200, 2400, Mol, Belgium
[2] Nagra, Hardstrasse 73, 5430, Wettingen, Switzerland
[3] Earth and Environmental Science, James Cook University, 4811, Townsville, Australia

Vigor[1,2], J. E., Prentice[3,4], D. P., Xiao[5,6], X., Bernal[1], S. A., & Provis, J. L. (2024)
The pore structure and water absorption in Portland/slag blended hardened cement paste determined by synchrotron X-ray microtomography and neutron radiography. *RSC Advances*, *14*(7), 4389-4405.
https://doi.org/10.1039/D3RA06489A
[1] University of Leeds, Leeds, UK
[2] Imperial College, London, UK
[3] University of Sheffield, UK
[4] University of California Los Angeles, Los Angeles CA, USA
[5] Argonne National Laboratory, Argonne IL, USA
[6] Brookhaven National Laboratory, Brookhaven NY, USA

Wang, D., Ma, B., Pang[1], L., & Wang[1], Q. (2024) Alkali-activated blast furnace ferronickel slag for Cr immobilization. *Cement and Concrete Composites*, *150*, 105560.
https://doi.org/10.1016/j.cemconcomp.2024.105560
[1] Tsinghua University, Beijing, China

Wang[1,2], L., Nerella[2], V. N., Li[2], D., Zhang, Y., Ma, B., Ivaniuk[2], E., Zhang[3], Y., Zhu[5], X., Yan[1,4], J., Mechtcherine[2], V., & Tsang[1,3], D. C. W. (2024) Biochar-augmented climate-positive 3D printable concrete. *Communications Materials*, *5*, 257.
https://doi.org/10.1038/s43246-024-00700-3
[1] Zhejiang University, Hangzhou, China
[2] Technische Universität Dresden, Dresden, Germany
[3] Hong Kong University of Science and Technology, Hong Kong, China
[4] Hohai University, Nanjing, China
[5] University of California, Berkeley, USA

Wang[1], L., Xia[1], Y., Zhang, Y., Guo[2], B., Sun[1], C., Ma, B., Tsang[1,3], D. C. W., & Yan[1], J. (2024)
Introducing reactive magnesia to activate chloride/sulfate in waste incinerator fly ash for immobilization of potentially toxic elements. *ACS Sustainable Chemistry & Engineering*, *12*(26), 9602-9611.
https://doi.org/10.1021/acssuschemeng.4c00522
[1] Zhejiang University, Hangzhou, China
[2] Hefei University of Technology, Hefei, China
[3] Hong Kong University of Science and Technology, Clearwater Bay, Hong Kong, China

Wei, X., Shi[1], X., Yang[1], M., Tan[1], Q., Xu[1], Z., Ma, B., Pan[1], D., & Wu[1], W. (2024)
Phosphate and illite colloid pose a synergistic risk of enhanced uranium transport in groundwater: A challenge for phosphate immobilization remediation of uranium contaminated environmental water. *Water Research*, *255*, 121514.
https://doi.org/10.1016/j.watres.2024.121514
[1] Lanzhou University, Lanzhou, China

Yang[1], Y., Churakov, S. V., Patel[2], R. A., Prasianakis N. I., Deissmann[1], G., Bosbach[1], D., & Poonoosamy[1], J. (2024)
Pore-scale modeling of water and ion diffusion in partially saturated clays. *Water Resources Research*, *60* (1), e2023WR035595.
https://doi.org/10.1029/2023WR035595
[1] Institute of Energy and Climate Research—Nuclear Waste Management (IEK-6), JARA-CSD, Forschungszentrum Jülich GmbH, Jülich, Germany
[2] Laboratory for Waste Management, Institute of Building Materials and Concrete Structures (IMB), Karlsruhe Institute of Technology (KIT), Karlsruhe, Germany

Yang[1], Y., Patel[2], R. A., Prasianakis, N. I., Churakov S. V., Deissmann G., & Bosbach[1] D. (2024)
Elucidating the role of water films on solute diffusion in unsaturated porous media by improved pore-scale modeling. *Vadose Zone Journal*, *23* (3), e20321.
https://doi.org/10.1002/vzj2.20321
[1] Institute of Energy and Climate Research (IEK-6): Nuclear Waste Management, and JARA-CSD, Forschungszentrum Jülich GmbH, Jülich, Germany
[2] Institute of Building Materials and Concrete Structures (IMB), Karlsruhe Institute of Technology (KIT), Karlsruhe, Germany

Zhang[1], Y., Zhu[2], X., Ma, B., Wang[3], L., Yan[3], J., & Tsang[1,3], D. C. W. (2024)
Insights into microstructural alterations in alkali-activated materials incorporating municipal solid waste incineration fly ash. *Construction and Building Materials*, *425*, 136129.
https://doi.org/10.1016/j.conbuildmat.2024.136129
[1] Hong Kong University of Science and Technology, Clearwater Bay, Hong Kong, China
[2] University of California, Berkeley, USA
[3] Zhejiang University, Hangzhou, China

Zwahlen[1], C., Gimmi, T., Jenni[1], A., Kiczka[1], M., Mazurek[1], M., Van Loon, L. R., Mäder[2], U., & Traber[3], D. (2024)
Chloride accessible porosity fractions across the Jurassic sedimentary rocks of northern Switzerland. *Applied Geochemistry*, *162*, 105841.
https://doi.org/10.1016/j.apgeochem.2023.105841
[1] RWI, Institute of Geological Sciences, University of Bern, Switzerland
[2] Rock-Water Consulting, Boll, Switzerland
[3] Nagra, Switzerland

8.2 Technical reports

Becker[1], D.-A., Xiaoshuo[2], L., Holt[3], E., Pfingsten[4], W., Coelho[5], D., Strusińska-Correia[6], A., & Göbel[6], A. (2024)
UMAN – Management options for different types of uncertainties and preferences of different actors. Final version as of 22.05.2024 of deliverable D10.19 of the HORIZON 2020 project EURAD. EC Grant agreement no: 847593. EC**:** 66.
[1] Gesellschaft für Anlagen- und Reaktorsicherheit (GRS) gGmbH, Theodor-Heuss-Straße 4, 38122 Braunschweig, Germany
[2] Nagra, Hardstrasse 73, 5430, Wettingen, Switzerland
[3] VTT, Kivimiehentie 3, Espoo, P.O. Box 1000, 02044 VTT, Finland
[4] PSI Center for Nuclear Engineering and Sciences, 5232 Villigen PSI, Switzerland
[5] ANDRA, F-92298 Chatenay-Malabry, France
[6] BGE Bundesgesellschaft für Endlagerung mbH, Forschung & Entwicklung / Wissensmanagement, Eschenstraße 55, 31224 Peine, Germany

Churakov, S. V., Dauzères, A., Fischer, C., Mokos, A., Perko, J., Prasianakis, N. I., Seetharam, S. C., Phung, T. P., Shao J.-F., & Xue, J. (2024)
Report on micro scale chemo-mechanical modelling of leaching and carbonation and parameters upscaling. Final version as of 19.01.2024 of deliverable D16.7 of the HORIZON 2020 project EURAD. EC Grant agreement no: 847593.

Claret, F., Prasianakis, N. I., Baksay, A., Lukin, D., Pepin, G., Ahusborde, E., Amaziane, B., Baksay, A., Bátor, G., Becker, D., Bednár, A., Béreš, M., Bérešová, S., Böthi, Z., Brendler, V., Brenner, K., Bˇrezina, J., Chave, F., Churakov, S. V., Hokr, M., Horák, D., Jacques, D., Jankovsky, F., Kazymyrenko, C., Koudelka, T., Kovács, T., Krejci, T., Kruis, J., Laloy, E., Landa, J., Ligurský, T., Lipping, T., López-Vázquez, C., Masson, R., Meeussen, J. C. L., Mollaali, M., Mon, A., Montenegro, L., Poonoosamy, J., Saâdi, Z., Samper, J., Samper-Pillar, A-C., Scaringi, G., Yoshioka, K., Yuankai, Y., Zuna, M., & Kolditz, O. (2024)
Development and Improvement Of Numerical methods and Tools for modelling coupled processes, Updated State Of The Art report. Deliverable D 4.2 of the HORIZON 2020 project EURAD. EC Grant agreement N° 847593.

Glaus[1], M. A., Kulik[1,2], D. A., Miron[1], G. D., van Loon[1,3], L. R., Wüst[4], R., Becker[4], J., & Li[4], X. (2024)
Diffusion Databases for Opalinus Clay, Confining Geological Units and Bentonite: Methods, Concepts and Upscaling of Data. *Nagra Technical Report NTB 23-08.*
[1] PSI Center for Nuclear Engineering and Sciences, Switzerland
[2] CONGINEER GmbH, 5200 Brugg, Switzerland
[3] CWL Solutions GmbH, 5314 Kleindöttingen, Switzerland
[4] Nagra, 5430 Wettingen, Switzerland

Kolditz, O., Prasianakis, N. I., & Claret, F. (2024)
Final report describing improvement and implementation of scale transition methods to model coupled processes. Deliverable D4.6 of the HORIZON 2020 project EURAD. EC Grant agreement no: 847593.

Kulik, D. A., & Miron, G. D. (2024)
Solubility limits for model Opalinus Clay porewaters as input for sorption (SDB) and diffusion (DDB) databases. *Nagra Arbeitsbericht NAB 23-07.*

Marinich[1], O., Marques Fernandes[1], M., Miron[1], G. D., & Kulik[1], D. A. (2024)
ClaySor 2023: Update of 2SPNE SC/CE Sorption Model for Illite and Montmorillonite in GEMS Implementation. *Nagra Technical Report NTB 23-05.*
[1] PSI Center for Nuclear Engineering and Sciences, Switzerland

Marques Fernandes[1], M., Marinich[1], O., Miron[1], G. D., & Baeyens[1], B. (2024)
Sorption of Cs, Ni, Eu, Th and U on rock samples of Opalinus Clay and confining geological units from deep boreholes in the potential siting regions Nördlich Lägern, Zürich Nordost and Jura Ost: Measurements and predictive sorption modelling. *Nagra Technical Report NTB 23-01.*
[1] PSI Center for Nuclear Engineering and Sciences, Switzerland

Miron G. D. (2024)
Si–Al Pitzer dataset: Consistent set of Pitzer activity model interaction parameters of Al and Si species, for modelling cements in saline systems with THEREDA. ChemRxiv.
doi:10.26434/chemrxiv-2024-m02f1-v2

Miron G. D. (2024)
Deliverable 7.5 Report on the Digital Twin of a cemented wase package, geochemical evolution and mechanical integrity modelling. PREDIS WP 7.4.

Miron[1], G. D., Marques Fernandes[1], M., Kulik[1,2], D. A., Marinich[1], O., Baeyens[1,3], B., Wüst[4], R. A. J., Becker[4], J., & Li[4], X. (2024)
Sorption databases for Opalinus Clay, confining geological units, and bentonite: Methods, concepts, and upscaling of data. *Nagra Technical Report NTB 23-06.*
[1] PSI Center for Nuclear Engineering and Sciences, Switzerland
[2] CONGINEER GmbH, 5200 Brugg, Switzerland
[3] CWL Solutions GmbH, 5314 Kleindöttingen, Switzerland
[4] Nagra, 5430 Wettingen, Switzerland

Pfingsten, W. (2024)
UMAN - Views of the different actors on the identification, characterization and potential significance of uncertainties on the near-field. Final version as of 16.05.2024 of deliverable D10.18 of the HORIZON 2020 project EURAD. EC Grant agreement no: 847593. EC**:** 140.

Prasianakis, N. I., Laloy, E., Jacques, D., Meeussen, J. C. L., Tournassat, C., Miron, G.-D., Kulik, D. A., Idiart, A., Demirer, E., Coene, E., Cochepin, B., Leconte, M., Savino, M., Samper II, J., De Lucia, M., Yang, C., Churakov, S. V., Samper, J., Kolditz, O., & Claret, F. (2024)
Report describing the result of the machine learning benchmark carried out during the WP DONUT: EURAD-DONUT. Deliverable 4.8. (EURAD Reports; No. D4.8). EURAD - European Joint Programme on Radioactive Waste Management.

Tits, J., Kunz, D., Lechleitner, S.[1], Szidat, S.[1], & Guillemot, T.[2] (2024)
3rd annual report of the IGD-TP Project: "LOng-term Monitoring of C-14 compounds released during corrosion of IRradiated steel" (LOMIR). *IGD-TP Report. Nagra, Wettingen, Switzerland.*
[1] LARA, University of Bern, Bern, Switzerland
[2] Nagra, Wettingen, Switzerland

Tits, J., & Wieland, E. (2024)
Radionuclide Retention in the Cementitious Near Field of a Repository for L/ILW: Development of the Cement Sorption Data Base for Use in the License Application. *Nagra Technical Report NTB 23-07.*

Van Loon, L. R., Bunic, P., Frick, S., Glaus, M. A., & Wüst, R. A. J. (2024)
Diffusion Measurements of HTO, $^{36}Cl^-$ and $^{22}Na^+$ on Rock Samples of Opalinus Clay and Confining Units from Deep Bore Holes at the Potential Siting Regions for a Deep Geological Repository for Radioactive Waste in Switzerland: Jura Ost, Nördlich Lägern and Zürich Nordost. *Nagra Arbeitsbericht NAB 23-26.*

White[1], M. J., Aihkisalo[2], T., Bertrand[3], J., Buchwald[4], J., Chinesta[4], F., Cotton[3], J. C., Graebling[5], N., Haines[1], T. J., Hu[6], G., Kuusela[2], P., Laikari[2], A., Manukyan[7], E., Muñoz[4], D., Pfingsten[6], W., Purhonen[2], A., Schoenball[7], M., Thomas[1], A. E., Verstricht[8], J., & Wetter[8], C. (2024)
Advancements in Monitoring Data Management, Modelling and Visualisation. Deliverable D17.6 of the HORIZON 2020 project EURAD. EC Grant agreement no: 847593. EC**:** 141.

[1] Galson Sciences Ltd, 5 Grosvenor House, Melton Road, Oakham, Rutland, LE15 6AX
[2] VTT, Kivimiehentie 3, Espoo, P.O. Box 1000, 02044 VTT, Finland
[3] ANDRA, F-92298 Chatenay-Malabry, France
[4] ENSAM, 151, boulevard de l'hôpital, 75013 Paris, France
[5] Helmholtz Centre for Environmental Research (UFZ), Permoserstraße 15 / 04318 Leipzig / Germany
[6] PSI Center for Nuclear Engineering and Sciences, 5232 Villigen PSI, Switzerland
[7] Nagra, Hardstrasse 73, 5430, Wettingen, Switzerland
[8] EURIDICE, c/o SCK•CEN, Boeretang 200, 2400 Mol, Belgium

Wolffers, M., Bosoppi, I., & Eggenberger, U. (2024)
RÜCKBAUMATERIALIEN - Verwertungspotential der Feinfraktionen als CO_2-neutrales Rohmaterial in der Klinkerproduktion und PFAS-Vorkommen. On behalf of the Wyss Academy for Nature and the Federal Office for the Environment.

Wolffers, M., Dörfler, P., Weibel, G., & Bosoppi, I. (2024)
Jahresbericht AWA-1 Projekt «Ersatzrohstoffe in der Kreislaufwirtschaft», Wyss Academy for Nature.

Wolffers, M., Gfeller, F. Bosoppi, I., & Eggenberger, U. (2024)
Grundlagenstudie zur Anrechenbarkeit von klimaneutralem CO_2 in der Klinkerproduktion am Beispiel der Papierasche. On behalf of cemsuisse.

8.3 Conferences/workshops/presentations

Aschwanden, L., Looser, N., Mazurek, M., Gimmi, T., & Traber, D. (2024, November 25-29)
Geochemical investigation of veins and evidence for paleo fluid flow in Opalinus Clay. 9th Clay Conference, International Conference on Clays in Natural and Engineered Barriers for Radioactive Waste Confinement, Hannover, Germany.

Aschwanden, L., Waber, H. N., Eichinger, F., & Gimmi, T. (2024, June 12-14)
Isotope diffusive exchange experiments for deriving porewater isotope composition in low-permeability rocks – Improvements in experimental procedure and data processing. NEA Clay Club Workshop on Porewater Chemistry of Clayrocks in Repository Environments, Bure, France.

Baur, M., Churakov, S. V., & Prasianakis, N. I. (2024, July 9-12)
High performance reactive transport model for cement-claystone interface simulations. 33rd Discrete Simulation of Fluid Dynamics conference (DSFD 2024), Zürich, Switzerland.

Baur, M., Churakov, S. V., & Prasianakis, N. I. (2024, November 25-29)
High performance reactive transport model for cement-claystone interface simulations. 9th Clay Conference, International Conference on Clays in Natural and Engineered Barriers for Radioactive Waste Confinement, Hannover, Germany.

Bettoni[1], S., Kallestrup[1], J., Boege[1], M., & Boiger, R. (2024, May)
Machine learning for orbit steering in synchrotrons. Journals of Accelerator Conference Website (JACoW). 15th International Particle Accelerator Conference Proceedings, 977-980.
https://doi.org/10.18429/JACoW-IPAC2024-TUCN2

Boiger, R., Churakov, S. V., Llagaria, I. B., Kosakowski, G., Wüst, R., & Prasianakis, N. I. (2024, April 11-12)
Direct Mineral Content Prediction from drill core images via transfer learning. Data Science for the Sciences (DS4S) conference, Bern, Switzerland.

Boiger, R., Churakov, S. V., Llagaria, I. B., Kosakowski, G., Wüst, R., & Prasianakis, N. I. (2024, May 7-8)
Direct Mineral Content Prediction from drill core images via transfer learning. Mont Terri Technical Meeting TM-41, Porrentruy, Switzerland.

Boiger, R., Churakov, S. V., Llagaria, I. B., Kosakowski, G., Wüst, R., & Prasianakis, N. I. (2024, November 25-29)
Direct Mineral Content Prediction from Drill Core Images via Transfer Learning. 9th Clay Conference, International Conference on Clays in Natural and Engineered Barriers for Radioactive Waste Confinement, Hannover, Germany. (poster)

Bok, F., Zechel, S., Miron, D., Marinich, O., & Marques Fernandes, M. (2024, March 17–21) *Sorption data: Enhancement of geochemical modeling by chemically evident surface speciation* [Abstract]. ACS Spring, New Orleans, LA, United States, and virtual.

Bosoppi, Ilona (2024, August 27) *Ersatzrohstoffe in der Kreislaufwirtschaft.* KSE Kieslunch.

Brooksbank, H., & Neumann, A. (2024, November 9) *Impact of redox cycling on the composition and redox reactivity of the Fe(II)/phyllosilicate system* [Paper presentation]. 22nd Swiss Geoscience Meeting, Basel, Switzerland.

Brooksbank, H., & Neumann, A. (2024, November 25-28) *Redox buffering by iron-bearing clay minerals in the ferrous iron/smectite system*. 9th Clay Conference, Hannover, Germany.

Churakov, S. V., Owusu, J., Karalis, K., Mokos, A., & Prasianakis, N. I. (2024, January 24-25) *Molecular scale understanding of gas transport in clays*. 1st Caprock Integrity & Gas Storage Symposium 2024, St-Ursanne, Switzerland. (Poster)

Churakov, S. V., Owusu, J., Mokos, A., Karalis, K., & Prasianakis, N. I. (2024, November 25-29) *Molecular scale understanding of gas transport in clays*. 9th Clay Conference, International Conference on Clays in Natural and Engineered Barriers for Radioactive Waste Confinement, Hannover, Germany.

Claret, F., Pepin, G., Cances, C., Kolditz, O., Prasianakis, N. I., Baksay, A., & Lukin, D. (2024, November 25-29) *Developpement and improvement of numerical methods and tools for modelling coupled process: Lessons learnt during EURAD joint programing initiative*. 9th Clay Conference, International Conference on Clays in Natural and Engineered Barriers for Radioactive Waste Confinement, Hannover, Germany.

Dähn, R. (2024, June 5) *Digital Twin summary*. PREDIS final conference. Avignon, France.

Gimmi, T., Krejci, P., Baur, M., Prasianakis, N. I., Churakov, S. V., & Jenni, A. (2024, October 22-25) *Of chances and challenges (when modelling reactive transport of ions in clays and cement).* Reactive Transport Workshop 2nd edition, Fontainebleau, France.

Gimmi, T., Wersin, P., Aschwanden, L., Ma, J., Waber, H. N., Mazurek, M., Zwahlen, C., Wanner, C., & Traber, D. (2024, November 25-29) *Profiles of natural tracers in porewater of a Mesozoic rock sequence in northern Switzerland.* 9th Clay Conference, International Conference on Clays in Natural and Engineered Barriers for Radioactive Waste Confinement, Hannover, Germany.

Hu, G., Miron, G. D., Prasianakis, N. I., Churakov, S.V., Dähn, R., & Pfingsten, W. (2024, April 11-12) *Machine learning and surrogate model for two-case studies in nuclear waste management.* Data Science for the Sciences 2024, Bern, Switzerland.

Hu, G., & Pfingsten, W. (2024, April 23-25) *Physics-Based and Data-Driven Digital Twins for 3D-temperature evolution in the near-field of FE tunnel.* EURAD Final Annual Event, Bucharest, Romania.

Hu, G., Miron, G. D., Pfingsten, W., & Dähn, R. (2024) *Digital twin and surrogate model for long-term geochemical processes in nuclear waste management.* In Proceedings of the 31st International Conference on Nuclear Engineering (ICONE31), Prague, Czech Republic. Vol. 8. Decontamination and decommissioning, radiation protection, and waste management (#135796; 7 pp.). https://doi.org/10.1115/ICONE31-135796

Jenni, A., Gimmi, T., & Mäder, U. (2024, September 24-26) *Can reactive transport models predict clogging in highly reactive systems?* SKB Task Force EBS, Hannover, Germany.

Jenni, A., Gimmi, T., & Mäder, U. (2024, October 22-25) *Coupling of porosity and diffusive transport in highly reactive systems.* Reactive Transport Workshop 2nd edition, Fontainebleau, France.

Jenni, A., Kiczka, M., Zwahlen, C., Mäder, U., Meeussen, H., & Gimmi, T. (2024, November 25-29) *Transport experiments in claystone: electrostatic effects and preferential pathways*. 9th Clay Conference, International Conference on Clays in Natural and Engineered Barriers for Radioactive Waste Confinement, Hannover, Germany.

Kosakowski, G., & Martin, L. (2024, July 22-25) *Reactive Transport Modelling of Material Interface Evolution in the HLW Near-field*. Reactive Transport Workshop, Fontainebleau, France.

Kosakowski, G., & Martin, L. (2024, November 25-28) *Reactive Transport Modelling of Material Interface Evolution in the HLW Near-field*. 9th Clay Conference, Hannover, Germany.

Kulik, D. A., & Miron, G. D. (2024, June 3-7)
Beyond GEMS: Integration of thermodynamic datasets, activity models, and parameter optimization. ThermoCon, Socorro, New Mexico.

Laloy, E., Prasianakis, N. I., Jacques, D., Meeussen, J. C. L., Tournassat, C., Miron, G. D., Kulik, D. A., Idiart, A., Demirer, E., Cochepin, B., Leconte, M., Savino, M., Marques-Fernandes, M., Samper, J. II, De Lucia, M., Yang, C., Churakov, S. V., Montoya, V., Samper, J., Kolditz, O., & Claret, F. (2024, April 14-19)
Geochemistry and Machine Learning benchmark within EURAD joint project. European Geosciences Union general assembly, EGU 2024, Vienna, Austria.

Marinich, O., Marques Fernandes, M., Miron, G. D., & Kulik, D. A. (2024, June 14)
ClaySor 2023: sorption model and its application for predicting sorption of radionuclides by opalinus clay. Workshop on porewater chemistry of clayrocks in repository environments. Centre de Meuse / Haute Marne, Bure, France.

Miron, G. D., & Kulik, D. A. (2024, June 3-7)
GEMS as an asset of geochemical modelling: 24 years of development and use. ThermoCon, Socorro, New Mexico.

Miron, G. D., & Kulik, D. A. (2024, October 14-23)
Geochemical modelling with GEMS, application to model pore waters and sorption on clay minerals. China Institute for Radiation Protection (CIRP) and North China Electric Power University (NCEPU), Taiyuan-Beijing China.

Miron G. D., & Lothenbach B. (2024, July 5)
Thermodynamic models and databases for cementitious repositories. ThermoChimie Expert Panel, London, UK.

Miron, G. D., Marinich, O., Marques Fernandes, M., Kulik, D. A., & Baeyens, B. (2024, September 16-17)
Predictive sorption modelling with the ClaySor (2SPNE SC/CE) model. Sorption data management and database development for radioactive waste management workshop, Barcelona, Spain.

Miron, G. D., Marinich, O., Marques Fernandes, M., Kulik, D. A., Baeyens, B., & Wüst R. A. J. (2024, September 16-17)
Development of Sorption Databases for host rocks and engineered barrier materials. Sorption data management and database development for radioactive waste management workshop, Barcelona, Spain.

Mokos, A., Churakov, S. V., & Prasianakis, N. I. (2024, July 9-12)
Pore-scale nucleate boiling simulations using a 3D multiphase Lattice-Boltzmann approach. 33rd Discrete Simulation of Fluid Dynamics conference (DSFD 2024), Zürich, Switzerland. (Gold medal award)

Mokos, A., Sato, Y., Niceno, B., Churakov, S. V., & Prasianakis N. I. (2024, October 20-24)
Nucleate boiling within a fuel assembly affected by CRUD, pp.1-7, Proceedings of the Joint International Conference on Supercomputing in Nuclear Applications + Monte Carlo, SNA + MC 2024, Paris, France.

Obaied, A., Poonoosamy, J., Peng, H., Kaspor, A., Bosbach, D., & Prasianakis N. I. (2024, August 19-23)
Insights into the metastability of amorphous calcium carbonate (ACC): Microfluidic experiments combined with an AI-assisted toolbox for quantifying mineral transformations, Goldschmidt Conference, Chicago USA, (Poster).

Peng, H., Rajyaguru, A., Curti, E., Grolimund, D., Churakov, S. V., & Prasianakis, N. I. (2024, August 18)
Towards Digital Twins of Capillary Mass Diffusion Experiments: A Physics-based Machine-Learning Framework for Inverse Modeling of Mass Transport Processes. Goldschmidt Conference.

Pfingsten W. (2024, April 23-25)
MODATS - Advancements in Monitoring Data Management, Modelling and Visualisation. EURAD Final Annual Event, Bucharest, Romania.

Pfingsten, W. (2024, December 2-6)
SITEX.Network benchmarks of safety case review and modelling approaches. International Conference on Enhancing Nuclear Safety and Security Through Technical and Scientific Support Organizations (TSOs): Challenges and Opportunities in a Rapidly Changing World, IAEA, Vienna, Austria. (Invited panellist and talk).

Pfingsten, W., Diaconu, D., & Dewoghélaëre, J. (2024, April 23-25)
UMAN WP 10 –Nearfield uncertainties -views of different actors on their identification, characterization and potential significance for safety and a pluralistic dialogue with CS. EURAD Final Annual Event, Bucharest, Romania.

Pfingsten, W., & Hu G. (2024, November 8-9)
Physics-based and data-driven digital twins for 3D temperature development in the near field of the FE experiment in the Mont Terri rock laboratory. 22nd Swiss Geoscience Meeting 2024 Basel, Basel, Switzerland, SCNAT.

Pfingsten, W., & Hu G. (2024, November 25-28)
Physics-Based and Data-Driven Digital Twins for 3D-Temperature Evolution in the Near-field of the FE Tunnel at Mont Terri. 9th Clay Conference, Hannover, Germany.

Poonoosamy, J., Kaspor, A., Schreinemachers, C., Prasianakis, N. I., Curti, E., Deissmann, G., Kowalski, P., Churakov, S. V., & Bosbach, D. (2024, October 7-11)
AI-assisted lab-on-a-chip experiments: Setting new frontiers in radio-geochemistry. ATAS-AnXAS 2024 Joint Workshop, Karlsruhe (Germany).

Prasianakis, N. I., Baur, M., Peng, H., Mokos, A., & Churakov, S. V. (2024, August 19-23)
Accelerating reactive transport simulations by combining machine learning, smart algorithms and high performance computing, Goldschmidt Conference, Chicago USA.
https://doi.org/10.46427/gold2024.23143

Prasianakis, N. I., Boiger, R., Kosakowski, G., Wüst, R., & Churakov, S. V. (2024, November 25-29)
Effective diffusivity prediction by considering multivariable regression and rock properties. 9th Clay Conference, International Conference on Clays in Natural and Engineered Barriers for Radioactive Waste Confinement, Hannover, Germany. (poster)

Provis, J. L. (2024, March 11)
Cements, from beamlines to beams. CemNet Meeting, Bern, Switzerland.

Rothwell, K., & Neumann, A. (2024, July 22)
Octets: when to fit them and what information can we gain? [Workshop session]. Workshop on Iron Mössbauer applied to environmental systems 2024, Bristol, UK.

Stotskyi, V., Di Lorenzo, F., Marques Fernandes, M., Krack, M., Scheinost, A. C., Lanson, M., Lanson, B., & Churakov, S. V. (2024, August 21)
Molecular scale understanding of Ni^{2+} and Zn^{2+} adsorption on swelling clay minerals. Goldschmidt Conference 2024, Chicago, USA.

Stotskyi, V., Di Lorenzo, F., Marques Fernandes, M., Krack, M., Scheinost, A. C., Lanson, M., Lanson, B., & Churakov, S. V. (2024, November 26)
Ab initio MD modelling of Ni^{2+}, Zn^{2+}, and Lu^{3+} cation adsorption on saponite edge surfaces. 9th International Conference on Clays in Natural and Engineered Barriers for Radioactive Waste Confinement, Hannover, Germany.

Su, Z., Yue, Z., Paul, P. P., Marsh, A. T. M., DiMichiel, M., Burnett, T. L., Provis, J. L., Bernal, S. A., & Withers, P. J. (2024, 16 July)
Impact of CO_2 exposure in the microstructure of alkali-activated slag cement – A time-resolved 3D synchrotron XRD-CT/μXCT analysis. FEMS Junior EUROMAT 2024, Manchester, UK.

Traber, D., Roy, N., Stopelli, E., Heidinger, M., Eichinger, F., Wanner, C., Gimmi, T., & Waber, H. N. (2024, November 25-29)
Exploring the dynamics of aquifer- aquitard systems: new in-sights by ^{81}Kr model ages. 9th Clay Conference, International Conference on Clays in Natural and Engineered Barriers for Radioactive Waste Confinement, Hannover, Germany.

Wang, D. (2024, August 14)
Utilizing Electrolytic Manganese Residue (EMR) as a SCM. 10th International Conference of the Asian Concrete Federation (ACF), Ulaanbaatar, Mongolia [invited talk].

Wang, D. (2024, August 14-20)
Technical code for application of steel slag powder in concrete. First meeting of ACF Technical Committee-Supplementary Cementious Material. Ulaanbaatar, Mongolia.

Wang, D. (2024, September 9)
New supplementary cementitious materials (SCMs). CemNet Meeting, Bern, Switzerland.

Wang, Q., & Wang, D. (2024, November 1-3)
Binding and leaching of heavy metals from cement pastes. 10th Annual Academic Conference of the Cement Branch of the Chinese Ceramic Society, Hebei, China. [keynote lecture]

Wang, Q., & Wang, D. (2024, December 20-22)
Characterization methods for the species of heavy metals in cement pastes. 4th Academic Symposium on "Modern Concrete Microstructure Testing and Analysis. Harbin, China [keynote lecture]

Yang, Y., Patel, R. A., Zhang, Y., Prasianakis, N. I., Poonoosamy, J., Deissmann, G., Churakov, S. V., & Bosbach, D. (2024, November 25-29)
Radionuclide transport in variably water-saturated compacted clays: a pore-scale view, 9th Clay Conference, International Conference on Clays in Natural and Engineered Barriers for Radioactive Waste Confinement, Hannover, Germany. (poster)

Yue, Z., Dhandapani, Y., Provis, J. L., & Bernal, S. A. (2024, November 19)
Carbonation Resistance of Alkali-activated Materials-Experimentation and Modelling. 2024 Beijing International Youth Innovation and Development Forum; Future Industry and Science and Technology Innovation Parallel Forum; The 8th International Young Scholars "Rixin Forum" of Beijing University of Technology. Beijing, China. [Invited talk]

Zwahlen, C., Gimmi, T., Jenni, A., Mazurek, M., Traber, D., & Wüst, R. (2024, November 25-29) *Influence of texture on the chloride accessible porosity fraction explored by SEM and µCT data.* 9th Clay Conference, International Conference on Clays in Natural and Engineered Barriers for Radioactive Waste Confinement, Hannover, Germany.

8.4 Invited Talks

Boiger, R., Peng, H., & Xi B. (2024, November 20) *Machine learning applications for nuclear waste disposal and beyond*. Machine Learning Luncheon, PSI, Center for Scientific Computing, Theory and Data, Switzerland.

Neumann, A. (2024, June 3-6)
Redox processes of clay mineral-bound iron. Annual Conference of The Clay Minerals Society 2024, Honolulu, HI, USA.

Neumann, A. (2024, August 18-23)
The interdependence of structure and redox properties of clay minerals. 4th European Mineralogical Conference 2024, Dublin, Ireland.

Neumann, A., Entwistle, J., Latta, D. E., Scherer, M. M., Blukis, R., Couasnon, T., & Benning, L. G. (2024, March 17-21)
Investigating reactive precipitates formed by interfacial redox reactions at the clay mineral-water interface. National Meeting of the American Chemical Society ACS Spring 2024; New Orleans, LA, USA.

Prasianakis, N. I. (2024, July 9)
Accelerating numerical simulations: from microfluidics to geological repository scale. The 33rd Discrete Simulation of Fluid Dynamics (DSFD) conference, Zürich, Switzerland.

Provis, J. L. (2024, February 1)
Can we focus cements research to benefit both the environment and human development? ECO Materials Workshop, NYU Abu Dhabi, Abu Dhabi, UAE.

Provis, J. L. (2024, July 17)
Can we focus cements research to benefit both the environment and human development? 10th International Congress on Ceramics, Montreal, Canada.

Provis, J. L. (2024, November 11)
Can we focus cements research to benefit both the environment and human development? FIB Symposium 2024, Christchurch, New Zealand.

8.5 Teaching

Churakov S.V., Di Lorenzo F.
Master Course: *Mineral Surface Characterization with AFM*, Universität Bern, Fall semester 2024.

Churakov S.V.
Bachelor Course: *Kristallographie I+II*,
Universität Bern, Spring and Fall semester 2024.

Churakov S.V.
Bachelor Course: *Kristalloptik*, Universität Bern, Fall semester 2024.

Churakov S.V.
Master Course: *Atomistic simulations of fluids and solids*, Universität Bern, Fall semester 2024.

Eggenberger, U., Wolffers, M., & Gfeller, F.
Master Course: *X-Ray Powder Diffraction*, Institut für Geologie, Universität Bern, Spring semester 2024.

Gimmi, T., Mazurek, M., & van den Heuvel, D.
Fluids in the Crust. Bern–Fribourg Master in Earth Sciences, Fall semester, 2024.

Prasianakis N. I.
Examiner at PhD defence of R. Santoso, *Process-based machine learning for multi-physics and chemistry in geothermal applications: Parameter estimation and optimization under uncertainties*, RWTH Aachen University and ETH-Zürich, Aachen, Germany, December 2024.

Prasianakis N. I.
Examinateur at PhD defence of M. Savino, *Statistical learning methods for nonlinear geochemical problems*, Université Paris-Saclay, Paris, France, 2024, September 30.

Provis, J. L.
Radiation effects in cement and concrete, Joint ICTP-IAEA International Workshop on Modelling of Encapsulated Intermediate Level Waste (ILW) and High-Level Waste (HLW), Trieste, Italy, 2024, February 26.

Provis, J. L.
PhD defence examination (committee member), A. Germann (ETH Zürich), *Potential use of a low-carbon magnesia (MgO) binder for construction purposes.*

Provis, J. L.
PhD defence (rapporteur) of Q. Yang (Centrale Lille, France), *Résistance au feu de géopolymère alcalin et géopolymère acide.*

Provis, J. L. PhD defence (external examiner) of G. Griffiths (University of South Wales, UK), *Development of slow-release fertiliser from digestate using alkali silicates.*

Weibel, G., Wolffers, M., & Ingold, P.
Master Excursion: From Waste to Resources and the Challenges in Between, Spring semester 2024.

Weibel, G., Wolffers, M., Ingold, P.
Master Course: Geochemical Analysis of Rocks, Institut für Geologie, Universität Bern, Fall semester 2024.

8.6 PhD thesis defences

Ingold P. (2024)
Pollutant dynamics of bottom ash landfills (PhD student/UBern, defence date 2024, January 2).

Jäger, T. (2024)
Micro Surface Functionalisation to Improve Membrane Distillation (University of Luxembourg, 2024, January 10). Dissertation supervisors: Leyer, S. & Prasianakis N. I.

Jin, Haoliang (2024)
Investigation of alkali-silica reactions in different cement systems by thermodynamic modelling (PhD thesis, University of Sheffield). Supervisors: Provis, J. L. & Kinoshita, H.

Luraschi, P. (2024)
Evolution of porosity, diffusivity and mineralogy of different cement-clay interfaces (PhD thesis, defence on 2024, June 24, Bern, Switzerland.) Supervisors: Gimmi, T.; Co-supervisors: Churakov, S. V. & Van Loon, L. R.; External referee: Fernández Martin, R.

Mahrous M. (2024)
From Pore-Scale to Continuum-Scale: Reactive Transport Modeling of Minerals Dissolution and Precipitation (University of Bern, Switzerland, 2024, January 29). Supervisors: Churakov S. V. & Prasianakis N. I.

Qian Y. (2024)
Adsorption of redox sensitive radionuclides on Fe-bearing clay minerals (PhD student, defence date 2024, January 2).

White, M. L. (2024)
Harnessing Microbially-mediated Redox Processes for Sustainable Water Treatment (unpublished PhD Thesis, Newcastle University).

Paul Scherrer Institut PSI
Forschungsstrasse 111
5232 Villigen PSI
Schweiz
www.psi.ch